In Search of
Slow-moving Ionizing Massive Particles

Thesis by

Gang Liu

In Partial Fulfillment of the Requirements
for the Degree of
Doctor of Philosophy

California Institute of Technology
Pasadena, California

1988

(Submitted September 23, 1987)

To my father and my wife

Acknowledgements

I first wish to thank my thesis adviser Professor, Barry C. Barish. In the several years that I have been his student, his profound understanding of the physics principles, his deep insight into physics problems, his vast knowlege and skills in experimental physics, and his devotion and commitment in the research work have earned my great respect and gratitude, benefitted me in various respects and deepened my interest in experimental physics. Professor Barish's patient help, invaluable advice and outstanding leadership were essential for the completion of this work.

I also wish to take this opportunity to thank the members of MACRO collaboration, especially Professor Charlie Peck and Charles Lane of the Caltech group. Many useful discussions with them and their valuable suggestions have been of great benefit to this work. It has been a great pleasure to work with them.

My entire graduate study has been supported by Caltech through fellowships and graduate research assistantships. I wish to express my appreciation for this support.

Thanks are also due to A. Bodek of Fermilab for the loan of the scintillator used in the experiment of Chapter 3 and to Mark Nelson and Ryzard Stroynowski of Caltech Mark II group for the loan of their equipment used in the MACRO prototype counter test.

I also owe thanks to the engineers, electronic technicians and machinists of the Caltech High Energy Physics group. Their great skills in building equipment have been indispensable for this work.

Finally, I wish to express my gratitude to a very special American family. The Graham family of Portola Valley gave me the warmest welcome when I first arrived in this wonderful but foreign land. In several years of my stay in the United States, their sincere friendship, affectionate care and generous help have made me able to cope with the "cultural shock," the language barrier and other difficulties and made my life during my graduate study so enjoyable and so much like home.

Abstract

Many particles proposed by theories, such as GUT monopoles, nuclearites and 1/5 charge superstring particles, can be categorized as Slow-moving, Ionizing, Massive Particles (SIMPs).

Detailed calculations of the signal-to-noise ratios in various acoustic and mechanical methods for detecting such SIMPs are presented. It is shown that the previous belief that such methods are intrinsically prohibited by the thermal noise is incorrect, and that ways to solve the thermal noise problem are already within the reach of today's technology. In fact, many running and finished gravitational wave detection (GWD) experiments are already sensitive to certain SIMPs. As an example, a published GWD result is used to obtain a flux limit for nuclearites.

The result of a search using a scintillator array on Earth's surface is reported. A flux limit of $4.7 \times 10^{-12}\,\mathrm{cm}^{-2}\mathrm{sr}^{-1}\mathrm{s}^{-1}$ (90% c.l.) is set for any SIMP with $2.7 \times 10^{-4} < \beta < 5 \times 10^{-3}$ and ionization greater than 1/3 of minimum ionizing muons. Although this limit is above the limits from underground experiments for typical supermassive particles (10^{16}GeV), it is a new limit in certain β and ionization regions for less massive ones ($\sim 10^{9}$GeV) not able to penetrate deep underground, and implies a stringent limit on the fraction of the dark matter that can be composed of massive electrically and/or magnetically charged particles.

The prospect of the future SIMP search in the MACRO detector is discussed. The special problem of SIMP trigger is examined and a circuit proposed, which may solve most of the problems of the previous ones proposed or used by others and may even enable MACRO to detect certain SIMP species with β as low as the orbital velocity around the earth.

Table of Contents

List of Figures

List of Tables

Chapter 1

Introduction

Imagine a particle coming with a velocity as low as $\beta \sim 10^{-3}$, leaving energy of 1GeV/cm on its path, but so massive that it travels through a large detector with virtually constant velocity and can even penetrate the earth. No such particle can be found in the particle data table today, yet detecting them has recently grown into an active area in physics. Searching for such strange particles is not merely due to curiosity about finding new phenomena, it has become a subject of profound importance in particle physics, astrophysics and cosmology. In this chapter, I will try to outline some of the reasons for the general search for such Slow-moving, Ionizing, Massive Particles (SIMPs).

1.1. Dark Matter Problem

Observations and theoretical work have revealed that most of the matter in the universe is dark and that the density of the luminous matter is only a small fraction of the total mass density of the universe[1]. The strongest evidence of the existence of dark matter is from the observation of the rotation velocities of spiral galaxies[2]. The rotation velocities at the edge of these galaxies do not fall off as would be expected if the galaxies were made only of luminous matter. The rotation velocities, as well as the stability of spiral galaxies, can be explained by assuming that the visible galaxies are each imbedded in a large, roughly

spherical distribution of dark matter, or a galactic "halo." The halo density near the sun is certainly of the greatest interest so far as the experimental detection is concerned. Several authors have made detailed models of the mass distribution of our galaxy and have estimated the local halo density. A model made by Caldwell and Ostriker[3] gives a local halo density of $0.006 M_{\odot}/\mathrm{pc}^3 \sim 0.4\mathrm{GeV}/\mathrm{cm}^3$, with other models giving estimates of the same order of magnitude[4].

The galactic halo is not the only unseen matter in the universe. If one believes the inflationary scenario[5-7], the universe should be flat and has a mass density essentially exactly the critical density $\rho_c \sim 2\times 10^{-29}\mathrm{g}/\mathrm{cm}^3 \sim 10^{-5}\mathrm{GeV}/\mathrm{cm}^3$. However, if one adds up the total mass of the galaxies, including the dark halos (which can be measured by their gravitational effects), one can only make up 20% of the critical density[8-9]. Therefore, 80% of the mass in the universe is still missing. Such intergalactic dark matter is usually assumed to be uniformly distributed throughout the universe.

Dark matter may simply be ordinary matter being dark, such as stars with the size of Jupiter, white dwarfs or even black holes that do not emit or scatter much light. This possibility, however, is very unlikely because of a more profound reason. The big bang cosmology has been very successful in calculating the ratios of the primordial abundance of light elements[10], such as D, ^{3}He and ^{7}Li. However, the calculation is correct only when the present ratio of the nucleon number to the photon number lies in the range from 3×10^{-10} to 10^{-9}. Since the photon number density is well known from the 2.7°K background radiation, an allowed

range of the nucleon mass density can be obtained. It turns out, even if every possible error is stretched to its limit, the nucleon mass density still cannot be more than 20% of the critical density ρ_c.

Since the dark matter is very unlikely to be ordinary matter, various exotic particles have been proposed as candidates of the dark matter at different scales and the list is still growing. To explain the absence of their detection, such particles must either be very weakly interacting or have very low number density, or both. If dark matter particles are very weakly interacting, direct experimental detection is very difficult. It is interesting to note that the ultracold bolometric detectors may make those invisible particles visible[11-12], but such detectors are only at the stage of prototypes and proposals. On the other hand, if dark matter particles are not very weakly interacting, for instance, if they carry an electric charge or a magnetic charge, or for any other reason have large enough dE/dx when passing through matter, their detection becomes much easier. In this case, their number density must be very low, and to make up the required mass density, they must be supermassive. Unless galactic field acceleration plays an important role, supermassive particles are naturally expected to have the virial velocity of our galaxy ($\beta \sim 10^{-3}$) if they are of galactic origin, and a velocity slightly higher than the escape velocity ($\beta \sim 3 \times 10^{-3}$) if they come from outside our galaxy.

To detect charged dark matter particles or to rule them out is the first reason that SIMPs should be sought for.

1.2. Magnetic Monopoles

The history of the conjecture that magnetic monopoles may exist in nature has probably existed as long as the history of physics. The serious monopole theories, however, only began in 1931 when Dirac showed that the existence of magnetic monopoles was consistent with Maxwell equations and could provide the reason for charge quantization[13,14].

More recently, 't Hooft and Polyakov[15-16] showed that magnetic monopoles were simply unavoidable in most of the non-Abelian gauge theories. Since then, interest in experimental search for such poles has markedly increased. Monopoles associated with non-Abelian gauge theories are predicted to have a mass of order of the unification mass scale divided by the coupling constant. Although most formulations of Grand Unified Theories (GUTs) predict a monopole mass of approximately 10^{16}GeV, there are models that have monopoles with mass ranging in value from as low[17] as 10^{5}GeV up to the Planck mass (10^{19}GeV).

Like any other supermassive particles, if galactic field acceleration is not important, GUT monopoles should have $\beta \sim 10^{-3}$ if they are confined to our galaxy and $\beta \sim 3 \times 10^{-3}$ if they come from outside our galaxy. For monopoles of mass 10^{16}GeV, the velocity gained by galactic magnetic field acceleration is the same order of magnitude as the virial velocity, while monopoles lighter than 10^{10}GeV may have been accelerated to near the speed of light. However, in some models involving certain symmetries or plasma oscillations, the galactic field acceleration does not necessarily happen[18].

The expected monopole flux is subject to various cosmological and astrophysical constraints. The most stringent astrophysical constraint is set by Turner and Parker[19,20] based on the survival of the galactic magnetic field. If the observed galactic magnetic field is produced by the dynamo action, as usually expected, then the flux of magnetic monopoles cannot exceed $10^{-15}\mathrm{cm}^{-2}\mathrm{s}^{-1}\mathrm{sr}^{-1}$. This limit is usually referred to as "Parker bound." To detect such a small monopole flux, one needs a detector of more than $10^3\mathrm{m}^2$ in the area.

Since GUT monopoles are supermassive, they are very unlikely to stop in the Earth's crust and the Moon's surface; therefore, previous searches in iron ores or moon rocks etc.[21,22] are irrelevant. It is also impossible to generate GUT monopoles in particle accelerators; the only place to find them seems to be in cosmic rays. The superconducting loop techniques, first used by Cabrera[23], can provide a clear and unique signature for cosmic ray magnetic monopoles, but there are limited possibilities for expanding to very large areas[24]. On the other hand, since slow GUT monopoles have quite large dE/dx in matter, they can be seen in detectors based on the ionization and excitation mechanism. Although such detectors do not provide a unique signature for monopoles, they can be easily expanded into very large areas[24].

Looking for GUT magnetic monopoles is another reason that large area searches for SIMPs are necessary.

1.3. Nuclearites

It has been suggested recently[25–27] that certain quark matter, called "nu-

clearites," which contain proper numbers of up, down and strange quarks may be absolutely stable and might be the true ground state of QCD at finite baryon numbers (instead of the usual nuclei). If nuclearites do exist, they may solve the dark matter problem in the framework of QCD, which, unlike the theories of many other candidates, is a theory well tested in experiments.

Within the allowed range of QCD parameters (the strange quark mass excess m, the coupling constant α_s, and B, the "bag constant"), the baryon number and mass of a nuclearite can be any value from that of a usual nucleus to that of a neutron star[28]($\sim 10^{56} m_p$).

Nuclearites are electrically charged but have extraordinarily low charge-to-mass ratio. A nuclearite with a baryon number of order of 1000 may carry a positive charge of, say, 53 and acts like a superheavy iodine nucleus, while a nuclearite with a baryon number of 10^{10} may carry a charge of 1000 to 10000. Positively charged nuclearites are expected to be surrounded by electrons and appear neutral. For a small nuclearite, the surrounding electrons are not much different from that of an ordinary atom of the same charge, while a very large nuclearite can have an electron "atmosphere" continually distributed into the nuclear body, like that of a neutron star.

While very light nuclearites can stop and thus be found in rocks, and very large ones can be detected by earthquakes, the most interesting region (from 10^{-14}g to a few milligrams) can be sought for in cosmic rays as slow-moving,

ionizing, massive particles. This is the third reason that SIMPs should be sought for.

1.4. Other Particles?

In addition to those mentioned above, there may be many other kinds of SIMPs that are possible in various theories. For instance, the superstring theories may contain superheavy particles of fractional charge (1/5 electron charge, say)[29]. I will not attempt to make a full list of all the SIMPs that are possible in various current and future theories, because such list can never be complete.

In the pursuing unification, modern particle theories have been seeking new symmetries at much higher energy scales than what is accessible by any conceivable accelerators. Most of the Grand Unification Theories have unification scales at 10^{15}GeV. Theories trying to unify with gravity have energy scales at the Plank mass (10^{19}GeV). Since accelerators are hopeless, one hopes that systematically searching for SIMPs in cosmic rays, with large area detectors, may provide a way to explore such high energy scales directly. A positive discovery of anything at such high energy is undoubtedly of great importance, but even a negative result with a flux limit is a very useful piece of information. In fact, the absence of GUT monopoles has already played a crucial role in showing that the standard GUT is not compatible with the standard cosmology and has provided an important reason for the inflationary scenario.

1.5. Stopping Power of Slow Particles

The most important question about the experimental detection of SIMPs is their $\frac{dE}{dx}$ or "stopping power" in various materials. Because of the lack of experimental data and the complexity of theoretical treatment, stopping power at very low β is still not fully understood. There are various models giving wide range of results. To get some estimates, I will use the models that seem most convincing to me.

Stopping power is usually calculated as the sum of electronic stopping power and nuclear stopping power.

$$\frac{dE}{dx} = \left(\frac{dE}{dx}\right)_e + \left(\frac{dE}{dx}\right)_n \tag{1.5.1}$$

Based on the Thomas-Fermi picture, J. Lindhard and M. Scharff have found an expression of electronic stopping power for electrically charged particles at very low velocity[30-31]:

$$\left(\frac{dE}{dx}\right)_e = 4\pi a_0 e^2 N \frac{2\beta}{\alpha} \frac{Z_1^{7/6} Z_2}{(Z_1^{2/3} + Z_2^{2/3})^{3/2}}, \tag{1.5.2}$$

where Z_1 is the charge of the traveling particle, Z_2 is the atomic number of the stopping material, N is the number of atoms in unit volume, a_0 is the Bohr radius of a hydrogen atom and α is the fine structure constant.

An expression for nuclear stopping power of electrically charged particles was also derived by J. Lindhard and M. Scharff based on the Thomas-Fermi

model, but the "average" model of W. D. Wilson *et al.* seems to fit experimental data better[32]. According to this "average" model,

$$\left(\frac{dE}{dx}\right)_n = 4\pi a e^2 N \frac{Z_1 Z_2 M_1}{M_1 + M_2} S_n(\epsilon), \tag{1.5.3}$$

where M_1 and M_2 are the masses of the projectile and the target atom respectively, $a = 0.8853 a_0/(Z_1^{1/2} + Z_2^{1/2})^{2/3}$, $\epsilon = aM_2E/[Z_1 Z_2 e^2(M_1 + M_2)]$, and $S_n(\epsilon)$ is a universal function approximately parameterized as

$$S_n(\epsilon) = \frac{0.5 \ln(1+\epsilon)}{\epsilon + 0.14120\epsilon^{0.42059}}. \tag{1.5.4}$$

For SIMPs, $M_1 \gg M_2$, therefore,

$$\left(\frac{dE}{dx}\right)_n = 4\pi a e^2 N Z_1 Z_2 S_n(\epsilon) \tag{1.5.5}$$

and

$$\epsilon = \frac{aM_2c^2}{2Z_1 Z_2 e^2}\beta^2, \tag{1.5.6}$$

where c is the speed of light.

For slow GUT monopoles, S. P. Ahlen and K. Kinoshita have derived both electronic and nuclear stopping powers and the sum is the following[33]:

$$\frac{dE}{dx} = 4\pi a_0 e^2 \left[N_e \frac{Z_m^2 \beta}{2\beta_F} \left(\ln \frac{1}{z_{min}} - \frac{1}{2} \right) + N \frac{Z_m^2 Z_2^2 m_e}{M_2} \ln \frac{M_2 \beta}{Z_m Z_2 \alpha m_e} \right], \tag{1.5.7}$$

where Z_m is the magnetic charge of the GUT monopole in units of e/α (for Dirac monopole $Z_m = 1/2$), m_e is the mass of electron, N_e is the number of electrons per unit volume in the stopping medium, $c\beta_F = (\hbar/m_e)(3\pi^2 N_e)^{1/3}$ is their Fermi velocity, and z_{min} is a cutoff parameter. For nonconductors, $1/z_{min} =$

$2k_f a_0$, where $k_f = m_e c\beta_F/\hbar$, and N_e and β_F should be calculated by the total number of electrons in the medium. For conductors, the contribution of the nonconducting electrons can be calculated in the same way as for nonconductors, and the contribution of the conducting electrons should be calculated separately using $1/z_{min} \approx 100k_f a_1 T_m/T$, where a_1 is the lattice constant, T_m is the melting temperature of the metal and T is the actual temperature.

Low Z nuclearites are not much different from usual electrically charged particles, and their stopping power is given by Equations (1.5.2) and (1.5.5). For a nuclearite of very large Z, the electron atmosphere is so dense that it effectively becomes an impenetrable hard ball and can displace all matter in its path. In this case, the stopping power of a nuclearite with velocity v is given by[27]

$$\frac{dE}{dx} = \pi r^2 \rho v^2, \tag{1.5.8}$$

where ρ is the density of the medium and r is the effective radius of the nuclearite, including the surrounding electrons. For nuclearites lighter than 1.5g, r is roughly the radius of an atom ($\sim 10^{-8}$cm) and for larger ones $r \sim (3M/4\pi\rho_n)^{1/3}$, where $\rho_n \sim 3.6 \times 10^{14}\mathrm{g/cm}^3$ is the density of the nuclear matter.

Figure 1.5.1 shows the stopping power of several species of SIMPs calculated by the above formulas. Note that conductors have much larger stopping power than insulators for magnetic monopoles. This is due to the interaction of the long-range magnetic field with the conducting electrons. Such long-range interaction does not happen for electrically charged particles, because the electric field is shielded by the abundant electric charges existing in the medium. As shown in

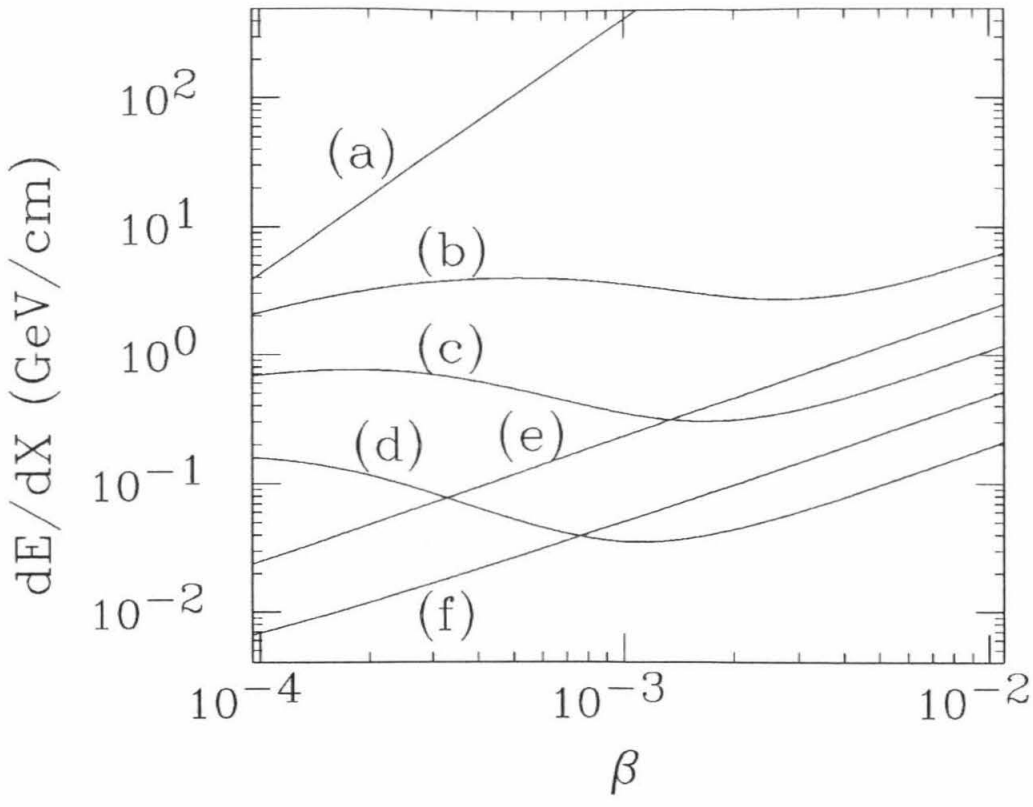

Fig. 1.5.1 — Stopping power versus β of various SIMPs. (a) nuclearites lighter than 1.5g in Si; (b) $Z = 6$ particles in Si; (c) unit charge particles in Si; (d) $\frac{1}{5}$ charge particles in Si; (e) monopoles in Al; (f) monopoles in Si.

Figure 1.5.1, the stopping power of various SIMPs in different materials differs by several orders of magnitude. However, for the convenience of later discussions, I will take 1 GeV/cm as a "typical value" of the stopping power of a SIMP and whenever possible, the explicit dependence on dE/dx will be given.

References of Chapter 1

[1]Lawrence M. Krauss, Scientific American **255**, 58 (Dec. 1986).
[2]S. M. Faber and J. S. Gallagher, Ann. Rev. Astron. Astrophys. **17**, 135 (1979).
[3]J. Caldwell and J. P. Ostriker, Astrophys. J. **251**, 61 (1981).
[4]See Table 4 of Ref. 3.
[5]A. H. Guth, Phys. Rev. D **23**, 347 (1981).
[6]A. D. Linde, Phys. Lett. **108B**, 389 (1982).
[7]A. Albrecht and P. J. Stainhardt, Phys. Rev. Lett. **48**, 1220 (1982).
[8]P. J. E. Peebles, Nature **321**, 27 (1986).
[9]G. A. Tammann and A. Sandage, Astrophys. J. **294**, 81 (1985).
[10]J. Yang, M. S. Turner, G. Steigman, D. N. Schramm, and K. A. Olive, Astrophys. J. **281**, 493 (1984).
[11]B. Cabrera, L. M. Krauss and F. Wilczek, Phys. Rev. Lett. **55**, 25 (1985).
[12]A. Drukier, K. Freese and D. N. Spergel, Phys. Rev. D **33**, 3495 (1986).
[13]P. A. M. Dirac, Proc. Royal Soc. London **A233**, 60 (1931).
[14]P. A. M. Dirac, Phys. Rev. **74**, 817 (1948).
[15]G. 't Hooft, Nucl. Phys. **B79**, 276 (1974).
[16]A. Polyakov, Sov. Phys. JETP Lett. **20**, 194 (1974).
[17]J. Kim, Phys. Rev. D **23**, 2706 (1981).
[18]R. Farouki, S.L. Shapiro and I. Wassermen, Astrophys. J. **284**, 282 (1984).
[19]M. S. Turner, E. N. Parker and T. J. Bogdan, Phys. Rev. D **26**, 1296 (1982).
[20] E. N. Parker, *Monopole '83* (Proceedings of Monopole '83 Workshop Oct. 6–9 1983 at Ann Arbor, Mich., ed. J. L. Stone), page 125 (Plenum Press, New York, 1984).
[21]R. R. Ross, P. H. Eberhard, and L. W. Alvarez, Phys. Rev. D **8**, 689 (1973).
[22]T. Watanabe and T. Ebisu, *Monopole '83*, page 503.
[23]B. Cabrera, M. Taber, R. Gardner, and J. Bourg, Phys. Rev. Lett. **51**, 1933 (1983).
[24]B. C. Barish, *Monopole '83*, page 367.
[25]E. Witten, Phys. Rev. D **30**, 272 (1984).
[26]A. De Rújula and S. L. Glashow, Nature **312**, 734 (1984).
[27]A. De Rújula, Nucl. Phys. **A434**, 605c (1985).
[28]E. Farhi and R. L. Jaffe, Phys. Rev. D **30**, 2379 (1984).
[29]X. Wen and E. Witten, Nucl. Phys. **B261**, 651 (1985).
[30]J. Lindhard and M. Sharff, Phys. Rev. **124**, 128 (1961).
[31]L. C. Northcliffe, Ann. Rev. Nucl. Sci. **13**, 67 (1963).
[32]W. D. Wilson, L. G. Haggmark and J. P. Biersack, Phys. Rev. B **15**, 2458 (1977).
[33]S. P. Ahlen and K. Kinoshita, Phys. Rev. D **26**, 2347 (1982).

Chapter 2

Acoustic and Mechanical Detection Methods

In order to detect SIMPs effectively and to address the related cosmological and astrophysical questions, very large area searches are needed. To make areas large, reducing the cost of the detector materials becomes important. Ordinary materials such as aluminum, etc. have large stopping power for SIMPs and are much cheaper than ordinary scintillators. B. Barish first noticed this and pointed out the possibility that such materials may be used for SIMP detection so that large areas can be covered with low cost[1]. Whether or not this goal can be realized is a rather practical question and can be answered only when the detection techniques are well understood and developed. Before this, some more immediate questions are: How can we detect the ionization energy deposited in a material that does not scintillate and is mostly opaque? What are the major factors that limit the sensitivity of such detection techniques? Are these limits merely due to some technical problems that can be solved by improving technology or are they inherently unavoidable? In this chapter, I attempt to answer these questions.

2.1. Acoustic Detection in Infinite Medium

I will first consider the method of detecting acoustic waves produced by a SIMP in infinite medium. Here, "infinite" means that the dimension of the

detector is much larger than the acoustic wave length and the attenuation length. The detection in the deep ocean (for instance in DUMAND[2]) is a good example of this case. The first Caltech prototype[1] does not really belong to this case, but the result can still be applied to obtain an approximate evaluation, since the attenuation length of the acoustic signal is not much larger than the size of the detector.

Acoustic radiation produced by traveling particles and showers in infinite fluid has been studied theoretically by J. Learned[3] and experimentally by L. R. Sulak[4] *et al.* In addition, C. Akerlof[5] has also made an estimation of acoustic signal produced by a GUT monopole in an infinite conductor. In order to simplify their calculations, the heat conductivity of the medium has been ignored and it has been assumed that the particle is infinitely fast and the track is infinitely thin, so that the acoustic source can be treated as a line source occurring instantly.

In the following, I will present another treatment explicitly containing the heat conductivity of the medium, the finite velocity of the particle and the finite size of the heat source it produces. Such an approach allows one to see explicitly how large these effects are and to estimate the errors. In case these effects are not negligible, they can be easily calculated.

The calculation is based on a simple picture: when the particle goes through the medium, the ionization energy loss turns into heat, raising up the temperature of the material near the track; then the thermal expansion of the material produces the acoustic signal. Such a "thermal expansion model" is supported

by the experiment[4] of L. R. Sulak *et al.* It was observed in their experiment that the acoustic signals in various liquids were proportional to the thermal expansion coefficient divided by the specific heat. Interesting enough, when the temperature of the tested water was reduced below 4°C, the thermal expansion coefficient became negative, and the signal was observed with reversed polarity.

For simplicity, I will ignore the difference between the isothermal elastic constants and the adiabatic ones and also the difference between the the specific heat under constant pressure and the specific heat with constant volume. The calculation starts with an isotropic solid, and the liquid case can be obtained by letting the Poisson's ratio be 1/2.

First, write down the equations for the heat conduction and the elasticity.

$$\frac{\partial T(\mathbf{x},t)}{\partial t} = \frac{K_H}{C_p}\nabla^2 T(\mathbf{x},t) + \frac{1}{C_p}Q(\mathbf{x},t) \tag{2.1.1}$$

and

$$\rho\frac{\partial^2 u_i}{\partial t^2} = \sum_{j=1}^{3}\frac{\partial s_{ij}}{\partial x_j}, \tag{2.1.2}$$

where $T(\mathbf{x},t)$ is the temperature distribution, $Q(\mathbf{x},t)$ is the heat source produced by the traveling particle, K_H is the heat conductivity, C_p is the specific heat, ρ is the density, u_i is the ith component of the displacement vector $\mathbf{u}$, and s_{ij}'s are the components of the stress tensor $\hat{\mathbf{s}}$.

In the usual theory of elasticity, the relationship between the stress s_{ij} and the strain $e_{ij} \equiv \frac{1}{2}(\frac{\partial u_i}{\partial x_j} + \frac{\partial u_j}{\partial x_i})$ for uniform isotropic material is given by

$$s_{ij} = K\theta\delta_{ij} + 2\mu(e_{ij} - \frac{\theta}{3}\delta_{ij}), \tag{2.1.3}$$

where $\theta = e_{11} + e_{22} + e_{33} = \nabla \cdot \mathbf{u}$, and K and μ are elastic constants related to the Young's modules Y and the Poisson's ratio σ by

$$K = \frac{Y}{3(1-2\sigma)} \qquad \text{and} \qquad \mu = \frac{Y}{2(1+\sigma)} \,. \tag{2.1.4}$$

When there is a temperature rise T, there will be thermal expansion αT in every direction, where α is the linear thermal expansion coefficient. If now the stress is kept unchanged, the strain will be increased by $\alpha T \delta_{ij}$. Since this additional amount of strain is not due to the applied stress, it should be subtracted from the total strain when calculating the stress. Thus, replacing e_{ij} by $e_{ij} - \alpha T \delta_{ij}$ in Equation (2.1.3) and also adding the friction stress, one gets the following modified strain-stress relation.

$$s_{ij} = K(\theta - 3\alpha T)\delta_{ij} + 2\mu(e_{ij} - \frac{\theta}{3}\delta_{ij}) + \eta\frac{\partial\theta}{\partial t}\delta_{ij} + 2\zeta(\frac{\partial e_{ij}}{\partial t} - \frac{1}{3}\frac{\partial\theta}{\partial t}\delta_{ij}), \tag{2.1.5}$$

where η and ζ are the bulk and shear viscosity constants.

Substituting (2.1.5) into Equation (2.1.2), one gets

$$\rho\frac{\partial^2\mathbf{u}}{\partial t^2} = (K+\frac{\mu}{3})\nabla(\nabla\cdot\mathbf{u}) + \mu\nabla^2\mathbf{u} + (\eta+\frac{\zeta}{3})\nabla\nabla\cdot(\frac{\partial\mathbf{u}}{\partial t}) + \zeta\nabla^2\frac{\partial\mathbf{u}}{\partial t} - 3\alpha K\nabla T. \tag{2.1.6}$$

Taking divergence of the above equation gives the following equation for the longitudinal waves:

$$\rho\frac{\partial^2\theta(\mathbf{x},t)}{\partial t^2} = (k+\frac{4}{3}\mu)\nabla^2\theta(\mathbf{x},t) + (\eta+\frac{4}{3}\zeta)\frac{\partial\nabla^2\theta(\mathbf{x},t)}{\partial t} - 3\alpha K\nabla^2 T(\mathbf{x},t). \tag{2.1.7}$$

Taking Fourier transforms of Equations (2.1.1) and (2.1.7) with respect to time and eliminating $T(\mathbf{x},\omega)$ from them, one obtains

$$(\nabla^2 + a^2)(\nabla^2 + b^2)\theta(\mathbf{x},\omega) = -\nu\nabla^2 Q(\mathbf{x},\omega), \tag{2.1.8}$$

where

$$a^2 = \frac{i\omega C_p}{K_H} \quad b^2 = \frac{\omega^2 \rho}{K + \frac{4}{3}\mu - i\omega(\eta + \frac{4}{3}\zeta)} \quad \nu = \frac{3\alpha K}{[(K + \frac{4}{3}\mu) - i\omega(\eta + \frac{4}{3}\zeta)]K_H}. \tag{2.1.9}$$

Equation (2.1.8) is a fourth order partial differential equation. Following the same route of proving the "Green's Function" method for usual second order equations, one can prove that if the "Green's Function" $G(\mathbf{x}, \mathbf{x}')$ satisfying

$$(\nabla^2 + a^2)(\nabla^2 + b^2)G(\mathbf{x}, \mathbf{x}') = \nabla^2 \delta(\mathbf{x} - \mathbf{x}') \tag{2.1.10}$$

is found, then the solution of Equation (2.1.8) is given by

$$\theta(\mathbf{x}, \omega) = -\nu \int Q(\mathbf{x}', \omega) G(\mathbf{x}, \mathbf{x}') d^3x'. \tag{2.1.11}$$

The solution of Equation (2.1.10) is easily found by the usual Fourier transform method, resulting in

$$G(\mathbf{x}, \mathbf{x}') = \frac{-1}{4\pi(a^2 - b^2)} \frac{a^2 e^{ia|\mathbf{x}-\mathbf{x}'|} - b^2 e^{ib|\mathbf{x}-\mathbf{x}'|}}{|\mathbf{x} - \mathbf{x}'|}. \tag{2.1.12}$$

Since a has a large imaginary part, the term containing $e^{ia|\mathbf{x}-\mathbf{x}'|}$ in the above equation can be ignored if the acoustic wave is detected at a reasonable distance from the source. For example, at 10MHZ and for $|\mathbf{x} - \mathbf{x}'| \sim 1$m, $e^{ia|\mathbf{x}-\mathbf{x}'|}$ is only order of $e^{-800000}$. Equation (2.1.11) thus becomes

$$\theta(\mathbf{x}, \omega) = \frac{-\nu b^2}{4\pi(a^2 - b^2)} \int \int e^{i\omega t'} Q(\mathbf{x}, t') \frac{e^{ib|\mathbf{x}-\mathbf{x}'|}}{|\mathbf{x} - \mathbf{x}'|} dt' d^3x'. \tag{2.1.13}$$

For a particle traveling along z-axis with velocity V_m and energy loss $\frac{dE}{dz}$, the heat source can written as

$$Q(\mathbf{x}', t') = V_m \frac{dE}{dz} f(r', z' - V_m t'). \tag{2.1.14}$$

where $r' = \sqrt{x'^2 + y'^2}$ and $f(r,z)$ is the distribution of the ionization energy around the traveling particle normalized as $\int f(r,z)d^3x = 1$.

Substituting Equation (2.1.14) into (2.1.13) and properly changing the variables in the integral, one gets

$$\theta(\mathbf{x},\omega) = \frac{-\nu b^2}{4\pi(a^2-b^2)}\frac{dE}{dz}\int F(x,y,z,x',y',z',z'')f(r',z'')d^3x'dz'', \qquad (2.1.15)$$

where

$$F(x,y,z,x',y',z',z'') = \frac{e^{i\omega(z'-z'')/V_m + ib|\mathbf{x}-\mathbf{x}'|}}{|\mathbf{x}-\mathbf{x}'|}. \qquad (2.1.16)$$

F can be expanded around $x' = y' = z'' = 0$, giving

$$F = F|_0 + x'\left.\frac{\partial F}{\partial x'}\right|_0 + y'\left.\frac{\partial F}{\partial y'}\right|_0 + z''\left.\frac{\partial F}{\partial z''}\right|_0 + \ldots\ldots, \qquad (2.1.17)$$

where $F|_0 \equiv F|_{x'=y'=z''=0}$ etc. Equation (2.1.15) can now be written as

$$\theta(\mathbf{x},\omega) = \frac{-\nu b^2}{4\pi(a^2-b^2)}\frac{dE}{dz}(q\ F|_0 + d_x\left.\frac{\partial F}{\partial x'}\right|_0 + d_y\left.\frac{\partial F}{\partial y'}\right|_0 + d_z\left.\frac{\partial F}{\partial z''}\right|_0 + \ldots\ldots). \qquad (2.1.18)$$

where

$$q = \int f(r,z)d^3x = 1 \qquad (2.1.19)$$

is the "monopole" of the heat source distribution and

$$d_x = \int xf(r,z)d^3x \qquad d_y = \int yf(r,z)d^3x \qquad d_z = \int zf(r,z)d^3x \qquad (2.1.20)$$

are the "dipole" components. According to the symmetry of $f(r,z)$, d_x and d_y are equal to zero. d_z also becomes zero when the origin of $f(r,z)$ is chosen properly. The reason that all the dipole components vanish is due to the fact that $Q(\mathbf{x},t)$

contains only sources and does not contain any "sinks." When quadrapoles and higher poles are ignored, one has

$$\theta(\mathbf{x},\omega) = \frac{-\nu b^2}{4\pi(a^2-b^2)}\frac{dE}{dz}\int F|_0\, dz'. \tag{2.1.21}$$

The integral in the above equation is easily carried out to be

$$\int F|_0\, dz' = i\pi e^{i\omega z/V_m} H_0^2(r\sqrt{b^2-\omega^2/V_m^2}), \tag{2.1.22}$$

where H_0^2 is the Hankel function of the second kind.

For longitudinal waves, the pressure P_n on a surface parallel to the wave front is given by

$$P_n = -\mathbf{n}\cdot\hat{\mathbf{s}}\cdot\mathbf{n} = -(K+\frac{4}{3}\mu)\theta - (\eta+\frac{4}{3}\zeta)\frac{\partial\theta}{\partial t}. \tag{2.1.22}$$

where $\mathbf{n}$ is a unit vector perpendicular to the wave front. This gives

$$P_n(\mathbf{x},\omega) = \frac{\alpha\rho}{4C_p}\frac{dE}{dz}\left(\frac{1+\sigma}{1-\sigma}\right)\frac{\omega e^{i\omega z/V_m} H_0^2(r\sqrt{b^2-\omega^2/V_m^2})}{(1-b^2/a^2)[1-i\omega(\eta+\frac{4}{3}\zeta)/(K+\frac{4}{3}\mu)]}. \tag{2.1.23}$$

One can now make estimations of the effects of the heat conductivity, the finite velocity of the particle and the finite size of the heat source.

The importance of the heat conduction is characterized by the dimensionless number:

$$\left|\frac{b^2}{a^2}\right| \sim \frac{\omega K_H}{V_s^2 C_p}, \tag{2.1.24}$$

where $V_s = \sqrt{(K+\frac{4}{3}\mu)/\rho}$ is the velocity of the sound. For aluminum at 10MHZ, this number is only 1.5×10^{-4}.

The effect of the finite velocity of the particle is given by the dimensionless number:

$$\left|\frac{\omega^2}{V_m^2 b^2}\right| = \frac{V_s^2}{V_m^2}. \tag{2.1.25}$$

For $\beta \sim 10^{-3}$ this number is $\sim 5 \times 10^{-4}$.

As for the effect of the finite size of the heat source, there are reasons[1,6] to believe that the size of the heat source cannot be much larger than 10^{-5}cm. Therefore, ignoring the quadrapoles and higher terms causes only an error of order $(\bar{r}/\lambda)^2 \sim 2 \times 10^{-8}$, where $\bar{r}$ is the size of the heat source and λ is the wavelength.

Letting $V_m \to \infty$, $K_H \to 0$, and ignoring the attenuation effects, Equation (2.1.23) reduces to

$$P_n(\mathbf{x},\omega) = \frac{\alpha\rho}{4C_p}\frac{dE}{dz}\left(\frac{1+\sigma}{1-\sigma}\right)\omega H_0^2(\frac{r\omega}{V_s}). \tag{2.1.26}$$

Letting $\sigma \to \frac{1}{2}$, the above equation becomes exactly twice the Equation (44) in Ref. 3 (note there is a factor of ρ difference in the definition of the specific heat). This is correct, since Equation (44) of Ref. 3 is for a line source from $z = 0$ to $z = \infty$, while our case is a line source from $z = -\infty$ to $z = +\infty$, the signal in our case should be twice as large as in the Ref. 3 case. This verifies that Equation (2.1.26) can be reduced to the correct form for liquid.

Taking the absolute value of Equation (2.1.26) and using the asymptotic expansion of the Hankel function at large distances, one gets

$$|P_n(\mathbf{x},\omega)| \approx \frac{\alpha\rho}{4C_p}\frac{dE}{dz}\left(\frac{1+\sigma}{1-\sigma}\right)\sqrt{\frac{2\omega V_s}{\pi r}}. \tag{2.1.27}$$

Taking the frequency ω and the effective band width $\Delta\omega$ as $\frac{1}{\Delta t}$ of Ref. 5, the signal size $|P_n(\mathbf{x},\omega)|\Delta\omega$ agrees with its equation (39).

In order to calculate the signal-to-noise ratio, one has to determine the noise spectrum. At this moment, I consider only the thermal acoustic noise from the infinite medium seen by the transducer and ignore the noise from the transducer itself and from the electronics. The thermal acoustic noise seen by a spherical transducer imbedded in an infinite medium has been calculated by Akerlof[5]. This has been done by assigning kT energy to each spherical harmonic normal mode in a large sphere and summing up their contributions to the pressure on the transducer. This may seem surpriseing, because the thermal noise has been calculated without putting any energy dissipation into the formalism! We know from the general fluctuation-dissipation theorem[7] that the thermal noise is always associated with energy dissipation, and a lossless system should be in principle noiseless. However, Akerlof's calculation is valid for infinite medium, in which the energy can be assumed to be dissipated at infinity. This, in fact, is completely analogous to the first derivation of the Nyquist law[8], where the voltage fluctuations due to the kT thermal energy of each normal mode of an infinitely long lossless cable, are summed up to calculate the fluctuation at a resistor of equivalent impedance. The second law of thermodynamics guarantees that the fluctuation at the end of an infinite lossless cable with impedance R is exactly equivalent to that of a resistor R.

Bearing this analogy in mined, finding the thermal acoustic noise on a *flat* transducer becomes extremely easy. A flat transducer attached to the surface of an infinite medium is analogous to a voltmeter connected to the end of an infinite cable. Therefore, the force fluctuation felt by the transducer is simply determined by the *mechanical impedance* of the surface it contacts. The mechanical impedance of a surface is defined as the following.

If a surface has such a property that when acted by a force F it acquires a velocity v proportional to the force, namely,

$$v = \frac{F}{Z_m}, \tag{2.1.28}$$

then the surface is said to have mechanical impedance Z_m. Equation (2.1.28) is analogous to

$$I = \frac{V}{R} \tag{2.1.29}$$

of an electric circuit. Such analogy can be used to discuss the energy dissipation and the noise because the power transfer in both cases is given by the analogous forms

$$W = VI \qquad \text{and} \qquad W = Fv\ . \tag{2.1.30}$$

The mechanical impedance of a surface depends on its shape and is generally a function of frequency. However, for a flat surface whose size is much larger than the wavelength, the mechanical impedance is independent of the frequency and is simply given by

$$Z_m = A\rho V_s, \tag{2.1.31}$$

where A is the area of the surface in contact with the transducer. By the analogy with an electric circuit, the rms of the force fluctuation at the transducer is $\sqrt{4kTZ_m\Delta f}$ and the *power spectral density* is[9]

$$\Phi(\omega) = 2kTZ_m = 2kTA\rho V_s. \tag{2.1.32}$$

Equation (2.1.27) is not valid for very large ω, not only because the attenuation is not negligible at high frequencies but also because the multipole expansion (2.1.18) is no longer valid when the acoustic wave length is comparable to the size of the heat source. Since the detection of very high frequency acoustic waves is not practical anyway, I assume that the transducer and electronics can handle signals only up to a cutoff frequency ω_c ($2\pi \times 10$MHZ say), and the effective signal spectrum is given by Equation (2.1.27) up to ω_c and equal to 0 for $|\omega| > \omega_c$.

The maximum signal-to-noise ratio that can be achieved by using an optimal filter is given by[9]

$$\frac{S}{N} = \int_{-\infty}^{\infty} \frac{|S(\omega)|^2}{\Phi(\omega)} \frac{d\omega}{2\pi}, \tag{2.1.33}$$

where $S(\omega)$ is the Fourier transform of the signal and $\Phi(\omega)$ is the noise spectrum; in the case here, $\Phi(\omega)$ is given by Equation (2.1.32). This gives

$$\frac{S}{N} = \int_{-\omega_c}^{+\omega_c} \frac{|AP_n(\mathbf{x},\omega)|^2}{\Phi(\omega)} \frac{d\omega}{2\pi} = \frac{Af_c^2\alpha^2}{8kT\rho r C_m^2} \left(\frac{1+\sigma}{1-\sigma}\right)^2 \left(\frac{dE}{dz}\right)^2, \tag{2.1.34}$$

where $f_c = \omega_c/2\pi$.

One may notice that the above equation agrees with equation (45) of Ref. 5 only when $A \sim \lambda^2$, where λ is the acoustic wave length. This is expected, because the size of a spherical transducer must be roughly equal to half a wavelength for

efficient acoustic detection, while a flat transducer can have a much larger area as long as its thickness is about half of the wave length.

For an aluminum medium at room temperature, with $A = 1\text{cm}^2$, $r = 100\text{cm}$ and $f_c = 10\text{MHZ}$, one gets

$$\frac{S}{N} \sim 9 \times 10^{-5} \left(\frac{dE/dx}{1\text{GeV/cm}} \right)^2 . \tag{2.1.35}$$

According to the noise level observed on the Caltech prototype, the actual S/N may be more than one order of magnitude lower than this ideal value[10].

According to Equation (2.1.35) and the dE/dx calculated in Chapter 1, it is obvious that the acoustic detection of most SIMPs in an infinite medium is simply hopeless, except for some highly ionizing nuclearites.

2.2. Is the Thermal Noise Limit "Intrinsic"?

Except for highly ionizing nuclearites, the expected acoustic signal from most of the SIMPs is much smaller than the thermal noise in infinite medium, and there is not much room left for improvements. Reducing temperature does not help much because even at 3°K, the S/N is still 9×10^{-3} for $dE/dx \sim 1\text{GeV/cm}$. One may increase the area A to enhance the signal-to-noise ratio, but this comes with a penalty, that the angular response of the transducer becomes so narrow (order of λ/D where D is the diameter of the transducer) that the solid angle acceptance for particle detection is severely limited. It is interesting to note that even if A is taken as the total vertical surface area of a cylinder 1m long and 1m in radius around the particle track, the S/N is still only an order of unity.

This agrees with the argument of Akerlof[11], that even if one can collect a large portion of the total acoustic energy, the maximum possible signal-to-noise ratio is only an order of unity. However, it should be kept in mind that the above discussions, as well as the calculations in Ref. 5, are only valid for the method of detection in infinite medium; it may not be applied to other cases, especially the case of an almost lossless finite detector.

Akerlof has gone too far to generalize the above limit[11]. He regards it as "intrinsic," meaning that no technical improvements are possible to give enough signal-to-noise ratio. It is "categorically infeasibe" at room temperature, even "a slightly greater hope" at low temperature has to be given up and "future work in this area seems pointless." All these conclusions were drawn for magnetic monopoles, but since the only property used in the discussion was its dE/dx, the conclusions should apply to any SIMP with $dE/dx \sim 1$ GeV/cm.

To prove something to be so "intrinsic," one should make some general statements without any assumption of the special properties of certain cases. Akerlof's argument certainly looks like this. His major point can be summarized as the following. The total acoustic energy E_a below 10MHZ produced by a particle of $dE/dx \sim 1$GeV is the same order of magnitude of kT, and $E_a/\frac{1}{2}kT$ is the maximum signal-to-noise ratio one can possibly get by using a matched filter. A practical device can extract only a very small portion of the total acoustic energy E_a (in order to extract a good portion of E_a, $2000^2 = 4 \times 10^6$ transducers are needed); thus, acoustic detection of particles is practically impossible. This

seemingly strong argument contains a major flaw: that is, the simple relation $S/N \sim E/kT$ is valid only for very special cases and is not at all universal and "intrinsic." In fact, Akerlof has already noticed an exception to this criterion; that is, in a high Q device, signal-to-noise ratio can be increased by a factor of Q since "signal can be coherently added over many cycles." However, he finally gave up the hope for such devices by saying that an effective temperature of a few microdegrees has to be reached to detect the acoustic signal. It will be shown in the next section that Akerlof's estimate of the capability of such devices is too pessimistic, but in this section, I will concentrate on the seemingly universal criterion:

$$\frac{S}{N} \sim \frac{E}{kT}. \tag{2.2.1}$$

Whether or not energy below kT is detectable has been argued at the very early stage of the development of gravitational wave antennae and the answer is definitely positive[12]. In fact, energy below kT is not only measured in gravitational wave antennae but is detected every minute in life. The fact that an amplifier can have a noise temperature lower than its physical temperature clearly means that energy below kT is detectable. A SQUID (Superconducting Quantum Interference Device) having a noise temperature of 10^{-6}°K when operating at 4°K is a device capable of measuring energy of $10^{-6}kT$. A theory that the threshold of hearing is quantum limit instead of the much higher thermal noise limit[13] implies that if energy below kT were not detectable, human hearing would be impossible.

In most of the above cases, instead of Equation (2.2.1), the optimal signal to noise ratio is given by

$$\frac{S}{N} \sim \frac{E}{kT}\frac{\tau^*}{\tau}, \tag{2.2.2}$$

where τ^* is the "relaxation time" of the system, the time scale the system approaches equilibrium once disturbed, and τ is the "signal acting time," the time during which the signal energy E is deposited and other changes necessary for signal detection are induced.

Equation (2.2.2) tells us that a signal with energy much smaller than kT can be detectable if the relaxation time of the system is much larger than the signal acting time. Although the sensitivity of a high Q device can be explained as "signal coherently added over many cycles," the fundamental reason is $Q = \frac{\tau^*\omega}{2}$.

The important role of the relaxation time τ^* of the system can be easily understood by the following discussion. Suppose a system of one degree of freedom is in equilibrium with a heat bath at temperature T and has a random motion energy of order of kT. Because of the friction or damping, the energy of the motion is dissipated into the heat bath with a characteristic time τ^* and the heat bath is putting it back randomly with the same characteristic time. This is what "equilibrium" means. The motion of the system thus randomly changes with a characteristic amplitude corresponding to kT energy in a characteristic time scale τ^*. Since the change in the amplitude of the motion is a random walk, the expected energy change of the system in a short time $\tau \ll \tau^*$ is only $kT\tau/\tau^*$. Therefore, when a signal deposits energy ΔE considerably larger than $kT\tau/\tau^*$

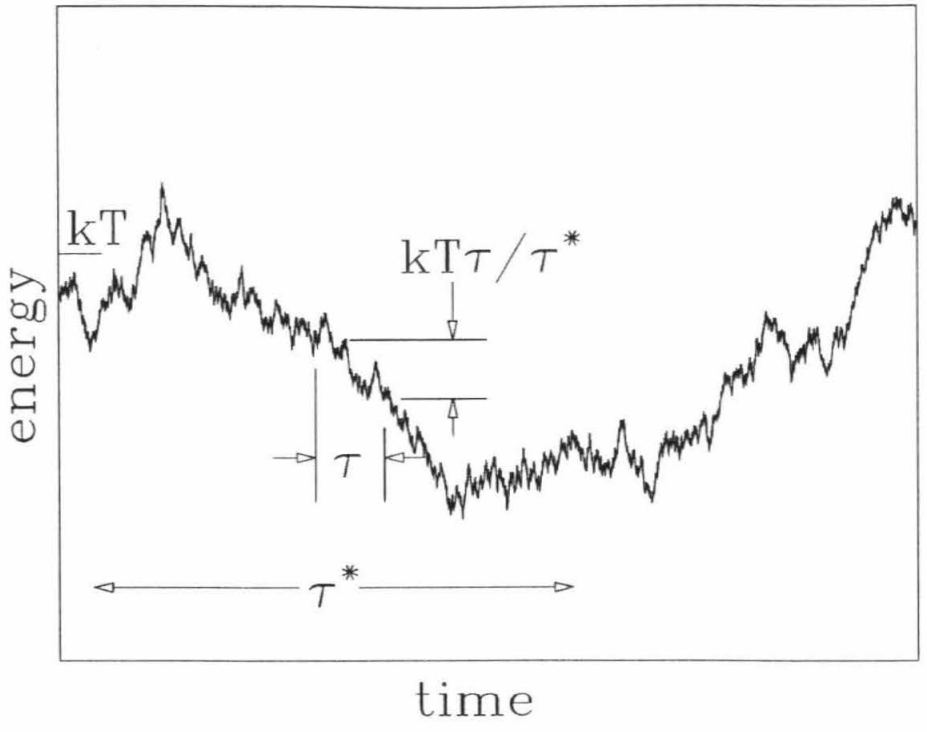

Fig. 2.2.1 — The energy fluctuation in a short time $\tau \ll \tau^*$ is much smaller than kT.

in time τ, this energy change is totally unexpected and can be recognized as a signal (see Fig. 2.2.1). It is not the *absolute value* of the thermal motion but its *unpredictable changes* that produce unavoidable noise. For many systems, the relaxation time is a measure of the energy dissipation. In principle, the only truly unavoidable noise is the generalized Nyquist noise associated with the energy dissipation[7]. Reducing energy dissipation, one reduces noise. A lossless system is noiseless. Equation (2.2.1) may be useful in many cases with $\tau > \tau^*$, but when applied to the case of $\tau \ll \tau^*$, it is wrong by a factor of $\frac{\tau^*}{\tau}$.

When energy dissipation is minimized, it is no longer correct to say that a practical device can extract only a very small portion of the total energy. Suppose the whole detector block is made almost lossless up to 10MHZ except at

one single transducer. The transducer has a reasonable bandwidth up to 10MHZ and can convert the acoustic energy into electric energy. Since the detector block is lossless, all the acoustic energy below 10MHZ, after bouncing around several times, will wind up being absorbed only at the transducer. In this way, a large portion of the total acoustic energy below 10MHZ can be collected by using only one transducer. $2000^2 = 4 \times 10^6$ transducers are not necessary. This idea has been vaguely expressed as the "focusing technique" in Ref. 10. It is now more clearly and correctly stated here.

As clearly shown above, "lossless" is the key word to reduce noise and enhance signal. Making a system lossless is a technical problem rather than a matter of principle; thus, no limit based on energy dissipation can be called "intrinsic." If the energy dissipation of the detector can be reduced without limit, then, in the regime of classical physics, the noise can be reduced without limit. In quantum mechanics, however, R. P. Giffard has shown that an ultimate limit imposed by the uncertainty principle cannot be avoided by any *linear* detector[14]. If one is not restricted to linear detectors, then various quantum nondemolition methods are possible to surpass the linear detector limit. A "back-action-evading" method has been proposed by C. Caves, K. Thorne R. Drever, *et al.* which, in principle, can make arbitrarily quick and accurate measurements of weak classical forces[15]. So far as the principle is concerned, there is no ultimate limit that applies, regardless of the measuring technique. Various limits exist only for certain measuring techniques.

2.3. Finite Detectors

Since there is no general "intrinsic" limit for measuring small forces, technical improvements to achieve enough signal-to-noise ratio for acoustic particle detection are always possible in principle.

It has been shown in the last section that the formidable noise in the infinite medium stems from the fact that the energy dissipation at infinity cannot be avoided; therefore, one obvious technical improvement is to make the detector finite and minimize energy dissipation. Acoustic particle detection going from the infinite ocean (DUMAND) to the finite Caltech prototype[1] is obviously on the right track, although its energy dissipation is not low enough, and geometry not ideal for achieving high sensitivity.

Resonant bar gravitational wave detectors having extremely low energy dissipation and simple geometry are ideal examples of finite detectors. The interaction of such a bar with a traversing particle has been studied by A. M. Allega and N. Cabibbo[16]. For the convenience of discussing energy dissipation and noise, I present a somewhat different approach here.

For a finite detector, Equation (2.1.6) can be formally solved by decomposing it into normal modes:

$$\mathbf{u} = \sum_n \mathbf{u}_n(\mathbf{x}) B_n(t). \tag{2.3.1}$$

The normal modes satisfy the equation:

$$-\rho\omega_n^2 \mathbf{u}_n = (K + \frac{\mu}{3})\nabla(\nabla \cdot \mathbf{u}_n) + \mu\nabla^2 \mathbf{u}_n \tag{2.3.2}$$

and are normalized as

$$\int (\mathbf{u}_n \cdot \mathbf{u}_m) d^3x = V\delta_{nm}, \tag{2.3.3}$$

where V is the volume of the detector.

With Equations (2.3.1), (2.3.2) and (2.3.3), the equation of motion (2.1.6) becomes:

$$M\ddot{B}_n + M\omega_n^2 B_n + \sum_k H_{nk}\dot{B}_k = F_n(t), \tag{2.3.4}$$

where $M = \rho V$ is the total mass of the detector,

$$F_n(t) = 3\alpha K \int T(\mathbf{x}, t)(\nabla \cdot \mathbf{u}_n) d^3x \tag{2.3.5}$$

and

$$H_{nk} = -\int [(\eta + \frac{\zeta}{3})\mathbf{u}_n \cdot \nabla(\nabla \cdot \mathbf{u}_k) + \zeta \mathbf{u}_n \cdot \nabla^2 \mathbf{u}_k] d^3x \tag{2.3.6}$$

It is easy to show that $H_{nk} = H_{kn}$. H_{nk}'s characterize the energy dissipation and the interactions between normal modes. For a complete treatment, Equation (2.3.6) should include terms that result from other sources of dissipation, such as damping at the surface and the friction caused by the supporting structure, etc.

Since the thickness of the particle track is much smaller than the wave length of most of the normal modes, and since the particle crossing time is much shorter than their periods, Equation (2.3.5) can be written as a line integral along the particle track and the time dependence can be regarded as a step function. Thus,

$$F_n(t) = \theta(t) F_n^0, \tag{2.3.7}$$

where $\theta(t)$ is the step function ($= 1$ for $t \geq 0$ and $= 0$ for $t < 0$) and

$$F_n^0 = \frac{3\alpha K}{C_p}\left(\frac{dE}{dx}\right)\int \nabla \cdot \mathbf{u}_n dl. \tag{2.3.8}$$

Equation (2.3.4) shows that the motion of the finite detector is equivalent to a series of mechanical oscillators; each is driven by a force $F_n(t)$ and is coupled to other modes through H_{nk}. If one considers only the normal modes decomposing as a mathematical way to solve Equation (2.1.6), the masses of the oscillators can be chosen arbitrarily. However, when the noise and the energy dissipation are under consideration, the mass of each oscillator must be chosen properly so that its energy is exactly equal to the energy associated with the corresponding normal mode. The choice $M = \rho V$ is correct since the kinetic energy of nth normal mode is given by

$$\mathrm{KE} = \frac{\rho}{2}\int |\dot{B}_n \mathbf{u_n}|^2 d^3x = \frac{\rho V}{2}\dot{B}_n^2 = \frac{M}{2}\dot{B}_n^2. \tag{2.3.9}$$

Because of the H_{nk} coupling, finding the exact solution of Equation (2.3.4) is extremely difficult. However, if one is only interested in those very weakly damped normal modes, H_{nk} can be ignored to obtain a solution that is valid for a time much shorter than the damping time. This gives

$$B_n(t) = B_n^0(t) + \theta(t)\frac{F_n^0}{M\omega_n^2}(1 - \cos\omega_n t), \tag{2.3.10}$$

where $B_n^0(t)$ is the solution without the signal (due to fluctuations).

When one considers the noise, H_{nk} can no longer be ignored, because they are the very source of the thermal noise. Taking Fourier transformation of Equation (2.3.4) one gets

$$\sum_k [M(\omega_n^2 - \omega^2)\delta_{nk} - i\omega H_{nk}]B_k(\omega) = F_n(\omega). \tag{2.3.11}$$

If the non-diagonal elements (interaction between normal modes) of the matrix $[M(\omega_n^2 - \omega^2)\delta_{nk} - i\omega H_{nk}]$ are treated as small perturbations, the above expression can be reversed as

$$B_n(\omega) = \sum_k \alpha_{nk}(\omega)F_k(\omega), \tag{2.3.12}$$

where

$$\begin{aligned}\alpha_{nk}(\omega) = &\frac{\delta_{nk}}{M(\omega_n^2 - \omega^2) - i\omega H_{nn}} + \\ &+ \frac{i\omega H_{nk}(1 - \delta_{nk})}{[M(\omega_n^2 - \omega^2) - i\omega H_{nn}][M(\omega_k^2 - \omega^2) - i\omega H_{kk}]} + O(H_{nk}^2)\end{aligned} \tag{2.3.13}$$

is the "generalized susceptibility." According to the generalized fluctuation-dissipation theorem, the fluctuation spectrum is given by[17]

$$\langle B_n^0 B_k^0\rangle_\omega \equiv \int_{-\infty}^{+\infty} \langle B_n^0(t+\tau)B_k^0(t)\rangle e^{i\omega t}dt = \hbar \mathrm{Im}(\alpha_{nk})\coth(\frac{\hbar\omega}{2kT}) \tag{2.3.14}$$

For $k \neq n$, the above equation gives the correlation between the fluctuations of different normal modes and may be useful for the consideration of making coincidence of two or more normal modes to enhance the noise rejection. For $k = n$, Equation (2.3.14) gives the noise spectrum of nth normal mode:

$$\langle (B_n^0)^2\rangle_\omega = \frac{\omega H_{nn}}{M^2(\omega_n^2 - \omega^2)^2 + \omega^2 H_{nn}^2}\hbar\coth\frac{\hbar\omega}{2kT} \approx \frac{2kTH_{nn}}{M^2(\omega_n^2 - \omega^2)^2 + \omega^2 H_{nn}}. \tag{2.3.15}$$

The above discussions apply to any finite detector with small energy dissipation. To be specific, I will consider a resonant bar of length L and radius R. The exact solution of normal modes for such a bar has been found[18], but unfortunately it cannot be put into finite analytical form. However, if $R \ll L$, good analytical approximations exist. For axial symmetric modes, I take[19]

$$\begin{aligned} u_n^r(r,z) &= A_n \sigma n\pi \frac{r}{L}\sin(\frac{n\pi z}{L}) + O((R/L)^3) \\ u_n^z(r,z) &= A_n[1 - \frac{\sigma}{2}(\frac{n\pi r}{L})^2]\cos(\frac{n\pi z}{L}) + O((R/L)^4) \end{aligned} . \tag{2.3.16}$$

This gives, for the leading order,

$$F_n^0 = -\lambda n \frac{E}{L}\sin[\frac{n\pi(z_1+z_2)}{2L}], \tag{2.3.17}$$

where $\lambda = \sqrt{2}\pi\alpha Y/C_p$ is a dimensionless number of order of 1, E is the total energy deposited in the bar by the particle, z_1 is the z-coordinate of the particle entry point and z_2 is its exit point.

One way to detect the signal is to measure the sudden change in the oscillation amplitude of a certain normal mode. For a particle going through the center of an aluminum bar at right angle, the amplitude change of the first normal mode is

$$B_{\mathbf{sig}} = \frac{-F_1^0}{M\omega_1^2} = 4.5 \times 10^{-17}\mathrm{cm}\left(\frac{10\mathrm{cm}}{R}\right)\left(\frac{dE/dx}{1\mathrm{GeV/cm}}\right). \tag{2.3.18}$$

This signal is very small indeed compared with the rms of the thermal motion amplitude:

$$\sqrt{\langle (B_1^0)^2\rangle} = \sqrt{\frac{kT}{M\omega_1^2}} = 4.4 \times 10^{-14}\mathrm{cm}\left(\frac{L}{1\mathrm{m}}\right)^{\frac{1}{2}}\left(\frac{10\mathrm{cm}}{R}\right)\left(\frac{T}{300^\circ\mathrm{K}}\right)^{\frac{1}{2}}. \tag{2.3.19}$$

However, since the signal is detected by monitoring the *change* of the oscillation amplitude, the true noise of the measurement is not the absolute amplitude of the thermal motion but its *unpredictable changes* during the signal acting time. The mean-square change of the thermal motion in a time τ is

$$\langle(\Delta B_1^0)^2\rangle \;=\; \langle(B_1^0(t+\tau)-B_1^0(t))^2\rangle \;=\; 2\langle(B_1^0)^2\rangle - 2\langle B_1^0(t+\tau)B_1^0(t)\rangle. \quad (2.3.20)$$

The autocorrelation function $\langle B_1^0(t+\tau)B_1^0(t)\rangle$ is the inverse Fourier transform of the noise spectral density given by Equation (2.3.15) and the result is, when certain non-critical small numbers are ignored:

$$\langle B_1^0(t+\tau)B_1^0(t)\rangle \;\approx\; \langle(B_1^0)^2\rangle e^{-|\tau|/\tau_1^{\rm m}}\cos\omega_1\tau, \quad (2.3.21)$$

where $\tau_n^{\rm m} = \dfrac{2M}{H_n}$ is the relaxation time of nth normal mode.

A convenient way to measure the amplitude change is to compare the amplitude at one time with the amplitude one or more cycles earlier. In such a case, τ is the multiple of the oscillation period and

$$\langle(\Delta B_1^0)^2\rangle \;\approx\; 2\langle(B_1^0)^2\rangle\frac{\tau}{\tau_1^{\rm m}} \quad (2.3.22)$$

for $\tau \ll \tau_1^{\rm m}$. The signal-to-noise ratio is then given by

$$\frac{S}{N} \sim \frac{B_{\rm sig}^2}{\langle(B_1^0)^2\rangle}\frac{\tau_1^{\rm m}}{2\tau}. \quad (2.3.23)$$

It can be much larger than $\dfrac{B_{\rm sig}^2}{\langle(B_1^0)^2\rangle} \sim \dfrac{E_{\rm sig}}{kT}$ if $\tau_1^{\rm m}$ is sufficiently larger than τ.

The above calculations have shown explicitly how energy below kT can be detected. The autocorrelation function of the noise has played a central role here.

Because of the strong correlation between the noise amplitudes at one time and a short time earlier, one can fairly accurately predict its behavior in a short time interval. Although predicting the oscillation amplitude without any knowledge of the system generally has uncertainty corresponding to kT energy, knowing the amplitude at one moment and predicting it a short time later can be done much more accurately. When the signal is detected by comparing the measured amplitude with the one predicted according to the autocorrelation function of the thermal motion, the true noise of the detection is not the actual value to be predicted but the *uncertainty* of this prediction, which can be many orders of magnitude smaller.

To get some actual numbers, I chose $\tau = \dfrac{2\pi}{\omega_1}$ and obtain

$$\frac{S}{N} \sim 1.7 \times 10^{-7} Q_1 \left(\frac{300^\circ\mathrm{K}}{T}\right)\left(\frac{1\mathrm{m}}{L}\right)\left(\frac{dE/dx}{1\mathrm{GeV/cm}}\right)^2, \qquad (2.3.24)$$

where $Q_1 = \dfrac{\tau_1^{\mathrm{m}}\omega_1}{2}$ is the quality factor of the first normal mode.

It is not very hard to have enough signal-to-noise ratio at low temperature. For example, at $T = 4^\circ$K, it requires only $Q_1 > 10^5$, while $Q_1 \sim 10^6$ is easy to achieve[20]. At room temperature, it requires $Q_1 > 10^7$. This may be difficult for a aluminum bar, but for a single crystal bar, $Q_1 \sim 10^8$ has been achieved[21].

Equation (2.3.24) shows a great improvement on the signal-to-noise ratio over the case of infinite medium. Note that in both cases, the noise of the devices used to pick up the signal has been ignored. In reality, the noise of such sensing devices can be very serious. It has been observed on the Caltech prototype that the preamplifier was the major noise source.

In order to evaluate the effect of the noise of the sensing devices, I assume that they have an effective displacement noise proportional to the square root of the bandwidth, and the bandwidth is roughly $\Delta\omega \sim \frac{1}{\tau}$, in order to measure the amplitude changes in a time τ. Thus, the total noise is

$$\langle B^2_{\rm noise}\rangle \sim \langle (B^0_1)^2\rangle \frac{2\tau}{\tau_1^{\rm m}} + \frac{D^2}{2\pi\tau}, \tag{2.3.25}$$

where D^2 is the mean-square noise per HZ of the sensing device.

It is obvious, when

$$\tau = \sqrt{\frac{D^2\tau_1^{\rm m}}{4\pi\langle (B^0_1)^2\rangle}}, \tag{2.3.26}$$

the noise gets its minimum:

$$\langle B^2_{\rm noise}\rangle_{\rm min} \sim 2\sqrt{\frac{D^2\langle (B^0_1)^2\rangle}{\pi\tau_1^{\rm m}}}. \tag{2.3.27}$$

This gives

$$\frac{S}{N} \sim 4.5\times 10^{-3}\left(\frac{1{\rm m}}{L}\right)^{\frac{1}{2}}\left(\frac{10{\rm cm}}{R}\right)\left(\frac{300^\circ{\rm K}}{T}\right)^{\frac{1}{2}}\left(\frac{Q_1}{10^8}\right)^{\frac{1}{2}}\left(\frac{10^{-15}{\rm cm}/\sqrt{\rm HZ}}{D}\right) \times\left(\frac{dE/dx}{1{\rm GeV/cm}}\right)^2 \tag{2.3.28}$$

At room temperature, even with $Q_1 \sim 10^8$ of a single crystal and $D \sim 10^{-15}$cm of an active cavity laser sensor[22], it is still three orders of magnitude away from detecting SIMPs with $\frac{dE}{dx} \sim 1$GeV/cm. However, there is nothing "intrinsic" and "categorical" here. It has been pointed out in Ref. 22 that the sensitivity of the active cavity laser sensor can be improved by three orders of magnitude if better materials and mirrors are used. If this can be achieved, then a marginal signal-to-noise ratio may be obtained at room temperature.

At low temperature, achieving enough signal-to-noise ratio should not be very hard. To see how well today's gravitational wave detectors are doing in practice, one may evaluate the signal in terms of the "temperature rise" of the normal modes. For a gravitational wave detector of $\sim$ 5000kg (L = 3m), the "temperature rise" in the first normal mode caused by a SIMP is

$$\delta T = \frac{M\omega_1^2}{2k} B_{\rm sig}^2 = 5.3 \times 10^{-5\circ}{\rm K} \left(\frac{dE/dx}{1{\rm GeV/cm}} \right)^2 . \qquad (2.3.29)$$

There is no major difficulty in obtaining an effective noise temperature of 1m°K in today's gravitational wave detectors of $\sim$ 5000kg, and this is not too far away for detecting $dE/dx \sim$ 1GeV/cm particles. It can be seen from Equation (2.3.28) that the S/N is inversely proportional to $\sqrt{M}$. Noting that Q-factors can be increased considerably in a small bar and cooling it off is much easier, a sizable signal to noise ratio should not be hard to achieve in a small bar of, say $\sim$ 5kg. In the above, only the information of the first normal mode has been used. Using the information contained in other normal modes may enhance the signal-to-noise ratio considerably. Therefore, in contrast to the previous belief that acoustic detection of SIMPs are "intrinsically" prohibited by the thermal noise, the techniques for today's gravitational wave detectors are already able to make a detector sensitive to $dE/dx \sim$ 1GeV/cm, although the goal of low cost can not be realized yet.

For the nuclearites of $\beta = 10^{-3}$, Equation (2.3.29) gives $\delta T \sim 13°$K. Detecting such a signal is very easy in low temperature gravitational wave detectors and can even be done at room temperature. It seems worthwhile to search for

nuclearites in the existing data of the gravitational wave detectors. In the published result of the Stanford gravitational wave search[23], 40 events above 0.25°K were rejected as gravitational waves because the second normal mode was also excited. This, however, happens to be a signature of nuclearites, so the 40 events may be the candidates of nuclearites. If these events can be rejected as nuclearites by looking at the phase and amplitude correlations between the first and second normal modes, then a flux limit of $F < 2 \times 10^{-12}\text{cm}^{-2}\text{s}^{-1}\text{sr}^{-1}$ (90% c.l.) can be set for $\beta > 3.7 \times 10^{-4}$ (corresponding to the 0.25°K cut). Even if the 40 events are not rejected, one still gets a limit of $F < 4.4 \times 10^{-11}\text{cm}^{-2}\text{s}^{-1}\text{sr}^{-1}$ which is only slightly higher than the limit of a scintillator search[24] performed three years later.

2.4. Measuring the Thermal Expansion of the Bar

It can be seen from Equation (2.3.10) that a crossing SIMP not only changes the oscillation amplitude of each oscillator, but also produces a sudden shift $\frac{F_n^0}{M\omega_n^2}$ in its equilibrium position. The origin of this equilibrium position shift is easy to understand. When the particle track is suddenly heated, it produces stress in the bar and suddenly changes its *equilibrium length.* Just because the actual length of the bar cannot follow this change so quickly, oscillation is induced. Although the new equilibrium length cannot actually be reached until the oscillation ceases, it can be easily and quickly detected by taking the average over several periods of the normal mode oscillations.

A displacement of the oscillator B_n corresponds to a stretch $B_n[u_n^z(L) - u_n^z(0)]$ of the bar. Adding up the contributions of all the normal modes and reducing the infinite sum to finite form by the Fourier series of certain functions, one obtains the net stretch of the equilibrium length of the bar immediately after the particle goes through:

$$l \equiv \Delta L = \sum_{n=1}^{\infty} \frac{F_n^0}{M\omega_n^2}[u_n^z(L) - u_n^z(0)] = \frac{\alpha E L}{V C_p} \qquad (2.4.1)$$

This is exactly equal to the thermal expansion of the bar after energy E is uniformly deposited. One now reaches a conclusion that the change in the *the equilibrium length* of the bar due to the thermal expansion of the heated particle track is exactly the same as if the heat is uniformly distributed in the whole volume of the bar (Fig. 2.4.1). One may worry that this conclusion may be approximate because of the use of the approximate expressions of the normal modes, but the following theorem ensures that the conclusion is exactly correct.

The theorem states that *when a certain amount of heat energy is deposited into a free bar with a uniform cross section, the change in its average equilibrium length depends only on the total heat energy deposited and is independent of its distribution inside the bar.* The following is the proof of the theorem.

The change in the average length of the bar is

$$l = \frac{1}{A}\int dxdy[u_z(x,y,L) - u_z(x,y,0)] = \frac{1}{A}\int e_{zz} d^3x, \qquad (2.4.2)$$

where A is the area of the cross section and $e_{zz} = \dfrac{\partial u_z}{\partial z}$. Taking the integral of Equation (2.1.5) and noting that $\int s_{ij} d^3x = 0$ for a free bar in *equilibrium*, one

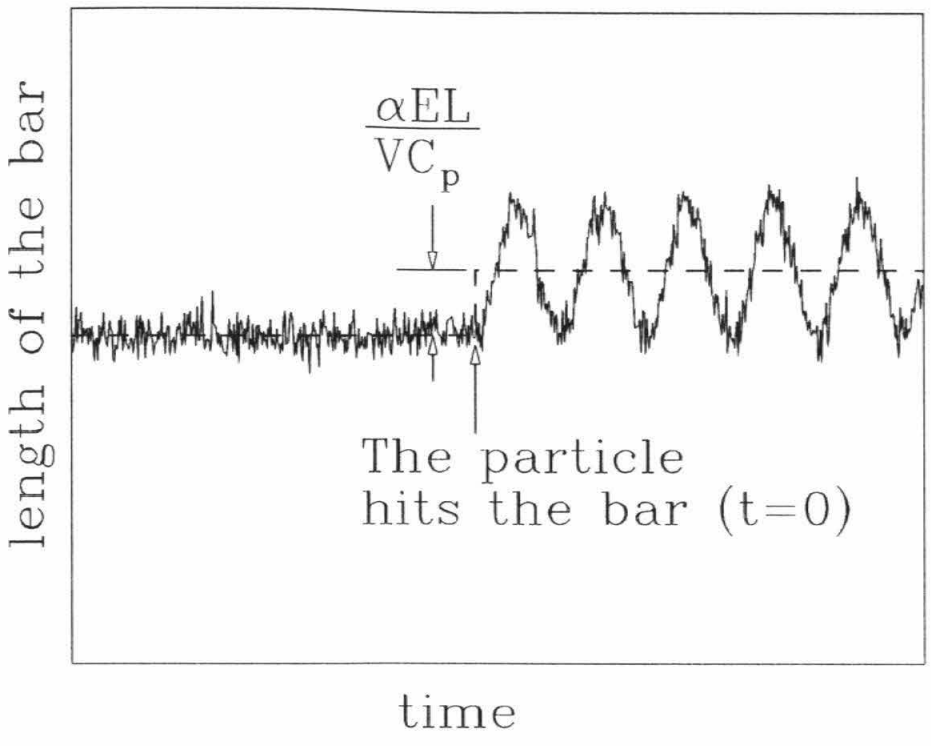

Fig. 2.4.1 — The change in the *equilibrium length* of the bar produced by a crossing particle is $\frac{\alpha EL}{VC_p}$. It is exactly equal to the thermal expansion of the bar, assuming the energy E is uniformly distributed in the whole volume.

gets

$$\int e_{zz} d^3x = \alpha \int T(\mathbf{x}) d^3x = \frac{\alpha E}{C_p}. \tag{2.4.3}$$

Equations (2.4.2) and (2.4.3) give exactly the same l as Equation (2.4.1) without any assumption about the distribution of $T(\mathbf{x})$.

According to the theorem, the thermal expansion of the bar, when interpreted as the change in its *average equilibrium length*, is only a function of the total energy deposited and is independent of its distribution inside the bar. Since the ionization energy is deposited promptly, the thermal expansion is a very quick process. It rises up almost like a step function as soon as the particle goes through and stays the same as long as the heat energy is still inside the bar. By taking

the average of the actual length of the bar over several cycles of the normal mode oscillations, the change of such *average equilibrium length* can be detected. The signal acting time of the thermal expansion is thus only a few times the fundamental period and is much shorter than the time for the heat to disperse into the whole volume of the bar.

The above theorem is also useful for noise considerations. It ensures that the fluctuation of the average length of the bar depends only on the fluctuation of the *total* thermal energy inside the bar, while the energy redistribution between different parts of the bar is irrelevant. The fluctuation of the total energy is[25]

$$\langle E_{\rm fl}^2 \rangle = kT^2 V C_p; \tag{2.4.4}$$

this gives the random thermal expansion:

$$\langle l_{\rm fl}^2 \rangle = \left(\frac{\alpha L}{V C_p} \right)^2 \langle E_{\rm fl}^2 \rangle = \frac{L \alpha^2 k T^2}{\pi R^2 C_p}. \tag{2.4.5}$$

For an aluminum bar,

$$\frac{l^2}{\langle l_{\rm fl}^2 \rangle} = 1.1 \times 10^{-4} \left(\frac{1\text{m}}{L} \right) \left(\frac{300^\circ\text{K}}{T} \right)^2 \left(\frac{dE/dx}{1\text{GeV/cm}} \right)^2. \tag{2.4.6}$$

Although the ratio of the signal amplitude to the noise amplitude is very small, the S/N can be much larger than this ratio if the relaxation time of the system is much larger than the signal acting time. The relaxation time here is actually the time for the bar to cool down, once it is heated. Indeed, it can be made extremely long, from several hours to several days (think about a thermos). In a reasonable vacuum, the energy exchange between the bar and the

environment is mainly through blackbody radiation. In this case, the relaxation time is given by

$$\tau_{\rm h} = \frac{VC_p}{4\sigma_{\rm b} ST^3}, \tag{2.4.7}$$

where $\sigma_{\rm b}$ is Stephen-Boltzman constant and S is the total surface area of the bar. For the example of an $L = 1$m, $R = 10$cm aluminum bar at room temperature, this gives $\tau_{\rm h} = 1.8 \times 10^4$sec if it is a blackbody. A polished metal surface can have reflectivity of 99% at the wave length of the black body radiation at room temperature. Thus, $\tau_{\rm h} \sim 1.8 \times 10^6$sec $= 500$hours can be achieved.

For quantitative discussions, one may write down the differential equation for the total energy of the bar:

$$\frac{dE_{\rm fl}}{dt} + \frac{E_{\rm fl}}{\tau_{\rm h}} = J_{\rm fl}(t), \tag{2.4.8}$$

where $J_{\rm fl}(t)$ is the power flow into the bar due to fluctuation. According to Equation (2.4.8), the power spectral density of $E_{\rm fl}$ is given by[9]

$$\langle E_{\rm fl}^2 \rangle_\omega = \frac{\langle J_{\rm fl}^2 \rangle_\omega}{|i\omega + 1/\tau_{\rm h}|^2}, \tag{2.4.9}$$

where $\langle J_{\rm fl}^2 \rangle_\omega$ is the power spectral density of $J_{\rm fl}$. Since $J_{\rm fl}(t)$ is mainly due to the uncorrelated bombardments of thermal photons and gas molecules, it should have a "white" spectrum and $\langle J_{\rm fl}^2 \rangle_\omega$ is basically a constant. The autocorrelation function of $E_{\rm fl}$ is then found by the inverse Fourier transformation of Equation (2.4.9), resulting in

$$\langle E_{\rm fl}(t+\tau) E_{\rm fl}(t) \rangle \;=\; kT^2 VC_p e^{-|\tau|/\tau_{\rm h}}. \tag{2.4.10}$$

This gives

$$\langle l_{\rm fl}(t+\tau) l_{\rm fl}(t)\rangle \;=\; \langle l_{\rm fl}^2\rangle e^{-|\tau|/\tau_{\rm h}}. \tag{2.4.11}$$

Similar to the case of measuring the change of the normal mode oscillations, if the *change* in the equilibrium length of the bar in a short time τ is measured, the noise is a factor of $\frac{\tau_{\rm h}}{2\tau}$ smaller than the random thermal expansion given by Equation (2.4.5).

When the noise of the sensing device is added, the total noise is similar to Equation (2.3.25):

$$\langle l_{\rm noise}^2\rangle \;\sim\; \langle l_{\rm fl}^2\rangle \frac{2\tau}{\tau_{\rm h}} + \frac{D^2}{2\pi\tau}. \tag{2.4.12}$$

For optimal τ,

$$\langle l_{\rm noise}^2\rangle_{\rm min} \;\sim\; 2\sqrt{\frac{D^2\langle l_{\rm fl}^2\rangle}{\pi\tau_{\rm h}}}. \tag{2.4.13}$$

This gives the signal-to-noise ratio:

$$\frac{S}{N} \sim 0.93 \left(\frac{1{\rm m}}{L}\right)^{\frac{1}{2}} \left(\frac{10{\rm cm}}{R}\right) \left(\frac{\tau_{\rm h}}{10^6{\rm sec}}\right)^{\frac{1}{2}} \left(\frac{300^\circ{\rm K}}{T}\right) \left(\frac{10^{-15}{\rm cm}/\sqrt{\rm HZ}}{D}\right) \times \left(\frac{dE/dx}{1{\rm GeV/cm}}\right)^2 \tag{2.4.14}$$

Comparing the above equation with Equation (2.3.28) and noting that $\tau_h \sim 10^6$sec is quite easy to achieve while $Q_1 \sim 10^8$ is very hard, it seems, at least in theory, measuring thermal expansion may be much easier than measuring the change in the amplitude of normal mode oscillations.

In the above discussions, it has been assumed that, in the measurement of the thermal expansion, the influence of the normal mode oscillations can be

eliminated by taking an average over several cycles. This assumption, however, is correct only when the normal mode oscillations are reasonably regular. If there are enough irregularities in the normal mode oscillations, this assumption may become invalid. In other words, if the normal modes do not have enough Q, their noise spectrum may be a wide distribution instead of narrow peaks and may have a considerable amount of low frequency components which cannot be averaged out. To determine the importance of this effect, I will consider the first normal mode as an example.

The noise spectrum of the first normal mode is

$$\frac{2kTH_1}{|M(\omega_1^2-\omega^2)+iH\omega|^2}. \tag{2.4.15}$$

Taking the average over several cycles implies $\omega \ll \omega_1$. In this low frequency region, the spectrum is rather flat and it is as though the noise of the sensing device D^2 is increased by an amount:

$$D'^2 = \frac{2kTH_1}{M^2\omega_1^4} = 2.4\times 10^{-33}\mathrm{cm}^2/\sqrt{\mathrm{HZ}}\frac{1}{Q_1}\left(\frac{L}{R}\right)^2\left(\frac{T}{300^\circ\mathrm{K}}\right). \tag{2.4.16}$$

This contribution is not important unless Q_1 is order of unity. The contribution of any higher normal mode is down by a factor of n^3 and is less important.

Since high Q is not necessary here, the choice of the materials becomes much wider. Plastics usually have a thermal expansion coefficient one order of magnitude higher than aluminum and may be a good choice. $\frac{dE}{dx}$ in pure plastic is less than in metal, but it may be possible to make certain plastic loaded with heavy metals so that $\frac{dE}{dx}$ is comparable or even higher than that in aluminum.

When high Q is not needed, the task for the sensing devices becomes much easier. In gravitational wave detectors, the electric field in the capacitance meter is limited to 10^4V/cm because of the low breakdown voltage of the air gap. Air or vacuum gap is necessary to retain high Q. When high Q is not required, one may put good insulating oil between the plates of the capacitance meter, then the electric field in the capacitance meter can probably be increased to 10^6V/cm. Using a FET preamplifier[26] developed for gravitational wave detectors, which has a noise of $e_n \sim 0.4\text{nV}/\sqrt{\text{HZ}}$, one may achieve $D \sim 4 \times 10^{-16}\text{cm}/\sqrt{\text{HZ}}$. In order to avoid the $1/f$ noise region, it is necessary to modulate the quasi-static distance changes with high frequency before it is amplified. A high frequency driven capacitance meter will do the job. It may be possible to connect the four capacitance meters of two identical bars into a bridge (Fig. 2.4.2), so that the noise and drifts of the high frequency driver can be canceled; the effect of the motion of each bar relative to the supporting structures without net expansion can be compensated while a particle going through one bar but not the other can be detected.

With all the above improvements possible, particle detection by measuring the thermal expansion of the bar seems very promising. However, because of the difficulties of working at relatively low frequency, it may not be easy to achieve enough sensitivity in practice. Whether or not the technical problems can be solved at low cost is certainly worth experimental investigation.

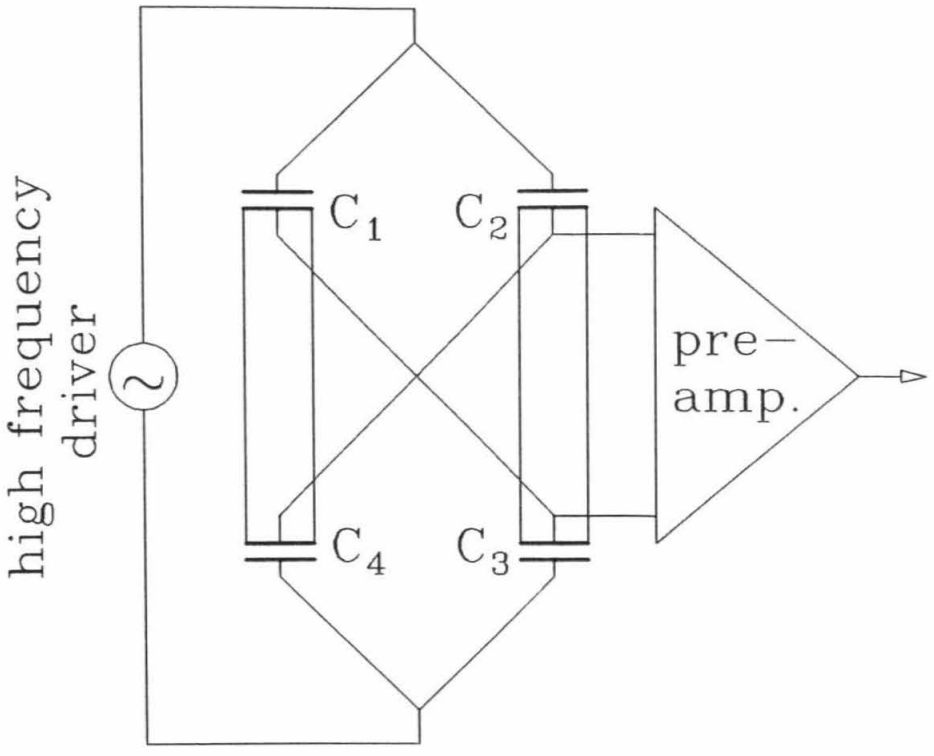

Fig. 2.4.2 — The four capacitance meters of two identical bars can be connected into a bridge.

From Equations (2.4.5), (2.4.7) and (2.4.13) and noting that α/C_p is approximately independent of the temperature (Grüneisen's Law[27]), the benefit of reducing temperature is easily seen. The noise is proportional to $T^{\frac{5}{2}}D$. Since D can also be reduced greatly at low temperature, it may be possible that this technique, when employed at low temperature, will be able to detect not only SIMPs but also usual relativistic particles.

2.5. Measuring the Stopping Force Directly

The stopping power $\frac{dE}{dx}$, in fact, is the *stopping force.* It is the force the travelling particle feels. According to Newton's third law, the stopping material feels a force of the same size in the opposite direction, the direction of the

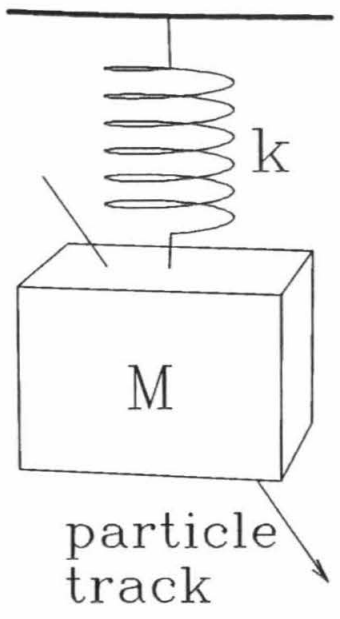

Fig. 2.5.1 — Mechanical oscillator for measuring stopping force produced by a SIMP.

particle's motion. To determine if this force can be detected, let us consider a mechanical oscillator of mass M, resonant frequency ω_0 and damping constant H (Fig. 2.5.1). The equation of motion is

$$M\ddot{x} + H\dot{x} + M\omega_0^2 x = F(t) \tag{2.5.1}$$

Since the particle's crossing time is very short, $F(t)$ can be treated as a δ-function and can be written as: $F(t) = I_0\delta(t)$, where $I_0 = \frac{dE}{dx}\tau$ and τ is the particle's crossing time. Since τ is inversely proportional the particle's velocity, this technique has advantages for very low β particles. According to the discussions of Section 1.5, $\frac{dE}{dx}$ of monopoles in the most interesting β region is virtually proportional to its velocity; therefore, the momentum transfer I_0 is independent of β. For nuclearites, I_0 is proportional to β although the stopping power is

proportional to β^2. For electrically charged SIMPs, I_0 at low β can be tremendously enhanced and almost goes as β^{-1} because of the contribution of the nearly constant nuclear stopping power.

For such a simple harmonic oscillator, a matched or nearly matched filter is not particularly difficult to build; thus, one can calculate the optimal signal-to-noise ratio by equation (2.1.33). In this case,

$$S(\omega) = \frac{I_0}{M(\omega_0^2 - \omega^2) + iH\omega} \quad \text{and} \quad \Phi(\omega) = \frac{2kTH}{M^2(\omega_0^2 - \omega^2)^2 + H^2\omega^2} + D^2, \tag{2.5.2}$$

where D^2 is the mean-square noise per HZ of the device for monitoring small displacements. Using Equation (2.1.33), one obtains

$$\frac{S}{N} = \int_{-\infty}^{\infty} \frac{I_0^2}{2kTH + D^2[M^2(\omega_0^2 - \omega^2)^2 + H^2\omega^2]} df. \tag{2.5.3}$$

Carrying out this integral and ignoring some noncritical small numbers, one gets

$$\frac{S}{N} = \frac{I_0^2}{8\sqrt{DM}} \left(\frac{\tau^*}{kTM}\right)^{3/4}, \tag{2.5.4}$$

where $\tau^* = 2M/H$ is the relaxation time of the oscillator.

To make the relaxation time as long as possible, using torsion pendulums may be a good idea. In an experiment using a torsion pendulum of a few grams for testing the equivalence principle of general relativity, $\tau^* \sim 3 \times 10^9$sec may have been achieved, although the actual measurement has set a lower limit of only $\tau^* > 6 \times 10^7$sec, because the damping was too small to be measured in a reasonable length of time[28]. If the damping is dominated by the residual gas in

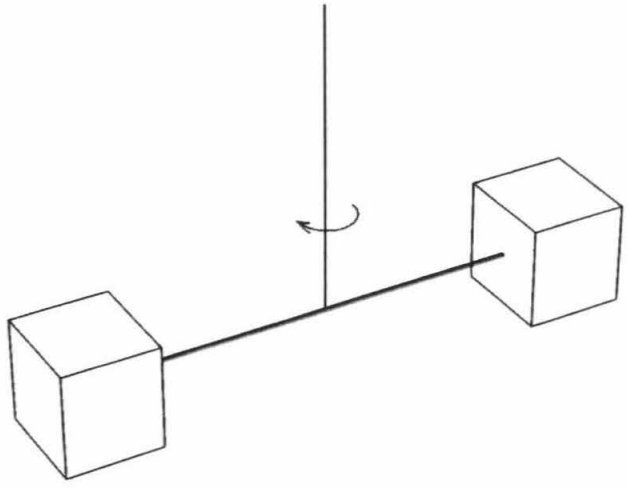

Fig. 2.5.2 — A torsion pendulum for measuring the stopping force.

the vacuum chamber, τ^* should be proportional to the ratio of the mass to the surface area. Thus, a torsion pendulum made of two $(10\text{cm})^3$ aluminum cubes (see Fig. 2.5.2) may have a relaxation time of $\tau^* \sim 10^{10}\text{sec}$. For such a torsion pendulum and a particle going through one of the two masses, one gets

$$\frac{S}{N} = 8.5 \left(\frac{10^{-15}\text{cm}/\sqrt{\text{HZ}}}{D} \right)^{\frac{1}{2}} \left(\frac{\tau^*}{10^{10}\text{sec}} \right)^{\frac{3}{4}} \left(\frac{300^\circ\text{K}}{T} \right)^{\frac{3}{4}} \left(\frac{10^{-3}}{\beta} \right)^2 \left(\frac{dE/dx}{1\text{GeV/cm}} \right)^2 . \tag{2.5.5}$$

In the above calculation, $F(t)$ is assumed to be a δ-function. For extremely slow particles, the crossing time may be quite long and this assumption becomes invalid. It is then important to determine how a finite crossing time affects the above results. A finite crossing time τ would modify the numerator of the integrand in Equation (2.5.3) by a factor of $(\frac{2}{\omega\tau} \sin \frac{\omega\tau}{2})^2$. Such modification does not change the value of the integral drastically if $\omega\tau \lesssim 1$ in the major contributing frequency region. It is seen from Equation (2.5.3) that the major

contributing frequency region is

$$|\omega| \lesssim \omega_{\rm cut} \equiv \left(\frac{2kTH}{D^2M^2}\right)^{1/4}. \tag{2.5.6}$$

Outside this region, the integrand dies away as ω^{-4}. The finite crossing time thus has litle effect on the above result if $\tau \lesssim 1/\omega_{\rm cut}$, or

$$\beta \lesssim 3\times 10^{-9}\left(\frac{10^{-15}{\rm cm}/\sqrt{\rm HZ}}{D}\right)^{\frac{1}{2}}\left(\frac{T}{300^\circ{\rm K}}\right)^{\frac{1}{4}}\left(\frac{10^{10}{\rm sec}}{\tau^*}\right)^{\frac{1}{4}}. \tag{2.5.7}$$

As long as this condition holds, the S/N for monopoles and electrically charged particles at low β is the same or even larger than that at higher β. There seem to be no other techniques that have any hope to detect SIMPs of such low β except for the superconducting ring,[29] which is sensitive only to monopoles.

Like the method of measuring thermal expansion, since the method of detecting stopping force works at low frequency, many practical problems may arise. Whether or not those problems can be solved can be answered only by experimental investigation.

The methods discussed in this chapter are only a few examples of the options for detecting small forces associated with a traveling particle. Except for the acoustic detection in the infinite medium, none of the methods is "intrisically" limited by the thermal noise, and their feasibility is only a question of the state-of-art of present technology.

Particle detection by measuring small forces is a very interesting area that is just beginning to be made possible by modern technology. Future work is certainly not "pointless."

References of Chapter 2

[1] B. Barish, *Magnetic Monopoles* (Proceedings of Magnetic Monopole Workshop at Wisconsin, 1982, ed. R. A. Carrigan, Jr. and P. W. Trower), page 219 (Plenum, New York, 1983).

[2] See *Proceedings of the 1976 DUMAND Summer Workshop,* ed. A. Roberts.

[3] J. Learned, Phys. Rev. D **19**, 3293 (1979).

[4] L. R. Sulak *et al.*, Nucl. Instr. Meth. **161**, 203 (1979).

[5] C. W. Akerlof, Phys. Rev. D **26**, 1116 (1982).

[6] E. J. Kobetich and R. Katz, Phys. Rev. **170**, 391 (1968).

[7] H. B. Callen and T. A. Welton, Phys. Rev. **83**, 34 (1951).

[8] H. Nyquist, Phys. Rev. **32**, 110 (1928).

[9] Carl. W. Helstrom, *Statistical Theory of Signal Detection* (Pergamon Press Inc., 1968)

[10] G. Liu, *Monopole '83* (Proceedings of Monopole '83 Workshop Oct. 6–9 1983 at Ann Arbor, Mich., ed. J. L. Stone), page 403 (Plenum Press, New York, 1984).

[11] C. W. Akerlof, Phys. Rev. D **27**, 1675 (1983).

[12] G. W. Gibbons and S. W. Hawking, Phys. Rev. D **4**, 2191 (1971).

[13] W. Bialek and A. Schweitzer, Phys. Rev. Lett. **54**, 725 (1985).

[14] R. P. Giffard, Phys. Rev. D **14**, 2478 (1976).

[15] Carlton M. Caves, Kip S. Thorne, Ronald W. P. Drever, Vermon D. Sandberg, and Mark Zimmermann, Rev. Mod. Phys. **52**, 341 (1980).

[16] A. M. Allega and N. Cabibbo, Lett. Nuovo Cimento **38**, 263 (1983).

[17] L. D. Landau and E. M. Lifshitz, *Statistical Physics, 3rd ed., Part 1*, page 333-400 (Pergamon Press, 1980).

[18] S. N. Rasband, J. Acoust. Soc. **57**, 899 (1975).

[19] Ho Jung Paik and Robert V. Wagoner, Phys. Rev. D **13**, 2694 (1976).

[20] J. Weber, *General Relativity and Gravitaion Volume 2* (ed. A. Held), page 435, (Plenum Press, New York, 1980).

[21] V. B. Braginsky and A. B. Manukin, *Measurement of Weak Forces in Physics Experiments* (ed. David H. Douglass, University of Chicago Press, 1977). See Fig. 32 on page 106.

[22] A. Abramovici, Z. Vager and M. Weksler, J. Phys. E **19**, 182 (1986).

[23] S. P. Boughn *et al.*, Astrophys. J. **261**, L19 (1982).

[24] K. Nakamura H. Horie, T. Takahashi, and T. Tanimori, Phys. Lett. **161B**, 417 (1985).

[25] David L. Goodstein, *States of Matter*, page 75-76 (Prentice-Hall, Inc., Englewood Cliffs, New Jersey, 1975).

[26] G. V. Pallottino and Giuliano Vannaroni, IEEE Trans. on Instru. and Meas. IM **34**, 676 (1985).

[27] Ref. 17, page 203.

[28] V. B. Braginsky and V. I. Panov, Sov. Phys. JETP **34**, 463 (1972).

[29] B. Cabrera, M. Taber, R. Gardner, and J. Bourg, Phys. Rev. D **51**, 1933 (1983).

Chapter 3

A Scintillator Search at Earth's Surface

Although the acoustic or mechanical detection of SIMPs is possible in principle and not far away from practice, the cheapest way to cover a large area is still the conventional ionization-scintillation techniques. In this chapter, I report the result of a search using a scintillator detector at Caltech.

3.1. Scintillation at Low β

Since SIMPs have large dE/dx, it may seem obvious that they can be detected by scintillators. However, this is not so *obvious* because a large stopping power does not always mean a high light yield. In order to produce light, electrons near the particle track have to be excited to higher energy levels and this can happen only when the electromagnetic field driving the electrons contains high enough frequency components. Since the frequency of the electromagnetic field near a travelling particle is proportional to its velocity, it is quite possible that a very slow particle may not be able to produce an electromagnetic field of high enough frequency to excite scintillation light, although it may have very large dE/dx due to low velocity collisions.

In order to determine whether or not scintillators can be used to detect slow particles, several theoretical and experimental studies have been carried out, and the results are very encouraging. A conservative calculation of the scintillation

yield of magnetic monopoles in organic scintillator has been done by Ahlen and Tarlé[1], which shows that for $\beta \geq 7 \times 10^{-4}$, the scintillation yield of a magnetic monopole is larger than a minimal ionizing muon. Although the calculation shows an abrupt cutoff below $\beta \sim 6 \times 10^{-4}$, it is speculated that there might still be a considerable amount of scintillation in this low β region due to other effects such as Zeeman splitting and energy level crossing, etc.[2,3]. An experiment at Brookhaven National Lab[4] has measured considerable scintillation light yields for protons with a velocity as slow as $\beta = 9 \times 10^{-4}$. A more recent measurement[5] down to $\beta = 2.5 \times 10^{-4}$ has indicated that the light yield of most SIMPs stays well above minimal ionization for the whole measured β range. There is no doubt that scintillator detectors are sensitive to nuclearites; let alone the scintillation mechanism, even the black body radiation of the heated track can produce enough light[6]. According to all these encouraging studies, it is clear that scintillation techniques are an effective way of SIMP detection.

3.2. The Caltech Scintillator Detector

The basic scheme employed in the Caltech experiment is a multilayer detector. In such a detector, the velocity of a traversing particle is measured by the interlayer timing, and a SIMP is recognized by its ability to penetrate the detector with constant low velocity ($10^{-3}c$). None of the known particles with such low velocity can penetrate several layers and keep its speed, while $\beta \sim 1$ cosmic rays are easily identified as signals occurring in all the layers almost simultaneously.

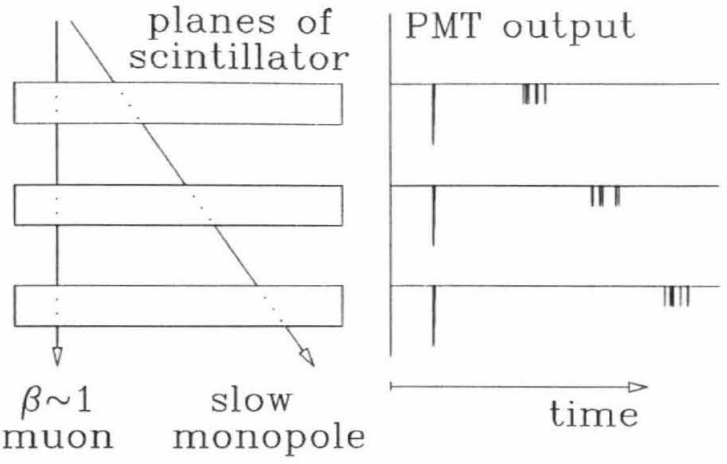

Fig. 3.2.1 — Comparison of signals produced by a $\beta \sim 1$ muon and a SIMP.

For a very slow SIMP, because of its extremely long crossing time, the signal in each layer becomes a train of single photoelectron pulses. (Figure 3.2.1).

The Caltech detector consisted of 6 planes of 1 inch thick NE 114 scintillator, measuring 5 by 10 feet. Each plane was made up of two pieces of scintillator, each having two 56 DVP photomultiplier tubes (PMTs) attached to the BBQ wave length shifter bars running along the sides, which were used to collect the light from the scintillator. The two PMTs on the same piece of scintillator were summed, yielding a signal for a minimum ionizing muon ranging from 12 to 16 photoelectrons, depending on the position. The spacing between the first and the second planes was 9 cm, with the other spacings all 20 cm (See Figure 3.2.2).

From these dimensions, the geometrical acceptance can be determined from the following formula derived by me, assuming the expected isotropic flux and requiring the particles to go through all six planes in one direction (down going),

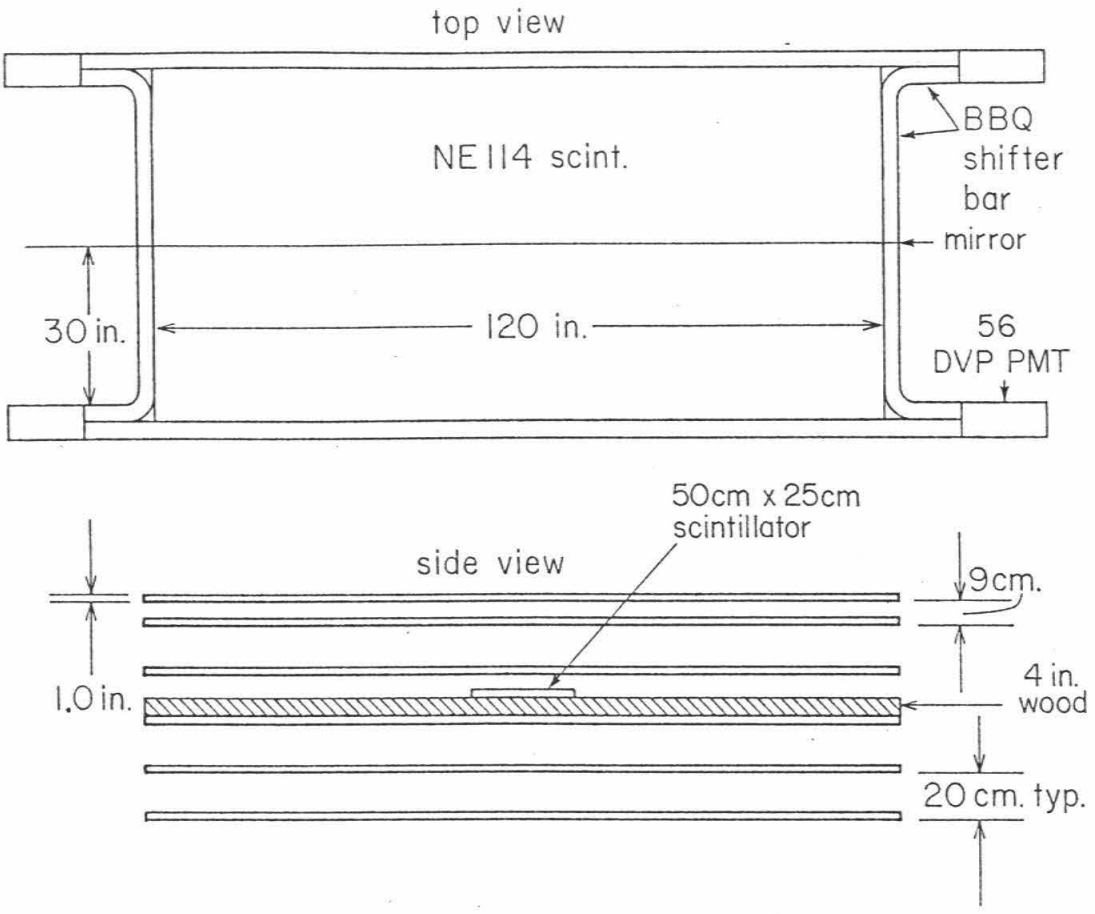

Fig. 3.2.2 — Geometry of the Caltech scintillator detector.

as in the experiment.

$$\begin{aligned} A \cdot \Omega = \; & 2b\sqrt{a^2+c^2}\,\operatorname{arctg}\frac{b}{\sqrt{a^2+c^2}} - 2cb\,\operatorname{arctg}\frac{b}{c} \\ & + 2a\sqrt{b^2+c^2}\,\operatorname{arctg}\frac{a}{\sqrt{b^2+c^2}} - 2ca\,\operatorname{arctg}\frac{a}{c} \\ & + c^2 \ln\left[\frac{(a^2+c^2)(b^2+c^2)}{c^2(a^2+b^2+c^2)}\right] \end{aligned} \tag{3.2.1}$$

a and b are the length and the width of the detector and c is the separation between the first and last planes. The formula yields a geometrical acceptance of 6.7 m^2sr for the Caltech detector. Equation (3.2.1) seems to be a useful formula, considering that most similar experiments have relied on Monte Carlo and numerical integration to find their acceptance.

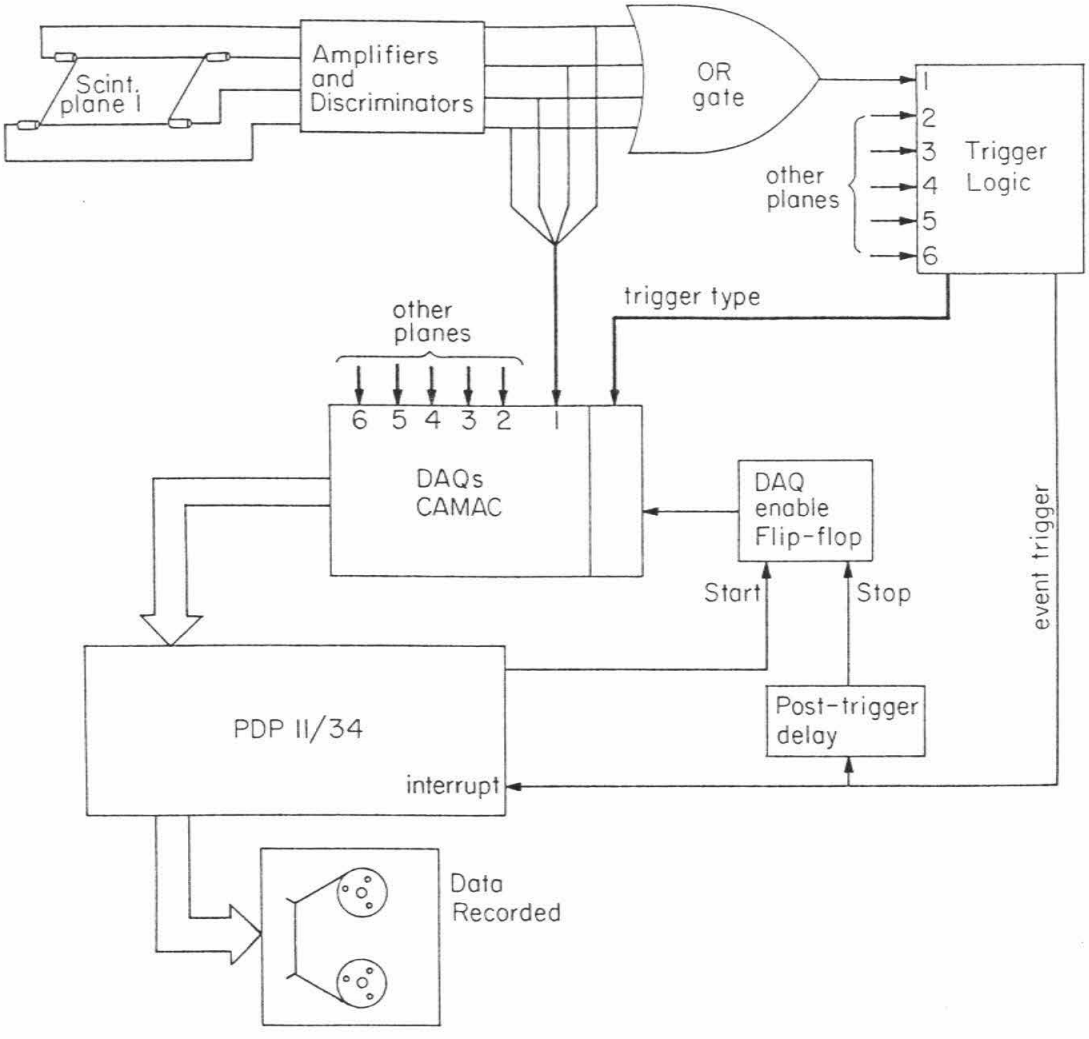

Fig. 3.2.3 — Overall electronics of the Caltech scintillator detector.

The overall electronics in this search is shown in Figure 3.2.3. The signal from each PMT was sent to a discriminator set at a threshold of 0.6 p.e. The output of the discriminator was sent to the trigger logic and the data acquisition system, which recorded the time of each pulse with a time resolution of 7ns. This timing information allowed the identification of long pulse trains characteristic of a SIMP. In addition, some pulse height information could be obtained by counting the number of pulses in the train.

The threshold setting of 0.6 photoelectrons resulted in some inefficiency because of the rather broad single photoelectron distributions of the PMTs. In order to determine this "single photoelectron discrimination efficiency," I measured the single photoelectron pulse height spectrum and determined that $\sim 75\%$ of the single photoelectrons yielded pulses above the 0.6 photoelectron threshold. At this level, the probability of missing a SIMP entirely in a given plane is very small since it produces a train of many single or multiple photoelectron pulses. For instance, a typical SIMP of $\beta \sim 6 \times 10^{-4}$ is expected to produce a pulse train of at least 12 photoelectrons per plane ($\approx$ minimal ionizing) spread over ~ 140 ns. The statistical probability of missing this signal is less than $\sim 10^{-4}$.

The trigger logic contained four separate triggers, which were ORed to generate the event trigger. The four triggers included a SIMP candidate trigger and three other triggers used for diagnostic studies (Fig. 3.2.4).

The four triggers are the following:

1) Muon Trigger: This trigger was a 3 out of 4 fast coincidence of the four center planes. The raw trigger rate was 1.27KHz. However, in actual data recording these triggers were prescaled to 0.0127Hz, resulting in a total sample of about 10^5 events. The prescaling was to prevent this trigger from creating too much dead time for data acquisition. The muon events were used to calibrate electronics, monitor efficiencies, etc.

2) Stopping Muon Trigger: This trigger was a fast coincidence between the top three planes and a small 25cm $\times$ 50cm scintillator detector placed in the

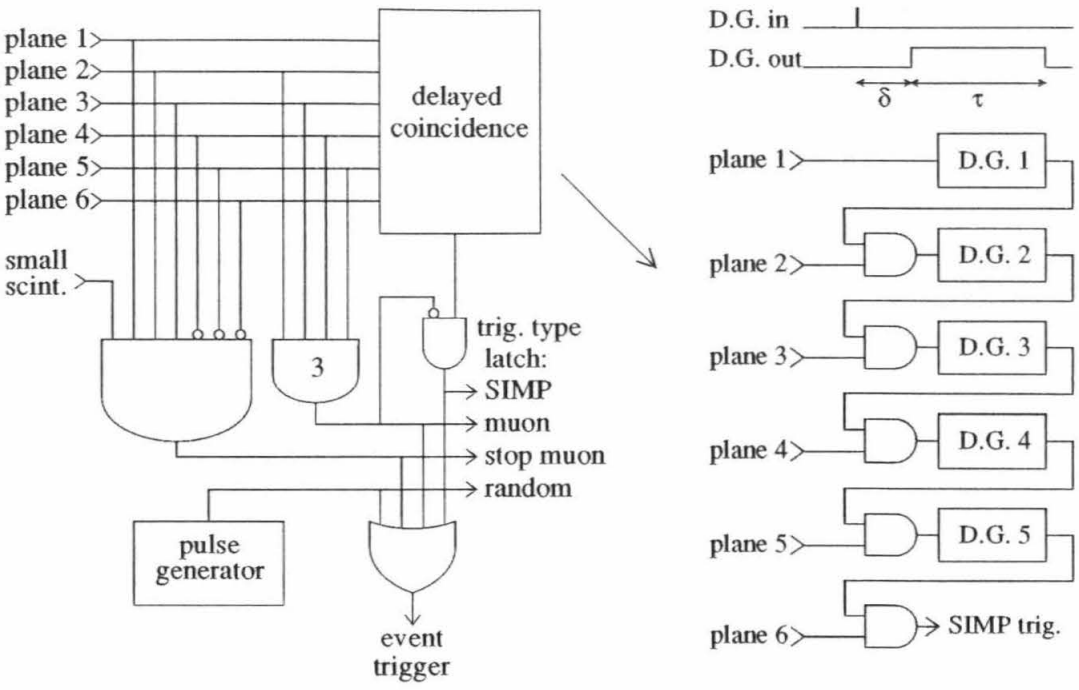

Fig. 3.2.4 — Trigger electronics of the Caltech scintillator detector. The SIMP trigger is a delayed coincidence of the six planes produced by a series of Delayed Gates (D.G.s). The delay δ was set at 70 ns and the gate width τ at 2.4 μs, resulting in a trigger β range from 5×10^{-3} to 2.7×10^{-4}.

center of the array, vetoed by any in-time signal from the lower three planes. 4 inches of wood were placed between the small scintillator and the fourth plane as a low-Z muon target. Stopping muon events provided a valuable check on the performance of the detector by measuring the muon lifetime. The stopping muon trigger rate was 0.15 Hz, and it was prescaled down to 0.015 Hz in the actual data recording.

3) Random Trigger: This trigger was generated by a pulse generator set at about 0.03 Hz. Events produced with this trigger contained random samples of background signals from the PMTs and have been used for off-line analysis of the background.

4) SIMP Trigger: This event trigger was a set of delayed coincidence between all six planes of the detector. I designed a simple TTL circuit to achieve this delayed coincidence. The function of this circuit is explained in Fig. 3.2.4. A pulse in the first plane generates a gate after a fixed delay; a pulse from the second plane arriving within this gate triggers a delay and gate for the third plane, etc. The delays were set at 70 ns and the gate widths at 2.4 μs, resulting in a β range from 5×10^{-3} to 2.7×10^{-4}. This trigger was vetoed by the cosmic ray muon trigger for about 30μs, to prevent cosmic ray muons from generating an excessive number of false triggers. Although the muon trigger rate was 1.27kHZ, the rate that the 30μs veto gates generated was only about 580HZ. This was because a cosmic ray muon often gave two or more muon triggers because of the timing spread of the BBQ wave shifter ($\sim$ 25ns) and the PMT afterpulses. From this veto rate, the veto dead time has been calculated to be only 1.7%.

The data acquisition system[7] (Fig. 3.2.5) consisted of 12 data acquisition (DAQ) timing modules. Two DAQ modules were used for each plane serving as a 32 bit $\times$ 15 location memory stack. 16 bits were used to register the time of a 70 MHZ greycode clock, 8 bits were used to register a code indicating which PMT of the plane fired and another 8 bits were reserved for future expansion. The memory contents were shifted by one location when any PMT of the corresponding plane fired and the content of the last cell was pushed out. In this way the DAQs always contained the latest 15 pulses of each plane and covered

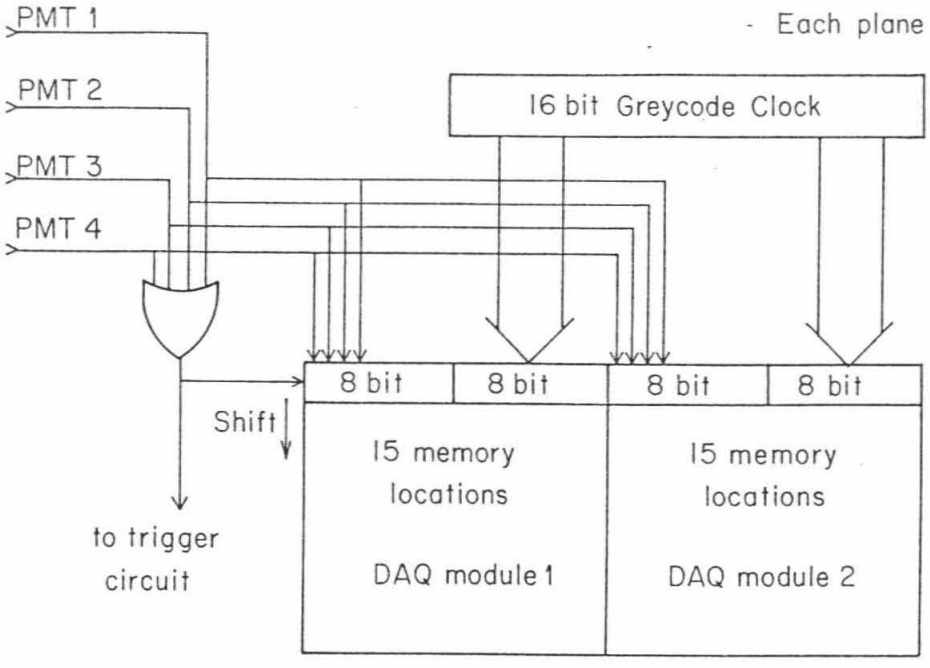

Fig. 3.2.5 — The data acquisition (DAQ) module of the Caltech scintillator detector.

approximately 450 μs. The on-line computer was a PDP11/34, using a modified version of "MULTI" as a data acquisition program.

The event triggers were used to stop the DAQs and interrupt the computer for reading the DAQs and writing the data on the magnetic tapes. A post-trigger delay was added to allow post-trigger data to be collected for about 7.7μs.

A sample of events (See Figure 3.2.6) presented at a variety of time scales illustrates the type of data available for off-line analysis from individual events. The tracks of $\beta \sim 1$ cosmic rays through the detector are clear and distinctive, and any residual contamination can be easily removed.

The data of cosmic ray muon events provided a valuable calibration of the efficiency of the detector. Since the muon trigger required at least 3 of the 4

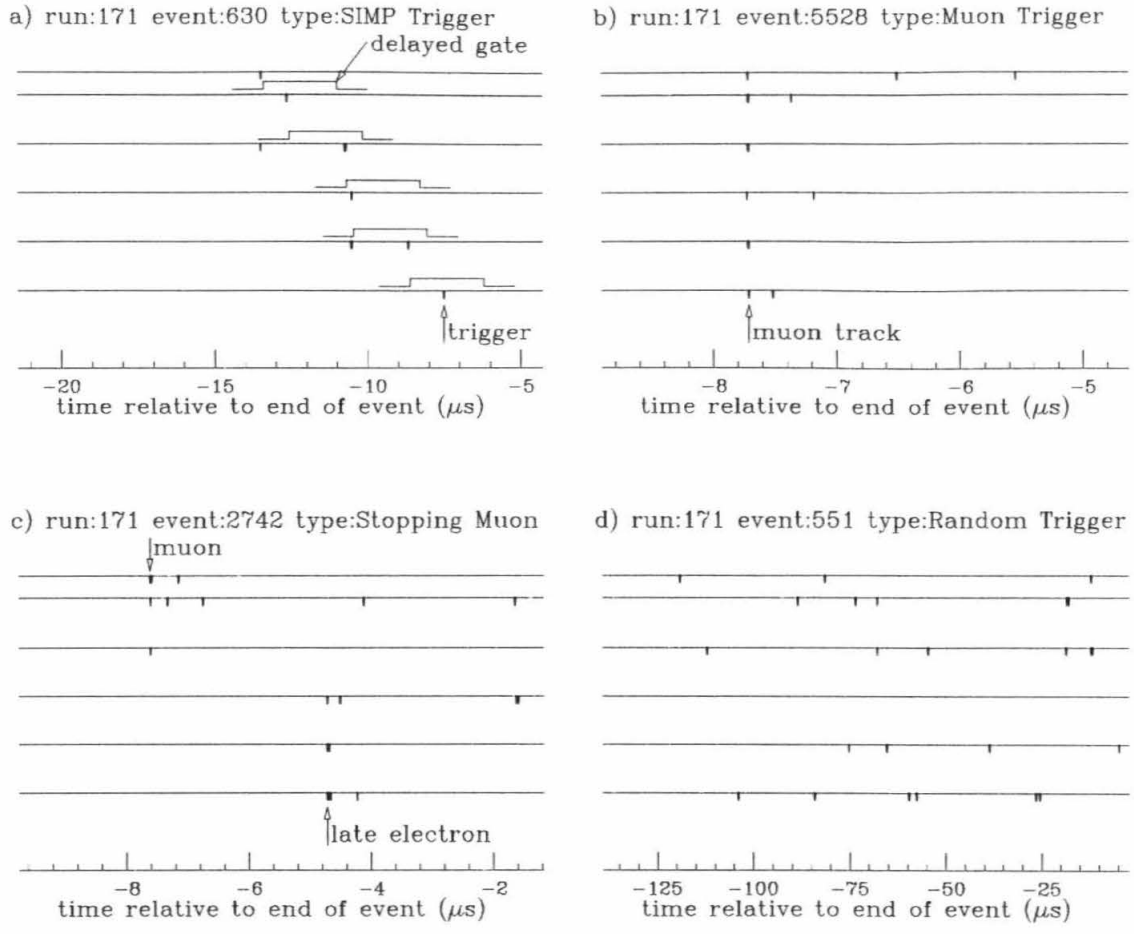

Fig. 3.2.6 — A Sample of events presented with different time scales. a) SIMP trigger event with the delayed gates indicated; b) muon trigger event with muon at $-7.7\mu s$; c) stopping muon trigger event with the muon and the late electron indicated; d) random trigger event containing only background noise.

center planes to have a signal, the inefficiency for muons can be measured by finding muon tracks that missed a given plane. By this method, I determined that the muon inefficiency of each plane was only about 1%.

The stopping muon events offered another convenient test of the performance of the detector. A measurement[7] of the muon lifetime from the stopping muon samples has yielded the expected value of about 2 μs.

3.3. Data Analysis

The experiment was run from December 3, 1983 through March 1984 for an effective running time of 8.2×10^6sec. The 195 data runs contained 985,495 events, of which 959,697 were "good" events not subject to equipment failure and data errors. About half of the data consisted of SIMP trigger events.

The basic object of off-line analysis was to search for any ionizing particle that penetrated through the detector with a low constant velocity, that is, to search for pulses that lined up in a straight line on the time versus distance graph. More specifically, my first pass through the data consisted of identifying SIMP candidate tracks by searching for the pulses having acceptable timing and patterns. The particles were required to go through all six planes and produce at least one pulse in each plane with relative timing indicative of a constant velocity. In order to ensure good efficiency and to account for any possible misalignments of the scintillator planes, I allowed time jitters up to 18% larger than the time for the particle to cross each plane. A high β cutoff at $\beta \approx 0.01$ was set to eliminate muons and a low β cutoff at $\beta = 2 \times 10^{-4}$ to speed up the search. These cutoffs were well beyond the triggering cutoffs; therefore, no additional inefficiency was produced. This data selection reduced the original data of 959,697 trigger events to 1,113 candidate events. The unshaded histogram of Fig. 3.3.1 shows the β distribution of these candidate tracks. Even though the trigger-type information was not used in the analysis (and roughly half the original triggers were of the diagnostic types), all surviving events came from the SIMP trigger.

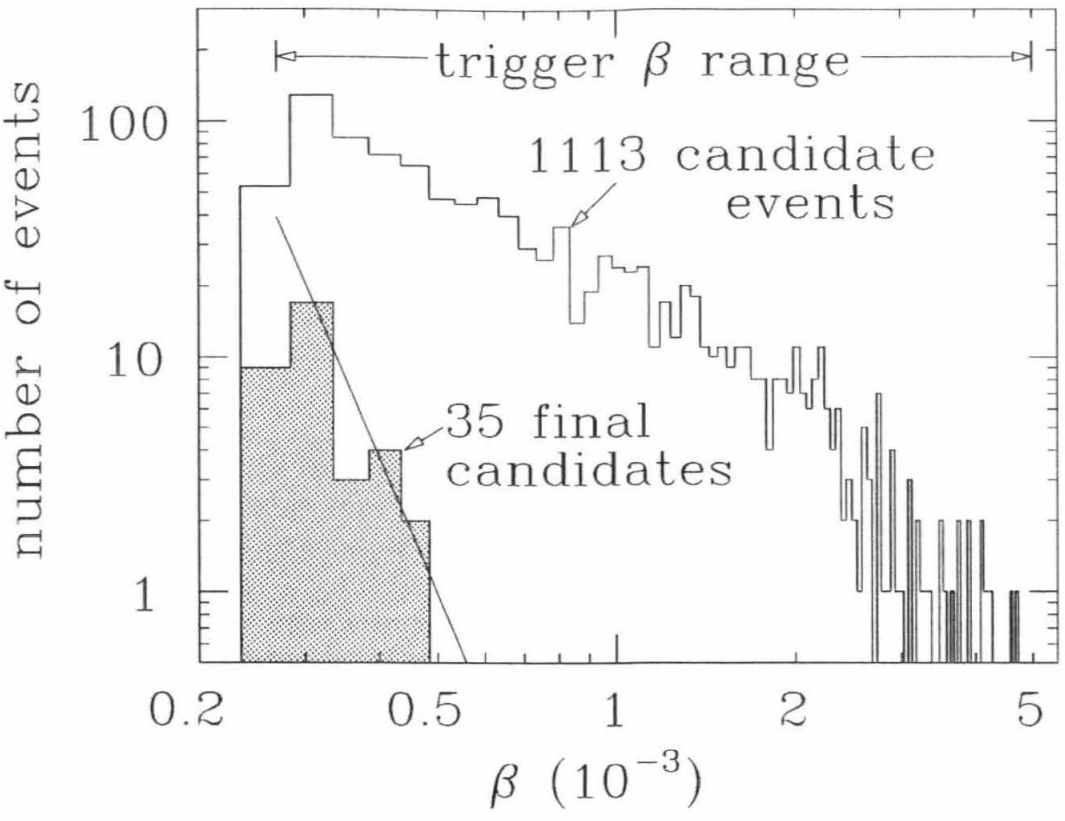

Fig. 3.3.1 — β distributions of the 1,113 candidate events (unshaded) and the 35 final candidates (shaded). The solid straight line is the calculated background.

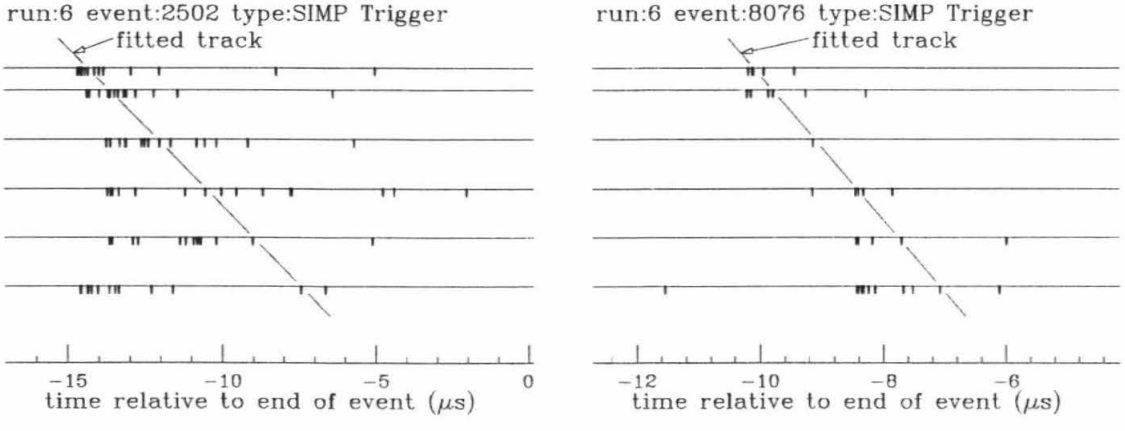

Fig. 3.3.2 — Typical SIMP candidate events.

I examined samples of the surviving 1,113 candidate events that had hits giving satisfactory timing and geometry (see Fig. 3.3.2), and found that most of

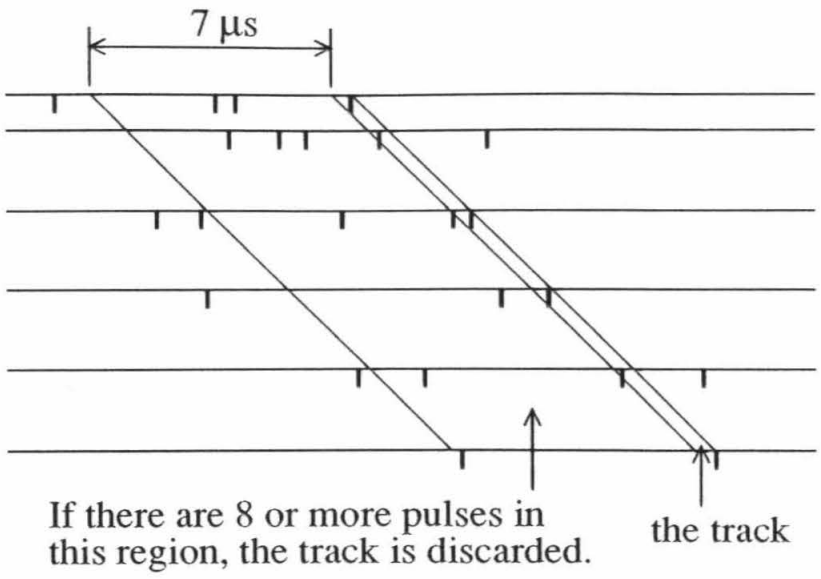

Fig. 3.3.3 — The events are required to be "quiet" before the candidate track; that is, the number of pulses in a $7\mu s$ window before the *earliest* candidate track must not exceed 7.

them had a large number of extra hits outside the allowed window. Also, many events were obviously caused by muons and the PMT afterpulses induced by them. It is impossible to determine the cause of all the spurious pulses from the recorded information, but they were likely to be caused by cosmic ray showers or some high energy interactions inside or near the detector.

In order to analyze these events systematically, I made a second pass. In this pass, the events were required to be "quiet"; that is, the number of pulses around a candidate track window does not exceed a certain value. Since heavily ionizing particles may have given rise to a large number of PMT afterpulses, it is only sensible to require the events to be quiet *before* the candidate track but *not after* it. Specifically, I required in this pass that the number of pulses in a $7\mu s$ window before the *earliest* candidate track not exceed 7 (Fig 3.3.3). Such a

value corresponds to a temporary noise rate of 1MHZ, which is about 6 times the average noise rate of the whole detector. SIMPs may interact (such as catalyzing baryon decays, etc.) with the concrete and atmosphere above and cause showers that arrive at the detector just before themselves and thus would be thrown away by this analysis. However, this is very unlikely unless the interaction cross section is unreasonably large. Additional requirements were also applied in this pass to remove muon pulses and their PMT after-pulses. Muon pulses were identified by fast coincidence between adjacent planes and after-pulses as those happening 100ns or less after a muon pulse.

The above analysis has relied on veto schemes, and therefore it is crucial to determine the veto dead time. I measured this in a realistic way by superposing random trigger events onto Monte Carlo generated SIMP tracks. As shown in Figure 3.3.4, 469 of the 500 background superposed Monte Carlo events have survived the above analysis. Therefore, the inefficiency due to these veto requirements is only 6.2%.

I applied the second pass analysis to the 1,113 candidate events surviving the first pass and obtained 35 final candidates, all having a measured $\beta < 5 \times 10^{-4}$ (see the shaded histogram in Fig. 3.3.1). In such a low β region, a particle needs more than 170ns to cross one scintillator plane; therefore, the signal from each plane must be either a wide pulse or a pulse train lasting for > 170 ns. The former corresponds to the case of relatively high ionization ($\gtrsim I_{min}$). Although only one pulse per plane could be registered in this case, the recorded pulses

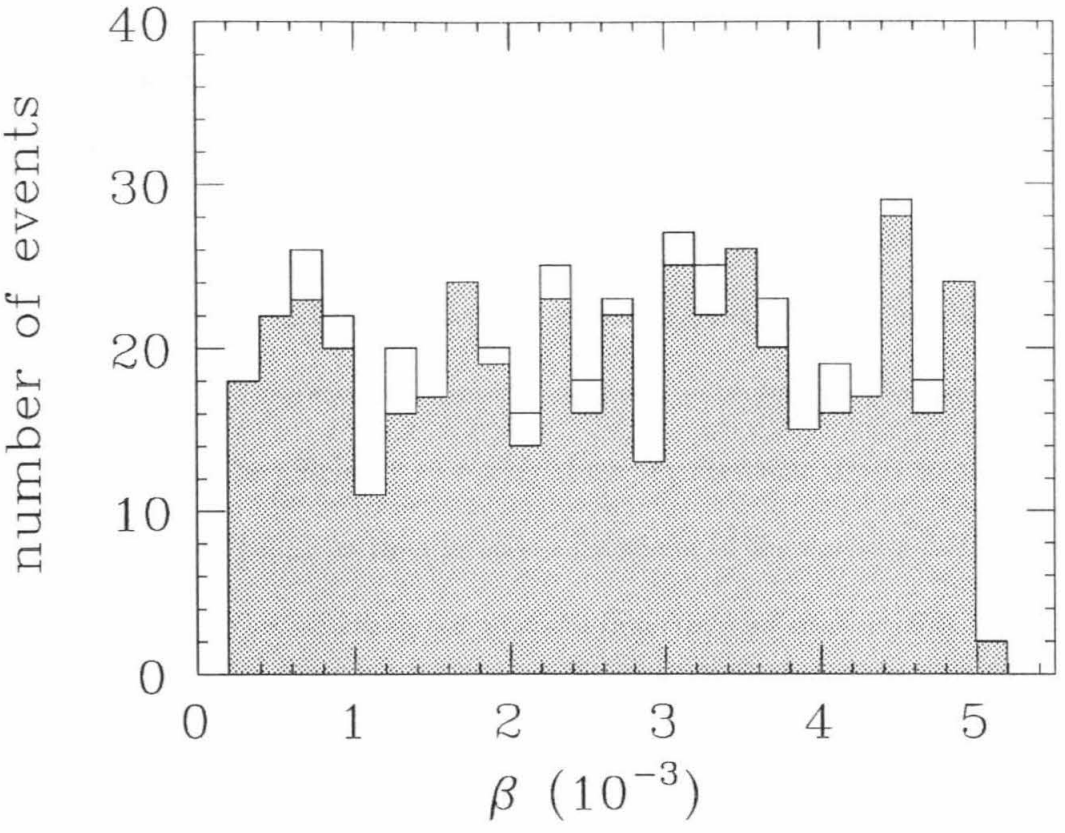

Fig. 3.3.4 — β distributions of the original 500 Monte Carlo events (unshaded) and the 469 events (shaded) that survived the same analysis that was applied to the actual data.

should have small time jitter and lie very close to a straight line. I examined the 35 final candidates and ruled out such a possibility, since all the slow particle tracks found in the 35 candidates deviated from an actual straight line by more than 90 ns. In order to study the latter case, I analyzed the 35 final candidates further to determine the number of planes that actually had pulse trains. A train was defined in the most minimal way as having at least two pulses. The result is the following:

Table 3.3.1 — Number of Planes Having a Pulse Train

number of planes having a pulse train	0	1	2	≥ 3
number of events	15	16	4	0

Therefore, there has been no indication that any of the 35 events came from slow moving particles crossing the detector.

The entire hardware β-range is eliminated for SIMPs if one requires at least three planes to have two or more pulses. This requirement and the requirement that each plane has to have at least one pulse set an ionization threshold for the detector. At 1/3 of the minimum ionization, each plane gets 4.5 photoelectrons on the average and the efficiency to satisfy these requirements drops to about 80%. Therefore, I take $\frac{1}{3}I_{min}$ as the ionization threshold of the detector, although the threshold cutoff is not a sharp one and the detector had considerable sensitivity even below this threshold.

The effective exposure time for the detector, corrected for the dead time, is 8.0×10^6 sec. Using this effective running time, the acceptance of the detector and applying efficiency corrections, I determined an upper limit for SIMP flux within the detector's β acceptance (90% confidence):

$$\begin{aligned} &\text{SIMP Flux} < 4.7 \times 10^{-12}\,\text{cm}^{-2}\text{sr}^{-1}\text{s}^{-1} \\ &\text{for} \qquad 2.7 \times 10^{-4} \leq \beta \leq 5 \times 10^{-3}. \end{aligned} \tag{3.3.1}$$

This flux limit applies to any particles having ionization above $\frac{1}{3}I_{min}$ in terms of scintillation yield.

3.4. Background Studies

The 35 final candidates have been rejected as SIMPs, but what caused them is still a question that should be answered. In the following, I will show that they can be explained as the coincidences of random background pulses.

In an n-layer detector in which slow particles are recognized only by inter-layer timing, the rate that random pulses happen to line up and fake a track of β in a small bin $\Delta\beta$ can be shown as

$$\Delta R = (n-1)H\nu_1 \cdots \nu_n \frac{W^{n-2}}{c^{n-1}} \frac{\Delta\beta}{\beta^n}, \tag{3.4.1}$$

where H is the height of the detector, ν_i is the noise rate of ith plane, c is the speed of light and W is the thickness of the scintillator used to calculate the allowed time jitter (I have taken it as 3 cm, which is 18% wider than the real thickness). If each plane has several pieces of scintillator, then the detector has some tracking ability and the above formula should be multiplied by a "geometrical factor." The geometrical factor is defined as the probability that a legitimate track in *space* can be formed if each plane is given one pulse randomly occurring in any piece of the scintillator. The geometrical factor of the Caltech detector is easily found to be $\frac{3}{16}$.

In order to find the actual random noise rate of each plane, highly correlated backgrounds such as muons and cosmic ray showers have to be removed. I have done this using the random trigger events and applying the same "quiet" requirement and muon and afterpulsing veto schemes as applied in the actual data analysis. The result is the following:

Table 3.4.1 — Random Noise Rate of Each Plane

plane	1	2	3	4	5	6
rate (kHz)	24.3	19.9	21.2	20.9	29.2	21.9

From these data, Equation (3.4.1) gives

$$\Delta n \;=\; 3.05 \times 10^{-16} \frac{\Delta\beta}{\beta^6}. \tag{3.4.2}$$

The calculated background is drawn on the histograms of the 1,113 candidate events and the 35 final candidates (Figure 3.3.1). The histogram of the 1,113 original candidates is far above the calculated background and has a different shape, indicating that the pulses from the cosmic ray showers and muons are highly correlated and tend to make many more coincidences than random noise. After removing the highly correlated backgrounds, the noise becomes truly random, and the histogram of the 35 final candidates agrees very well with the calculated background. Considering that there is no free parameter here, the agreement is remarkable. From this, I conclude that the final 35 candidates came from the coincidence of the uncorrelated random noise.

3.5. Comparison with Other Experiments and Implications

To compare this result with other reported experiments, I divide them into two types, underground experiments and surface experiments. Several underground experiments have reported lower flux limits than this experiment. Although some of them covered a very different β and ionization region (for instance, the Baksan experiment[8] had an ionization threshold at least $5I_{min}$ because of their improper integration time), there are those that have both a wider β range and lower ionization threshold than this experiment and have reported

lower flux limit[9]. The relevance of this surface measurement, therefore, is to particles that would not be detected underground.

The differences in sensitivity between the experiments at Earth's surface and the underground experiments are for particles having masses such that they penetrate the atmosphere with low velocity but do not penetrate to the depth of the deep underground detectors. I call such particles "medium heavy," with masses $\sim 10^9$GeV, in contrast to the more penetrating "superheavy" particles with masses $\sim 10^{16}$GeV typical of the GUT scale. For these medium heavy particles, the flux limits set by underground experiments do not rule out a much higher flux on Earth's surface.

For certain medium heavy SIMPs such as magnetic monopoles, one may expect them to be accelerated to $\beta \sim 1$ by the galactic magnetic field. However, this is not true in certain models involving symmetries or plasma oscillations[10-11]. If the galactic magnetic field acceleration is avoided, the Parker bound does not apply. The monopole candidates observed by Cabrera[12] and the Imperial College group[13], which imply flux well above the Parker bound, have motivated such models.

As an example, Figure 3.5.1 shows the lower mass limit versus the original β of various SIMPs that can reach the Caltech detector and fall into its β window, as compared with the experiment in Kamioka Mine[9], 250 m deep, the only published underground experiment that has reported lower flux limit and had a wider β window and a lower ionization threshold than ours. I calculated these

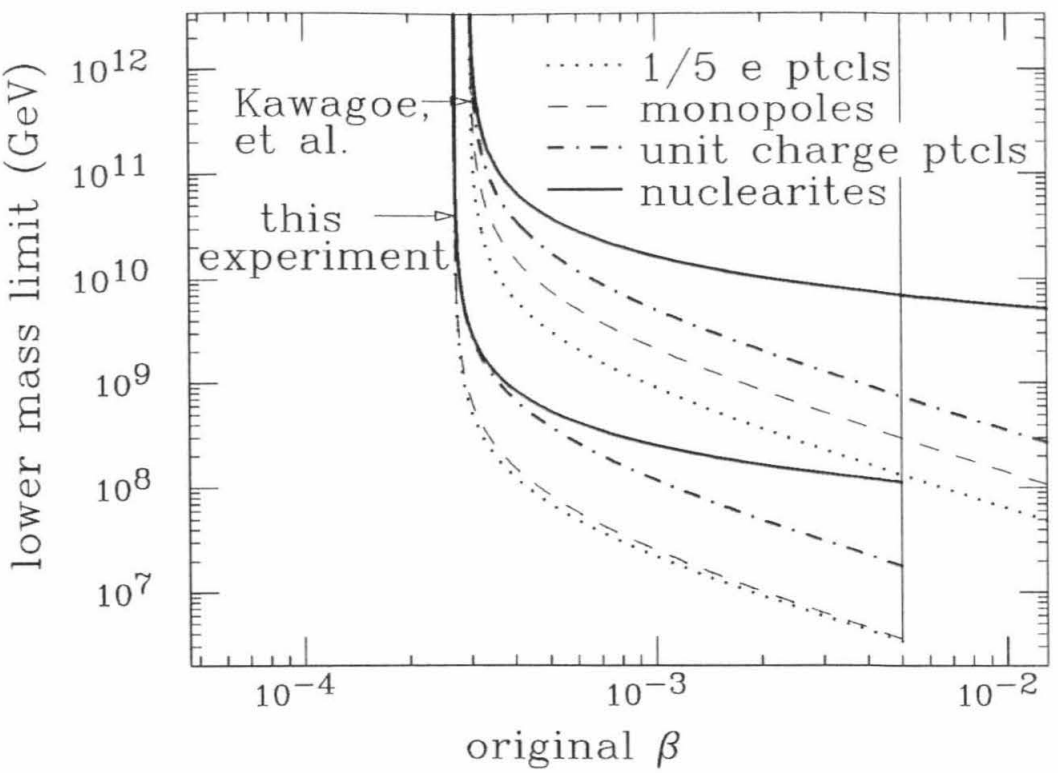

Fig. 3.5.1 — The lower mass limit versus the original β of various SIMPs that can reach our detector and have β within its β acceptance. The similar limit of the experiment in Kamioka Mine is also drawn for comparison.

curves according to the stopping power formulas discussed in Chapter 1, using the average values of $Z_2 = 7.3$ $M_2 = 14.7m_p$ for the atmosphere and $Z_2 = 12.2$ $M_2 = 24.7m_p$ for Earth's crust. Our experiment is calculated as a 60cm deep "underground" experiment to account for the concrete building above the detector. Note that our experiment is sensitive to particles having masses two orders of magnitude lower than those accessible to underground experiments.

Table 3.5.1 is a compilation[14] of the upper flux limits of several experiments on Earth's surface that have similar a β range and ionization sensitivity to this experiment. The ionization threshold I_{thr} is shown in units of minimum ioniz-

Table 3.5.1 — Flux Limits from Surface Experiments (90% c.l.)

experiment	I_{thr}	β range	flux limit
BNL (p)	2.0	$3 \times 10^{-4} - 1.2 \times 10^{-3}$	3.4×10^{-11}
Tokyo (s)	1.2	$10^{-2} - 0.1$	1.5×10^{-11}
Tokyo (s)	0.025	$2 \times 10^{-4} - 5 \times 10^{-3}$	1.5×10^{-11}
BNL-Brown-KEK (s)	0.3	$10^{-3} - 0.2$	5.2×10^{-12}
Tokyo(Kajino) (sp)	1/20	$10^{-4} - 10^{-2}$	1.6×10^{-12}
Akeno (p)	10	$7 \times 10^{-4} - 1$	1.2×10^{-13}
Indiana-Berkeley (s)	0.6	$6 \times 10^{-4} - 2.1 \times 10^{-3}$	9.4×10^{-13}
This experiment (s)	1/3	$2.7 \times 10^{-4} - 5 \times 10^{-3}$	4.7×10^{-12}

ing muons and the letter in the brackets after each experiment name indicates whether it uses proportional counters (p) or scintillator detectors (s), or both (sp).

For superheavy particles, the result of this experiment does not improve on the limit set by Kajino *et al.* in any β region, However, for the more relevant "medium heavy" particles that cannot penetrate deep underground, their limit (and others) must be reconsidered. It must be immediately doubled since their acceptance for up-going particles is no longer relevant. In addition, their detector had sensitivity mainly to large zenith angles because of the geometry using vertical layers. This greatly reduced the sensitivity to medium heavy particles, since they must pass through a large amount of matter to reach the detector. Furthermore, because of the 3m iron absorber between the layers, medium heavy particles could be slowed considerably in the detector and be thrown away in the analysis which essentially looked for objects with constant velocity. The same arguments apply to the limit of the BNL-Brown-KEK experiment since it also

uses vertical layers. The limit from the Indiana-Berkeley experiment must also be doubled, because of their up-going acceptance, making their limit comparable to this experiment but with somewhat different β coverage and ionization threshold as shown in Table 3.5.1. Lastly, the experiment in the Akeno Air Shower Observatory has yielded a limit one order of magnitude lower than this experiment but only for particles exceeding their ionization threshold, which is 30 times higher.

Since medium heavy particles stop in matter, our flux limit might also be compared with the results of searches in bulk matter. There is no bulk matter limit for electrically charged particles that is comparable to our flux limit, but monopole searches in lunar rock and iron ores are very sensitive, and much lower flux limits have been reported[15]. The results of these bulk matter searches, however, are actually limits on the monopole density in certain samples. To interpret the results in terms of a monopole flux limit in cosmic rays, many assumptions are necessary regarding the age of the samples, how deep they have been buried, whether or not they have been heated in their entire history over a few million years, etc., and therefore the results should be regarded as indirect.

Experiments using track etch techniques[16-18] have also been reported with very impressive flux limits. Such techniques, however, are sensitive only to highly ionizing particles ($\sim 30 I_{min}$); therefore, the results are often quoted as having a low β cutoff in the order of 10^{-2}, although there are arguments[19] suggesting that such techniques may be sensitive to particles as slow as $\beta = 3 \times 10^{-5}$.

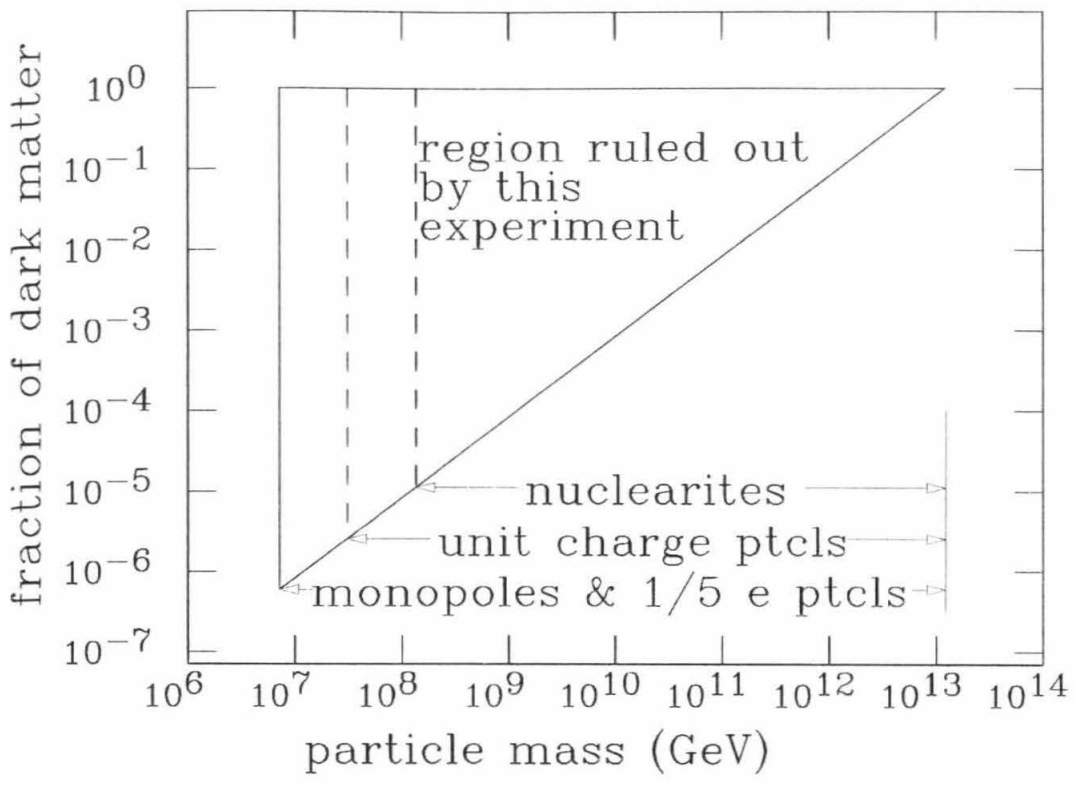

Fig. 3.5.2 — The limit of the fraction of the dark matter that can be attributed to massive charged particles, as a function of mass.

In summary, the limit presented here represents a flux limit for any ionizing ($> \frac{1}{3} I_{min}$) medium heavy particles that can penetrate the atmosphere but not deep underground. After correcting other results for the sensitivity to such particles, none would be more sensitive than the result reported here, and none has been analyzed in such detail to address medium heavy particles, which are the only relevance of surface experiments when a much lower limit has been set by underground detectors.

A major implication of this result is that it can be used to address the dark matter of the universe. Assuming an isotropic flux and a nominal velocity of $3 \times 10^{-3} c$ for the dark matter, I calculated the upper limit of the fraction of the

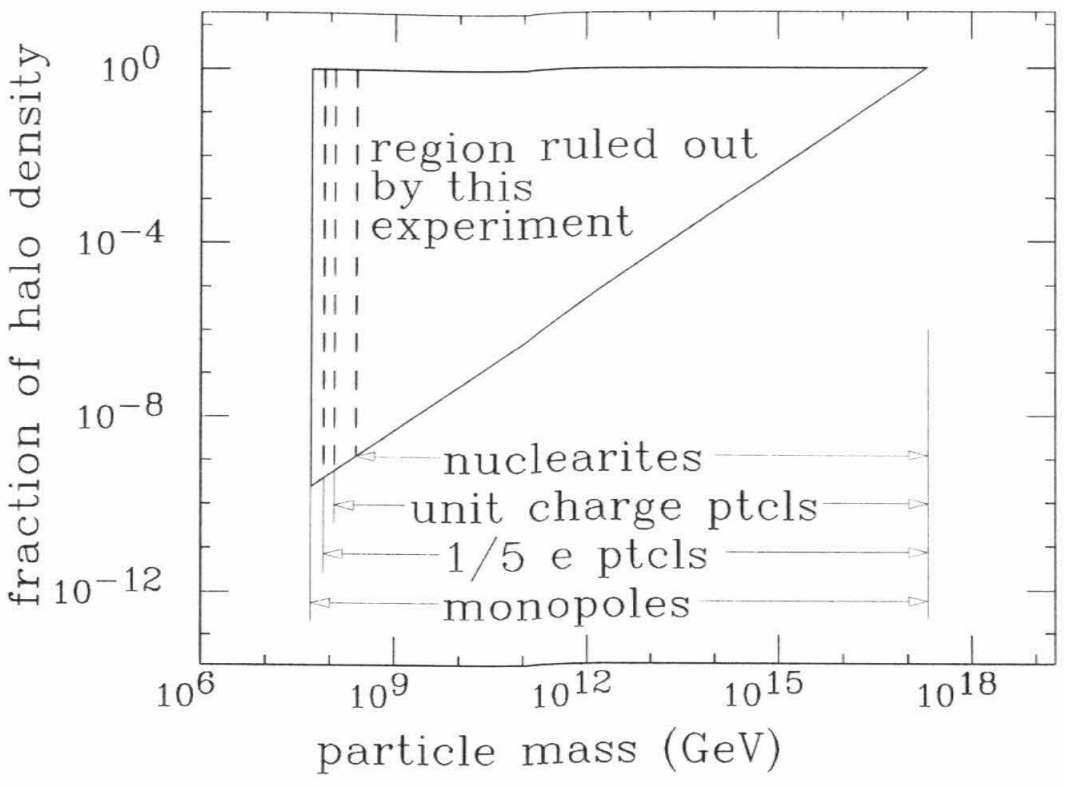

Fig. 3.5.3 — The limit of the fraction of the galactic halo that can be attributed to massive charged particles, as a function of mass.

dark matter that can be attributed to charged massive particles, as implied by our flux limit (Fig. 3.5.2). Lower mass cutoffs for different particles are determined using the stopping power models mentioned in Chapter 1, and the detector's β acceptance is truncated at 6.5×10^{-4} for monopoles and at 8×10^{-4} for 1/5 charge particles in accord with the conservative light yield estimation in Ref. 5. It is obvious that the major dark matter component cannot be monopoles or 1/5 charge particles with mass $7 \times 10^7\,\mathrm{GeV} < M < 10^{12}\,\mathrm{GeV}$, nor can it be unit charge particles with $3 \times 10^7\,\mathrm{GeV} < M < 10^{12}\,\mathrm{GeV}$ or nuclearites of $1.4 \times 10^8\,\mathrm{GeV} < M < 10^{12}\,\mathrm{GeV}$. For some particles and certain mass, a fraction as low as 10^{-6} has been excluded.

Similar limits for the halo dark matter are even more stringent. Fig. 3.5.3 shows such limits, calculated assuming an isotropic flux and a nominal velocity of $10^{-3}c$. Because of many uncertainties in the density, velocity and direction of the dark matter, Figs. 3.5.2 and 3.5.3 should be regarded as a rough estimation and give only the correct order of magnitude.

References of Chapter 3

[1]S. P. Ahlen, G. Tarlé, Phys. Rev. D **27**, 688 (1983).

[2]S. Drell, N. Kroll, M. Mueller, S. Parker and M. Ruderman, Phys. Rev. Lett. **50**, 644 (1983).

[3]S. P. Ahlen, *Monopole '83* (Proceedings of Monopole '83 Workshop Oct. 6-9 1983 at Ann Arbor, Mich., ed. J. L. Stone), page 629 (Plenum Press, New York, 1984).

[4]S. P. Ahlen, T. M. Liss, C. Lane and G. Liu, Phys. Rev. Lett. **55**, 181 (1985).

[5]D. J. Ficenic, S. P. Ahlen, A. A. Marin, J. A. Musser and G. Tarlé, Phys. Rev. D **36**, 311 (1987).

[6]A. De Rújula and S. L. Glashow, Nature **312**, 734 (1984).

[7]The data acquistion system and on-line computer programs are due to the work of C. Lane. See C. Lane, *GUT Monopole Detection With Scintillator*, Ph.D. thesis, California Inst. of Tech. (1987).

[8]E. N. Alexeyev *et al.*, Lett. Nuovo Cim. **35**, 413 (1982).

[9]K. Kawagoe, T. Mashimo, S. Nakamura, M. Nozaki, and S. Orito, Lett. Nuovo Cim. **41**, 315 (1984); T. Mashimo, S. Orito, K. Kawagoe, S. Nakamura, and M. Nozaki, Phys. Lett. **128B**, 327 (1983)

[10]R. Farouki, S. L. Shapiro and I. Wassermen, Astrophys. J. **284**, 282 (1984).

[11]J. Arons and R. D. Blanford, Phys. Rev. Lett. **50**, 544 (1983).

[12]B. Cabrera, Phys. Rev. Lett. **48**, 1378 (1982).

[13]M. Chown, New Scientist **108**, 11 (1985).

[14]G. Tarlé, S.P. Ahlen and T.M. Liss, *Monopole '83*, page 551; F. Kajino, S. Matsuno, Y.K. Yuan, and T. Kitamura, *Monopole '83*, page 589; Philip L. Connolly *Monopole '83*, page 617; T. Hara, *et al.* Phys. Rev. Lett. **56**, 553 (1986) and the rewiew article of G. Giacomelli *Monopole '83*, page 637. Note that the published limit of the Indiana-Berkeley experiment is a single event significance, but it is mistaken as having 90% confidence level in G. Giacomelli's review article. It is corrected here.

[15]R. R. Ross, P. H. Eberhard, L. W. Alvarez, and R. D. Watt, Phys. Rev. D **8**, 698 (1973); T. Watanabe and T. Ebisu *Monopole '83*, page 503.

[16]K. Kinoshita and P.B. Price, Phys. Rev. D **24**, 1707 (1981).

[17]S.W. Barwick, K. Kinoshita and P.B. Price, Phys. Rev. D **28**, 2338 (1983).

[18]S. P. Ahlen, P.B. Price, S. Guo and R.L Fleisher, *Monopole '83*, page 383.

[19]P.B. Price, Phys. Lett. **140B**, 112 (1984).

Chapter 4

Future Searches — the MACRO Experiment

The MACRO detector[1] (Monopole, Astrophysics and Cosmic Ray Observatory), now being built in the Gran Sasso Laboratory in Italy, will soon be the world's largest SIMP search detector. The present design of the detector consists of three layers of thick (25 cm) scintillator planes, 18 layers of streamer tubes and one layer of track etch detector, enclosed on the four sides by one layer of vertical scintillator plane and five layers of vertical streamer tubes. With an acceptance of over 10000 m^2sr, the detector can reach a flux sensitivity of 10% of the Parker bound[2] after five years' running, and can rule out any electrically and/or magnetically charged particles with mass below 10^{17}GeV as the major component of the dark matter of the universe. In this chapter, I report the work I have done toward developing this future SIMP search detector.

4.1. The Test of the First MACRO Scintillator Counter Prototype

The MACRO scintillator detector will utilize about $1000m^3$ of liquid scintillator contained in 484 counters. Each counter is a 12m long PVC tank lined inside with FEP teflon and viewed by 8 inch hemispherical PMTs at both ends. The counters in the three horizontal layers have a cross section of 75cm × 25cm and those in the vertical layers, 25cm × 50cm. FEP teflon has a refraction index of 1.33, giving the teflon-oil interface a total reflection angle of about 23°.

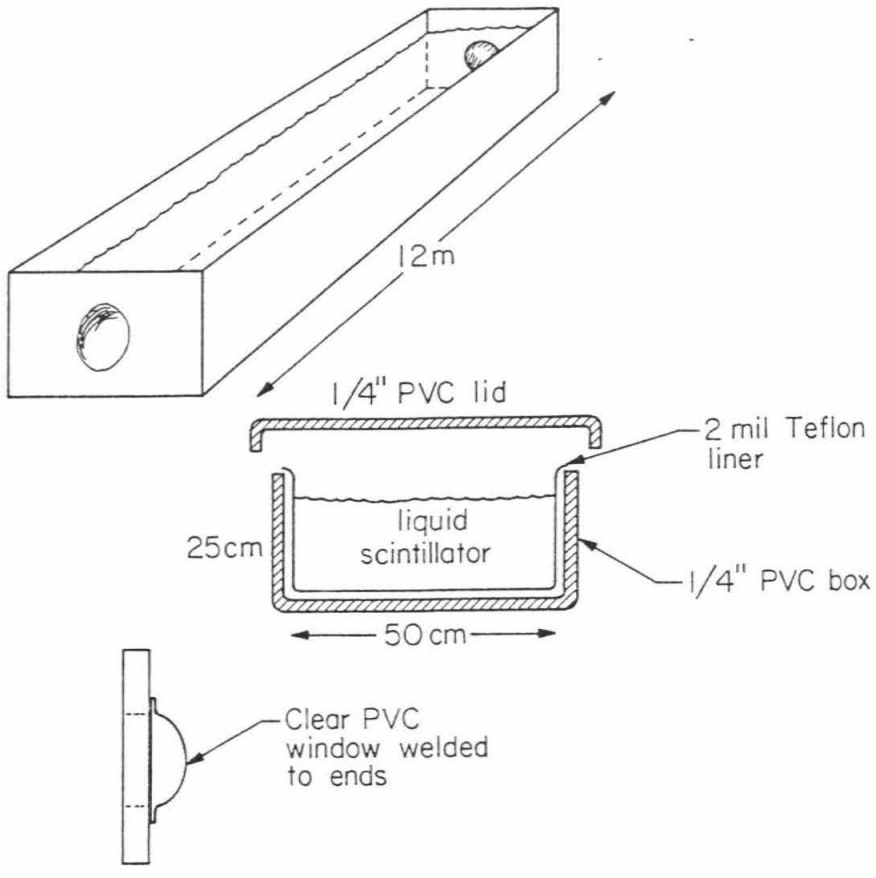

Fig. 4.1.1 — The first prototype of the MACRO scintillator counter built at Caltech.

In order to achieve MACRO's physics goals, the scintillator counters must meet very special requirements. It must have high light level and long attenuation length so that a low energy event (5MeV, say) occurring near one end of the counter can be seen at the opposite end. Seeing by both ends is necessary to determine the energy and the position of the event. The MACRO scintillator counters must also have good time resolution in order to distinguish up-going and down-going cosmic rays and to determine the position of an event by the time difference of the signals from the two ends of the counter.

The first prototype of the MACRO scintillator counter was a box 12m long

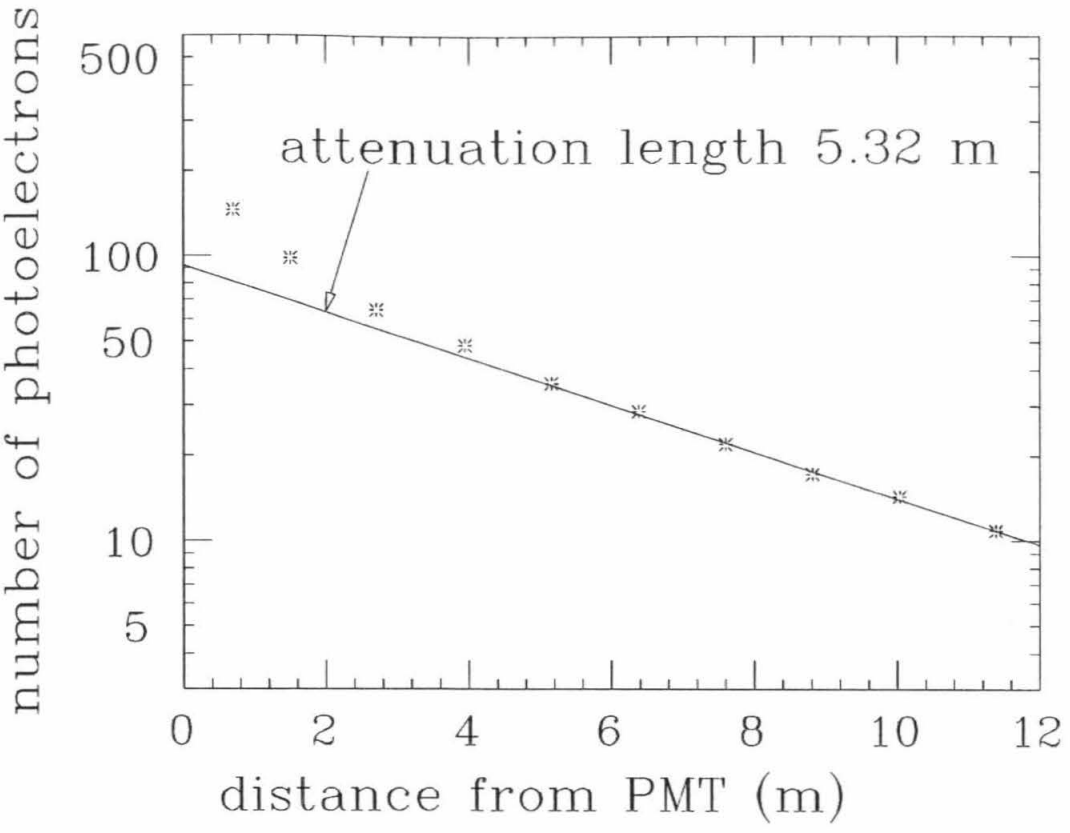

Fig. 4.1.2 — The light level of cosmic ray muons versus distance, measured on the first prototype of the MACRO scintillator counters. After various improvements, the expected light level of the present design is a factor of 10 higher than these data.

and 50cm wide containing 25cm high liquid scintillator with two 8 inch PMTs coupled to the two ends (Fig. 4.1.1). Figure 4.1.2 shows the light level I measured for cosmic ray muons penetrating at various distances from one end of this prototype. Except for the nearest 2 meters, the data points lie very close to a straight line corresponding to an "attenuation length" of 5.3m. Since this first light level measurement, various improvements have been made or proposed, and now the light level of the present design of the MACRO counter is expected to be about a factor of 10 higher than that shown in Figure 4.1.2. This means that a minimal ionizing muon crossing one end of the counter can produce more than

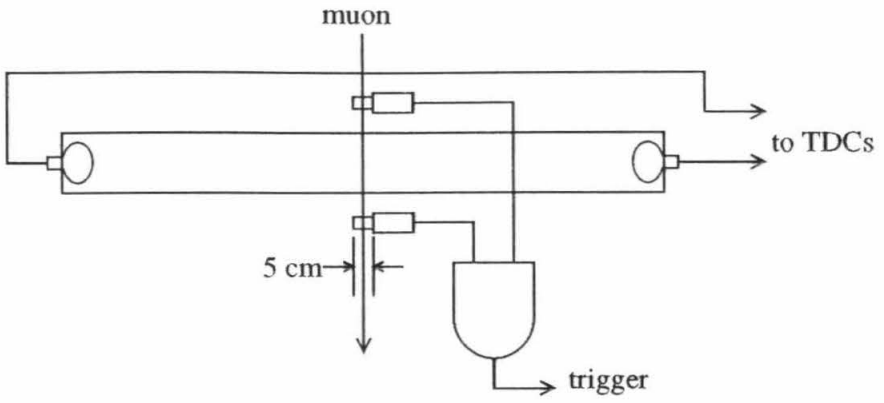

Fig. 4.1.3 — The setup for measuring the time resolution of the MACRO prototype counter.

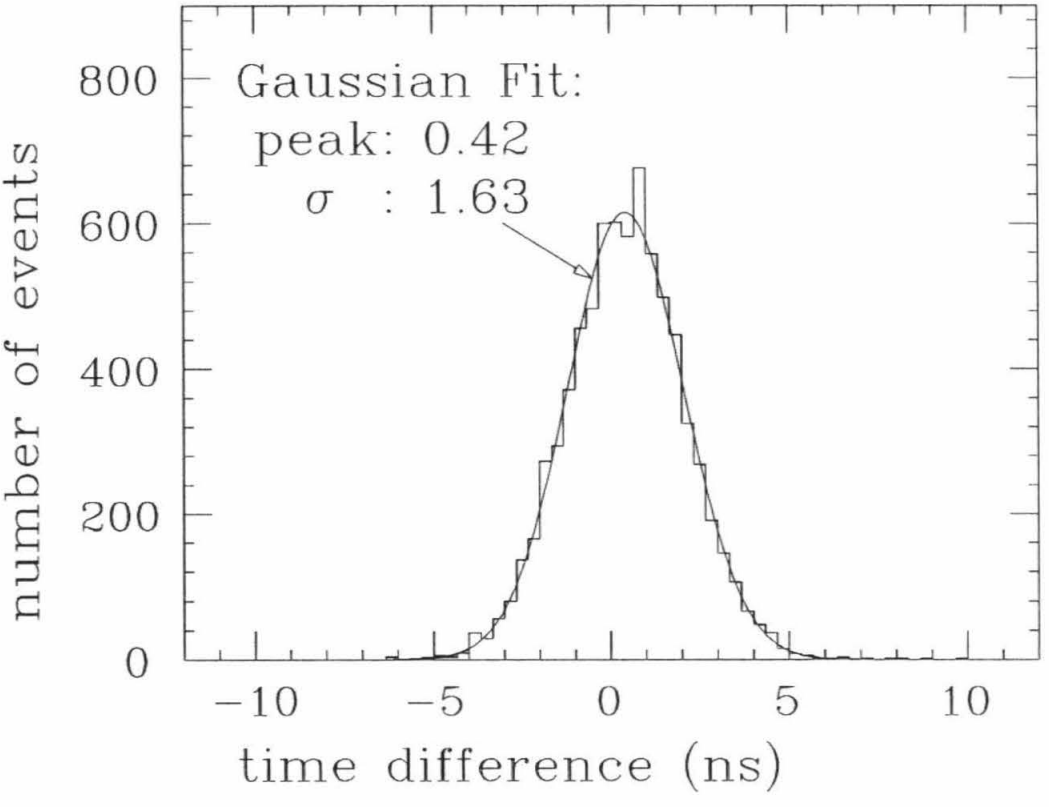

Fig. 4.1.4 — The histogram of the time difference between the two ends of the counter.

100 photoelectrons at the opposite end.

I also measured the timing characteristics of the counter, using cosmic rays. The setup of this measurement is shown in Fig. 4.1.3. Two small scintillators

5cm wide placed at the center of the MACRO counter, one above and one below, were used to trigger a data acquisition system which recorded the time of the signal from each end of the counter. The histogram of the time difference between the two ends is shown in Fig. 4.1.4. The σ of the distribution is 1.63ns. Since this jitter includes the contributions of both ends, the jitter of each end is about $1.63\text{ns}/\sqrt{2} = 1.15\text{ns}$.

Such a time resolution allows one to determine the position of an event according to the time difference between the signals from the two ends. Since the effective light speed in the counter has been measured to be 18.5cm/ns, a time difference resolution of 1.63 ns corresponds to a position resolution of about 15cm. Using the time difference to determine position, I measured the attenuation length of the counter in another way. The setup is shown in Fig. 4.1.5. The coincidence of the two ends of the counter was used to trigger the data acquisition system, which then recorded the time and pulse height of the signal from each end. The ratio of the pulse height from the two ends versus the time difference is shown in Fig. 4.1.6. The linear regression of the central part of Fig. 4.1.6 gives a straight line of slope 0.0343 ns^{-1} corresponding to 5.4m attenuation length, which agrees with the measurement mentioned earlier.

The time resolution of the prototype also made it possible to measure the time of flight of cosmic ray muons. The test setup is shown in Fig. 4.1.7. A pair of small scintillators were put close to each other and 4.5 m below the MACRO prototype (the same distance as the separation of the scintillator planes of the

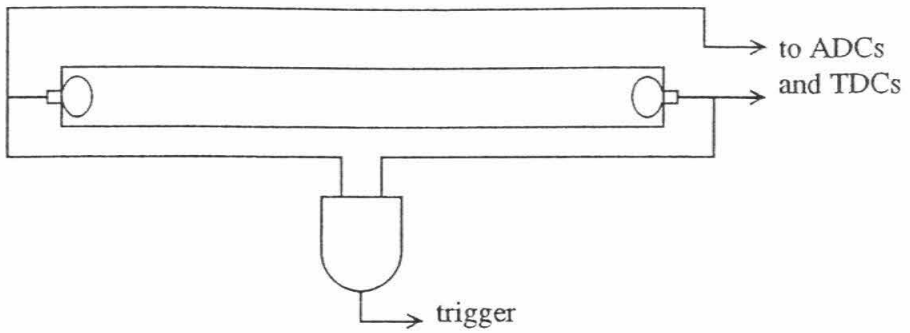

Fig. 4.1.5 — A way to measure the attenuation length using timing to determine position.

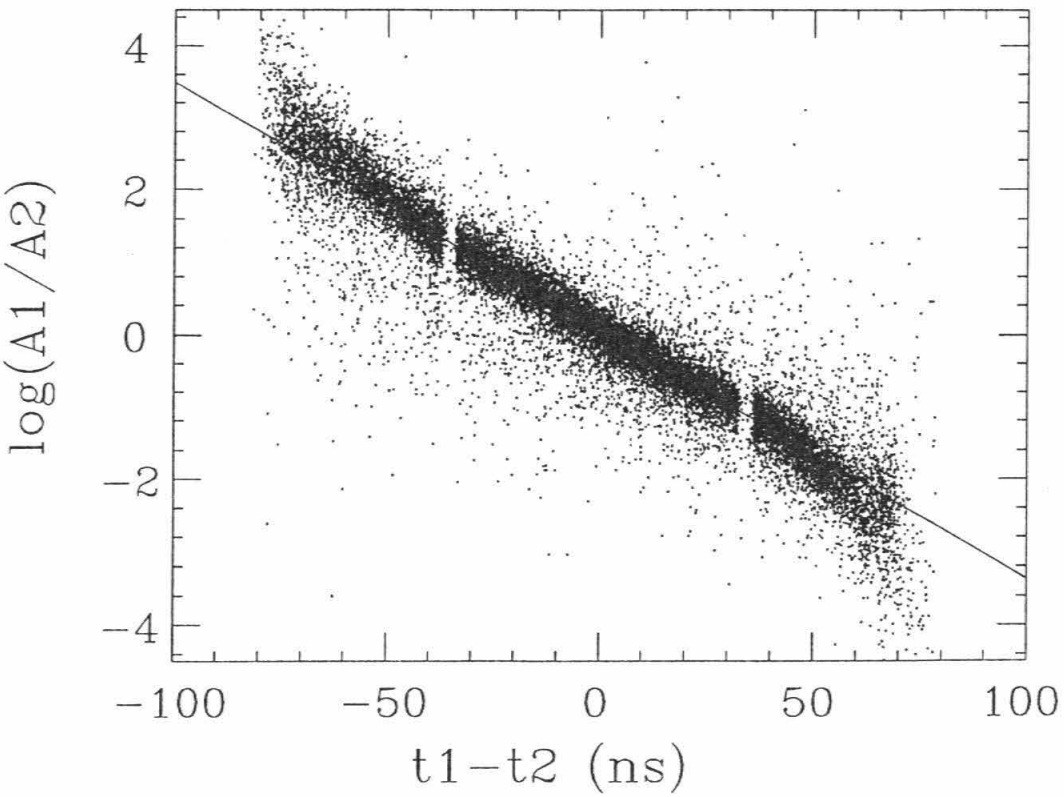

Fig. 4.1.6 — The scatterplot of the ratio of the pulse height from the two ends versus the time difference. The straight line is the linear regression of the central part of the scatterplot, corresponding to 5.4m attenuation length.

MACRO detector). The trigger was produced by the coincidence of the MACRO prototype with the two small scintillators, and the time and pulse height of the signals from all the PMTs were recorded. Using the time differences of the signals

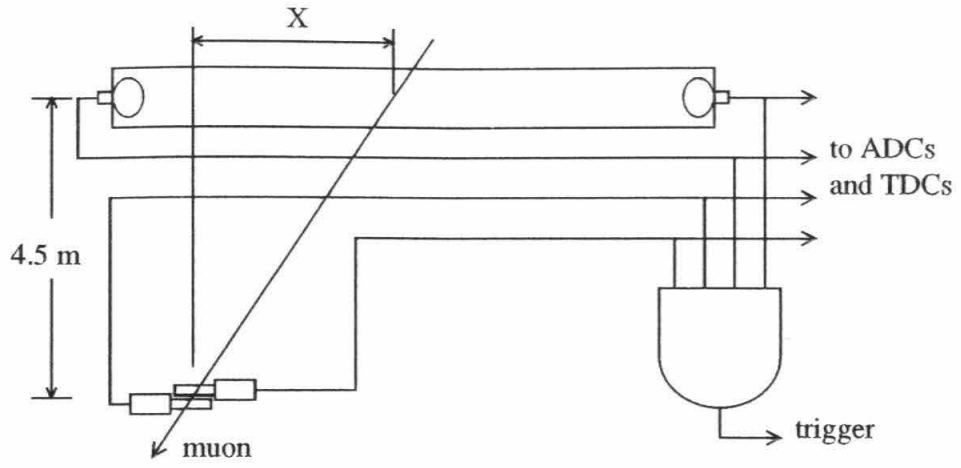

Fig. 4.1.7 — The setup for measuring the time of flight of cosmic ray muons.

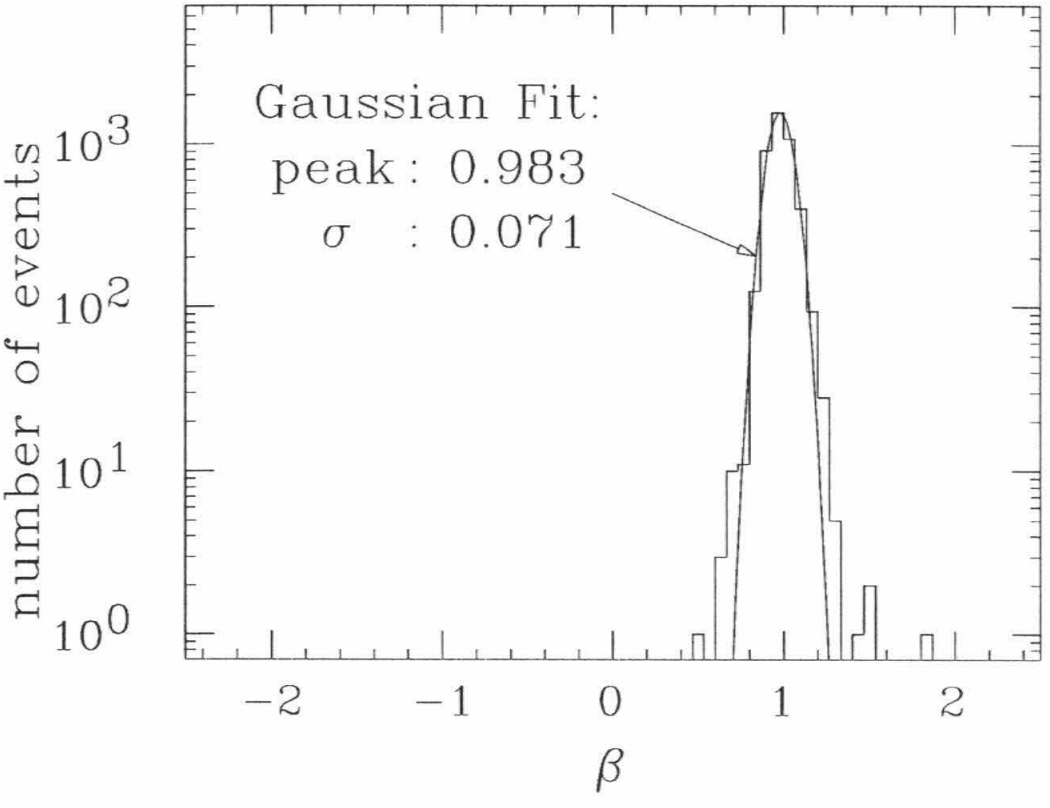

Fig. 4.1.8 — The measured β of the cosmic ray muons. It is obvious that the MACRO counter is capable of distinguishing up-going ($\beta = -1$) and down-going ($\beta = 1$) muons.

to determine the time of flight and the horizontal distance X, the velocity of the muons can be calculated. The measured β of the muon events from a 10 hour run

is shown in Fig. 4.1.8. The σ of this distribution agrees exactly with the value calculated according to the 1.15 ns time jitter of the MACRO prototype counter. It is obvious that the MACRO counter is capable of distinguishing up-going and down-going muons. Up-going muon events correspond to $\beta = -1$ in Fig. 4.1.8; none has been observed in the 10 hour run.

To summarize, the test of the prototype has shown that the MACRO scintillator counter has adequate light level and time resolution to achieve its physics goals, including SIMP detection.

4.2. Slow Particle Trigger of MACRO Detector

Because of the wide range of the possible velocity and ionization of various SIMPs, developing triggering electronics for them presents a very special challenge. Unlike the usual particle detection, which often uses fast coincidences to generate triggers, there is no such coincidence available for SIMPs. The delayed coincidence scheme for the search described in the last chapter could be used in MACRO, but it would not work as well since MACRO has only three scintillator planes. On the other hand, each layer of MACRO's scintillator counters are made 25cm thick, giving another handle on the passage of a slow particle. A SIMP needs a much longer time ($\sim 1\mu$s) to cross each scintillator layer compared with usual relativistic particles and therefore can be recognized by the *duration* of its signal.

Although this feature is very clear, the task of using it to generate triggers is not trivial, because of the extremely wide range of possible β and ionization

of various SIMPs.

At the high β end, in order to connect the β range of the SIMP trigger to that of the fast particle trigger, β as high as 10^{-2} should be covered. At this β, a SIMP produces a large pulse of ~ 83 ns wide.

For the low β region, if possible, one would like to extend it to include the earth's escape velocity ($\beta = 3.7 \times 10^{-5}$) and even the orbital velocity around the earth ($\beta = 2.6 \times 10^{-5}$). Although the scintillation yield at such extremely low β is not well understood, there are indications that this goal may be achievable at least for some species of SIMPs. If one extrapolates the dyon's dL/dx curve from the recent low β scintillation experiment[3] down to $\beta = 2.6 \times 10^{-5}$, it gives a light yield about 1/10 of the minimal ionizing muons. A unit charge particle is expected to have a light yield 4/5 of that of a dyon; higher charged particles, including nuclearites, may produce a much higher light yield. For the central 3/5 of the total length of the counter, a crossing particle with $\beta = 2.6 \times 10^{-5}$ and $I = \frac{1}{10} I_{min}$ produces for each end of the counter a pulse train 32μs long containing 16 to 60 single photoelectron pulses. Note that the pulse rate in such a train is at least 20 times the typical noise rate (25kHZ) of the counter measured in the Gran Sasso tunnel, and the probability that such pulse trains arise from random noise fluctuations is extremely small.

The difficulty of the SIMP trigger is now obvious: it has to trigger on signals that are qualitatively different, ranging from a short pulse of 83ns to a long pulse train of 32μs containing only 16 single photoelectron pulses.

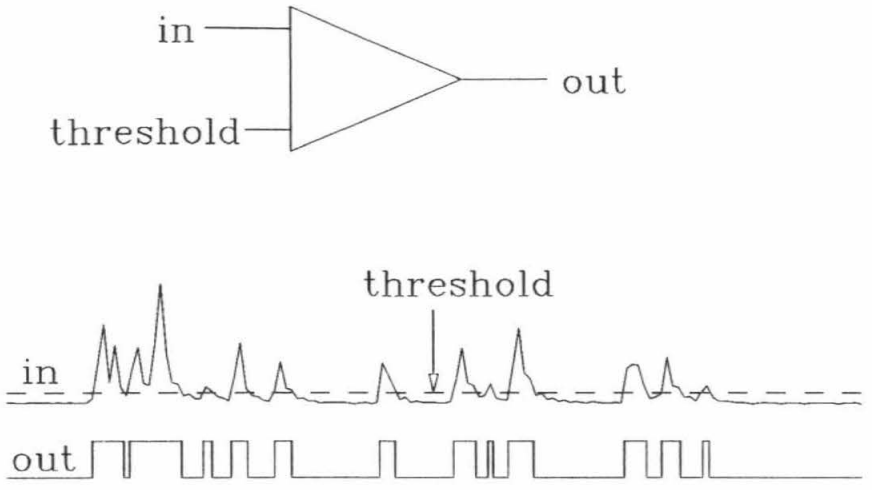

Fig. 4.2.1 — Time over threshold (TOT) discriminator.

The first trigger electronics that relies on the signal duration instead of on the time of flight to recognize SIMPs has been used in the Indiana-Berkerly monopole search experiment[4], where the pulse durations have been actually measured to generate triggers. This scheme, however, is not suitable for MACRO, because it cannot trigger on pulse trains of very low β particles.

A circuit that triggers on pulse trains has been proposed by M. Severi *et al.*[5] This circuit, however, has several problems making it not optimal for the MACRO detector. The Severi circuit works as the following: First, a time over threshold discriminator (TOT) set below the single photoelectron level converts the PMT signal to a series of logic pulses with variable widths and gaps (Fig. 4.2.1). Then, a digital circuit looks at the gaps and the train lengths of the TOT signal. Whenever it finds a train longer than a given value T_0 in which no gaps larger than the "gap threshold" t_0 have ever occurred, a trigger is generated. A single pulse lasting for longer than T_0 is itself a qualified train and can cause a trigger.

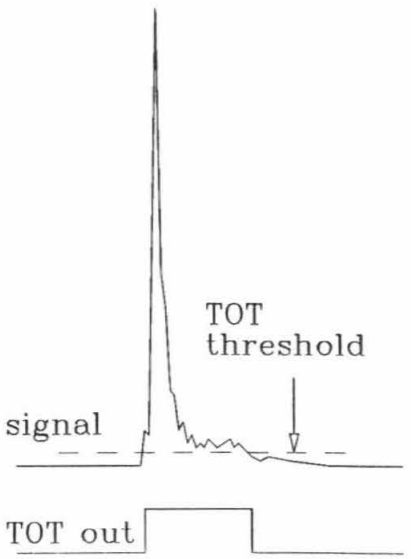

Fig. 4.2.2 — Large muon or radioactivity pulses can be very wide at the single photoelectron level and give wide TOT outputs faking SIMP signals.

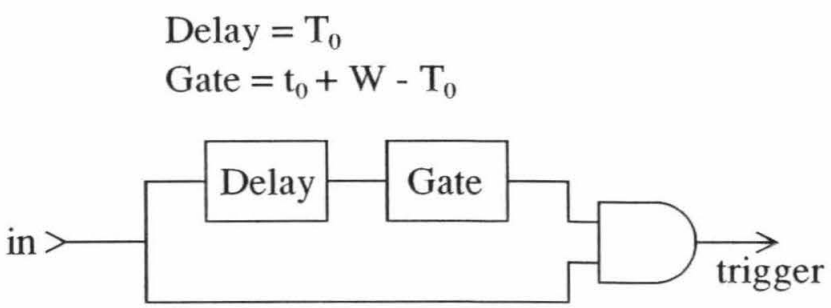

Fig. 4.2.3 — When the Severi circuit is set with $t_0 > T_0$, it is equivalent to this simple self-delayed coincidence logic with Delay $= T_0$ and Gate $= t_0 + W - T_0$, where W is the width of the single photoelectron TOT pulse.

The weakness of the Severi circuit is obvious. First, since the TOT threshold is set below the single photoelectron level, large muon or radioactivity pulses (200-2000 photoelectrons), although intrinsically narrow, can be very wide at the single photoelectron level and can give wide TOT outputs, faking relatively fast SIMPs (Fig. 4.2.2). The second problem of this circuit is a dynamical range problem due to the use of a *fixed* gap and train length criterion. As discussed above, a SIMP signal in the full region of $2.6 \times 10^{-5} < \beta < 10^{-2}$ and $I \geq 0.1 I_{min}$,

ranges from a short pulse of 83ns to a 32μs long pulse train containing 16 single photoelectron pulses spread with an average gap of 2μs. This immediately puts Severi's circuit into a dilemma, that the train length requirement T_0 has to be less than 83 ns while the gap threshold t_0 must be longer than 2 μs. In spite of the conceptual difficulty of imagining a pulse train having gaps larger than the total train length, one may technically set $t_0 \geq T_0$. However, in such a case, the Severi circuit would trigger on any two pulses close to each other to within t_0 and could be replaced by a much simpler "self-delayed coincidence" logic shown in Fig. 4.2.3. Such a loose trigger criterion is obviously very vulnerable to random noise. The Severi circuit is inherently incapable of covering the whole interesting β and ionization region and, when forced to do so, it becomes vulnerable to random noise and also becomes unnecessary because a much simpler self-delayed coincidence logic can have the same function.

In order to solve the problems of the Severi circuit, I proposed to the MACRO collaboration a new SIMP trigger circuit for the experiment. First, instead of TOT, I proposed that a TOHM (Time Over Half Maximum) discriminator should be used. This discriminator dynamically raises up its threshold to about half of the pulse peak and produces a logic output pulse with width equal to the time over half-maximum of the input pulse (Fig. 4.2.4). In order to treat the narrow single photoelectron pulses consistently, any pulse narrower than a minimal width W is extended to W and pulses wider than W are unaltered. The TOHM output is then sent to an integrator and discriminated at a certain level

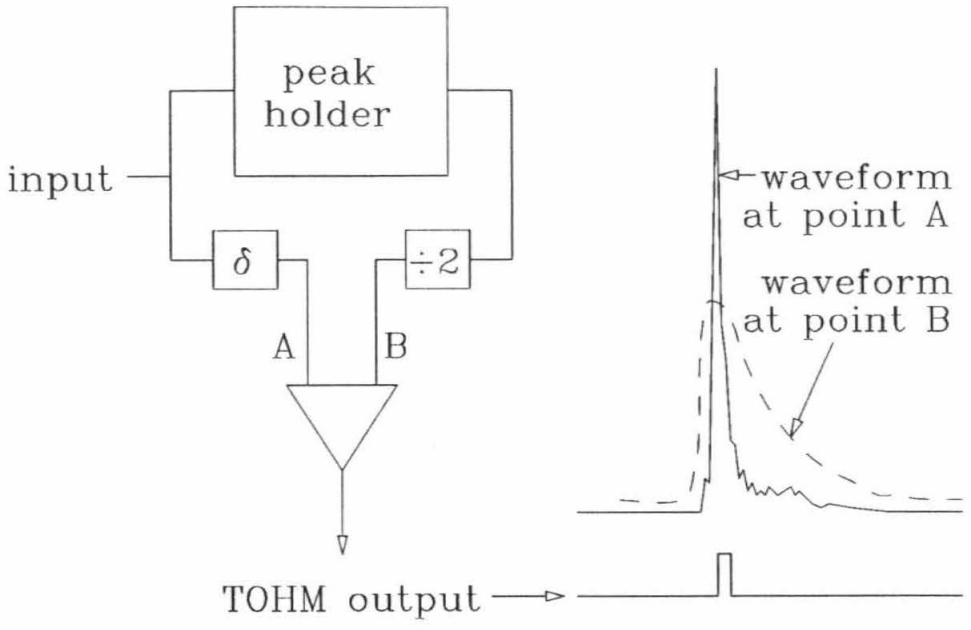

Fig. 4.2.4 — Time Over Half Maximum (TOHM) discriminator.

to generate SIMP triggers. The integrator can be an ordinary RC integrator or a digital version (Fig. 4.2.5). The digital version uses an up/down counter counted up and down with different rates (R_u and R_d) to simulate the charging and leaking processes of the RC circuit, and the trigger occurs whenever the content of the counter reaches a threshold value C_{th}. Since the leakage of the integrator here is not a shortcoming of the circuit, but rather an important feature that plays a crucial role, I call it "Leaking integrator" and the circuit "LI circuit."

The advantage of the TOHM discriminator is obvious. Since its output is independent of the pulse height and counts for only the half-maximum width, the signals of all prompt processes such as muons and radioactivity are greatly suppressed, while slow particle signals, which are widely spread in time, are amplified. For instance, a muon pulse of 300 photoelectrons may have a half-maximum width not much larger than W and gives the integrator only the same

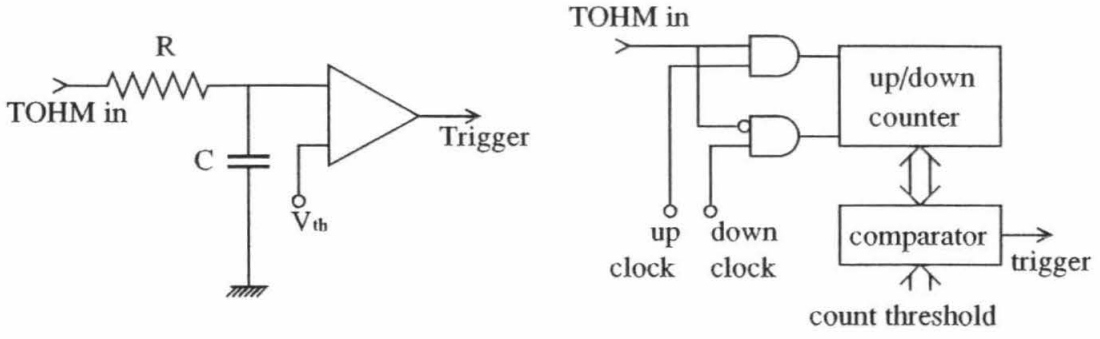

Fig. 4.2.5 — Analog and digital versions of the LI circuit.

amount of charge as a single photoelectron pulse. A preliminary test has shown that TOHM replacing TOT can improve the muon and radioactivity rejection rate by several orders of magnitude.

The advantage of the LI circuit is that it can solve the dynamical range problem of the Severi circuit. To show this, let us consider the analog version as an example. For a relatively fast SIMP, the TOHM output is a short pulse having the logic high level V_H and a duration equal to the particle's crossing time. Since the time needed for V_H to charge up the capacitor to the threshold V_{th} is

$$T_{min} = -RC\ln(1 - \frac{V_{th}}{V_H}). \tag{4.2.1}$$

The LI circuit acts as a discriminator on the *pulse width* or the particle crossing time.

For pulse trains lasting longer than RC, the integrator acts as a *rate meter*, and the LI circuit is a discriminator on the pulse rate with a *rate threshold*:

$$r_{min} = \frac{V_{th}}{V_H W}. \tag{4.2.2}$$

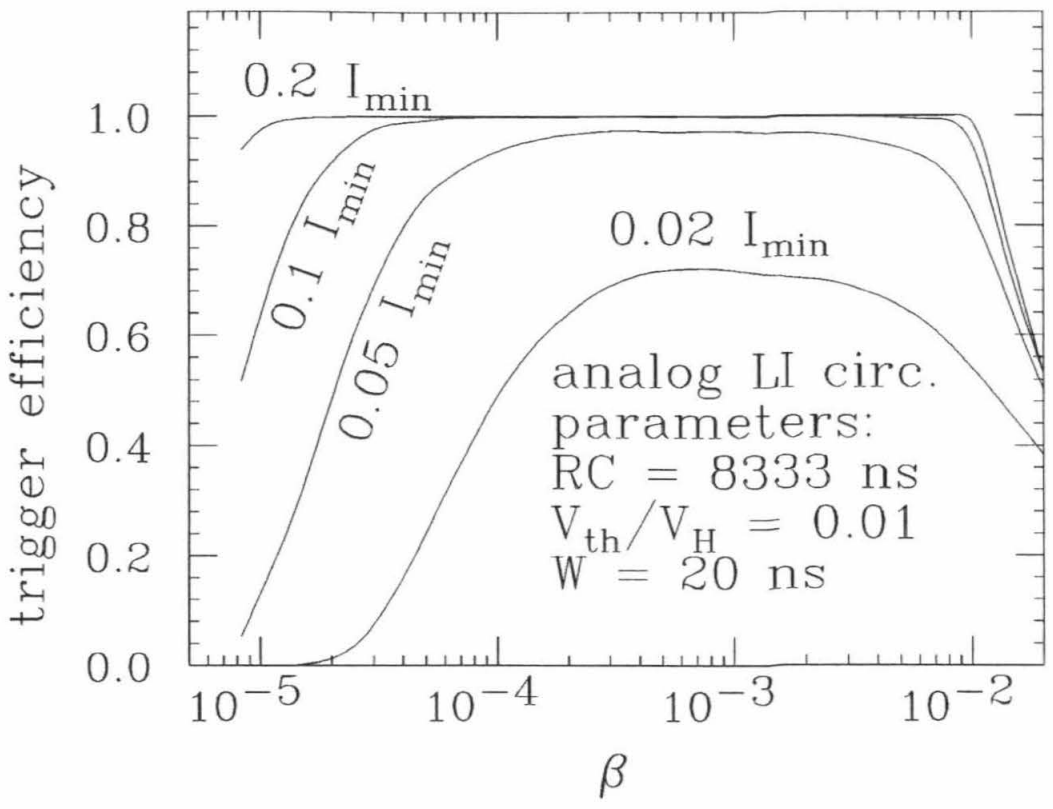

Fig. 4.2.6 — Trigger efficiencies using the analog LI circuits.

In order to trigger on a range of SIMP signals from a 16 pulse train of 32 μs long to a single pulse 83 ns wide, one only needs to set the parameters of the circuit so that T_{min} = 83 ns and r_{min} = 0.5 MHZ. This is easily accomplished by letting W = 20 ns, V_{th}/V_H = 0.01 and RC = 8.33 μs. With these parameter settings, I calculated the trigger efficiencies as a function of β and ionization, assuming that the trigger is generated by the coincidence of the two LI circuits, each connected to one end of the counter (Fig. 4.2.6). All the curves are calculated by a Monte Carlo program, assuming an isotropic particle flux, a response curve exponentially decaying by a factor of 10 from the near end to the far end and a light level of 100 photoelectrons for a minimal ionizing muon crossing the far

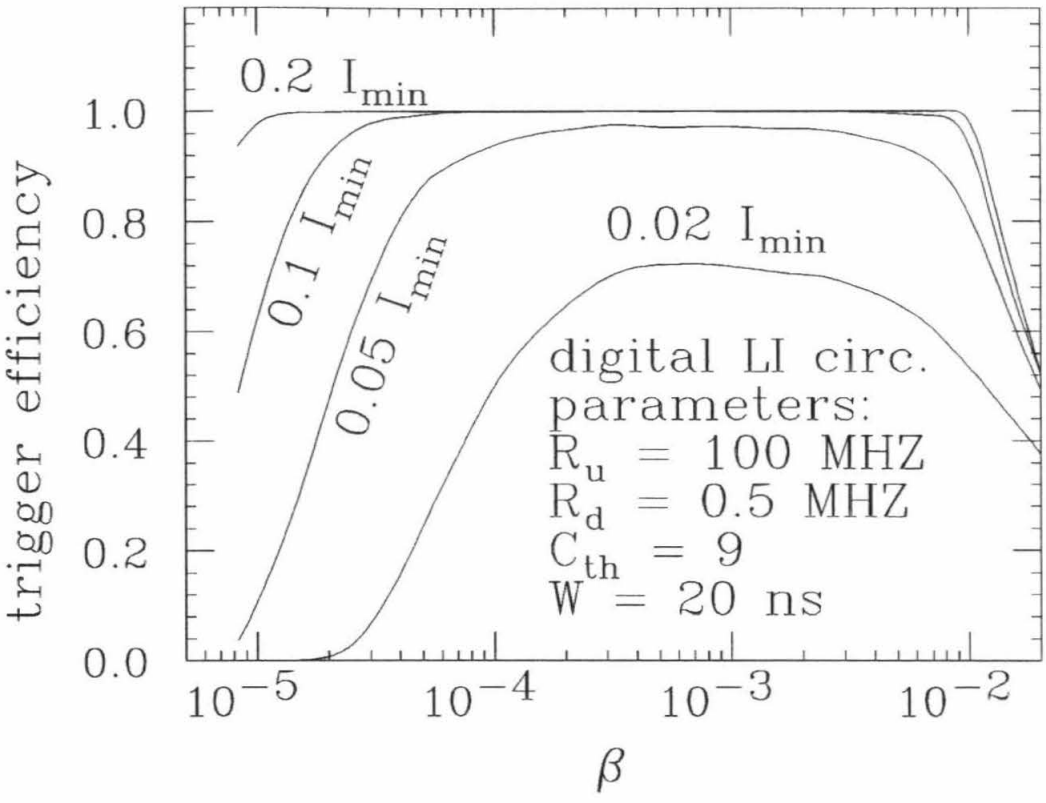

Fig. 4.2.7 — Trigger efficiencies using the digital LI circuits.

end. For $I \geq \frac{1}{10} I_{min}$, the whole range of $2.6 \times 10^{-5} < \beta < 10^{-2}$ is completely covered with efficiency close to 100%. The efficiency curves of the digital version (Fig. 4.2.7) are almost identical to those of the analog version, if the parameters of the circuits are chosen properly. In order to match those efficiency curves, the Severi circuit has to be awkwardly set with $t_0 > T_0$. Fig.4.2.8 is an example of such parameter settings and the corresponding efficiency curves.

With the same trigger circuit parameters used in generating the above efficiency curves, the background trigger rate is calculated as a function of the noise rate and is shown in Fig. 4.2.9. At the typical 25kHZ noise rate, the background trigger rate of the LI circuits is about 3 orders of magnitude lower than that of

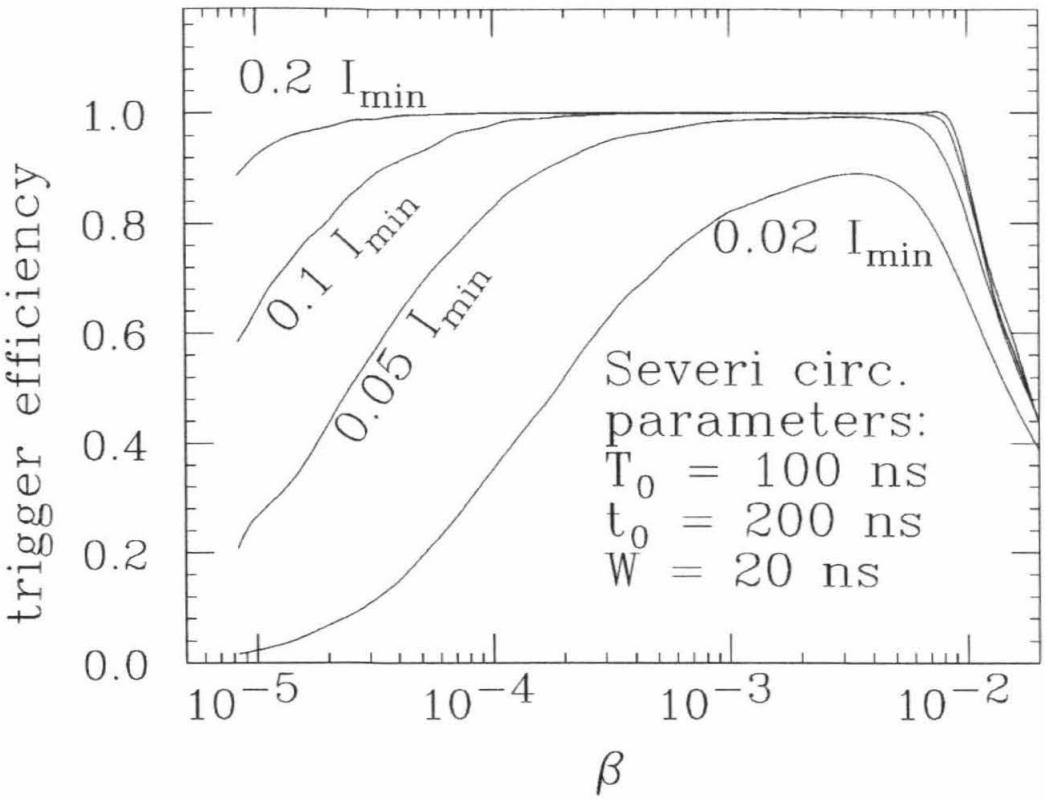

Fig. 4.2.8 — Trigger efficiencies using the Severi circuits with $T_0 < t_0$.

the Severi circuit. Even under a random noise rate of 50 KHZ, the background trigger rate from a single LI circuit is only an order of 1 HZ. The coincidence of the two circuits connected to the two ends of the counter may reduce the false trigger rate to a level of 10^{-6} HZ. Although the background may be highly correlated and the real background trigger rate may not be as low as calculated, it may still be low enough to be tolerable.

Fig. 4.2.10 shows what kind of new physics might be available when MACRO uses the LI circuit instead of the Severi circuit. The efficiency contours of the two circuits are drawn on the β versus ionization plane together with the extrapolated tails of the dL/dX curves from Ref. 3. In these contours, I have chosen the loosest

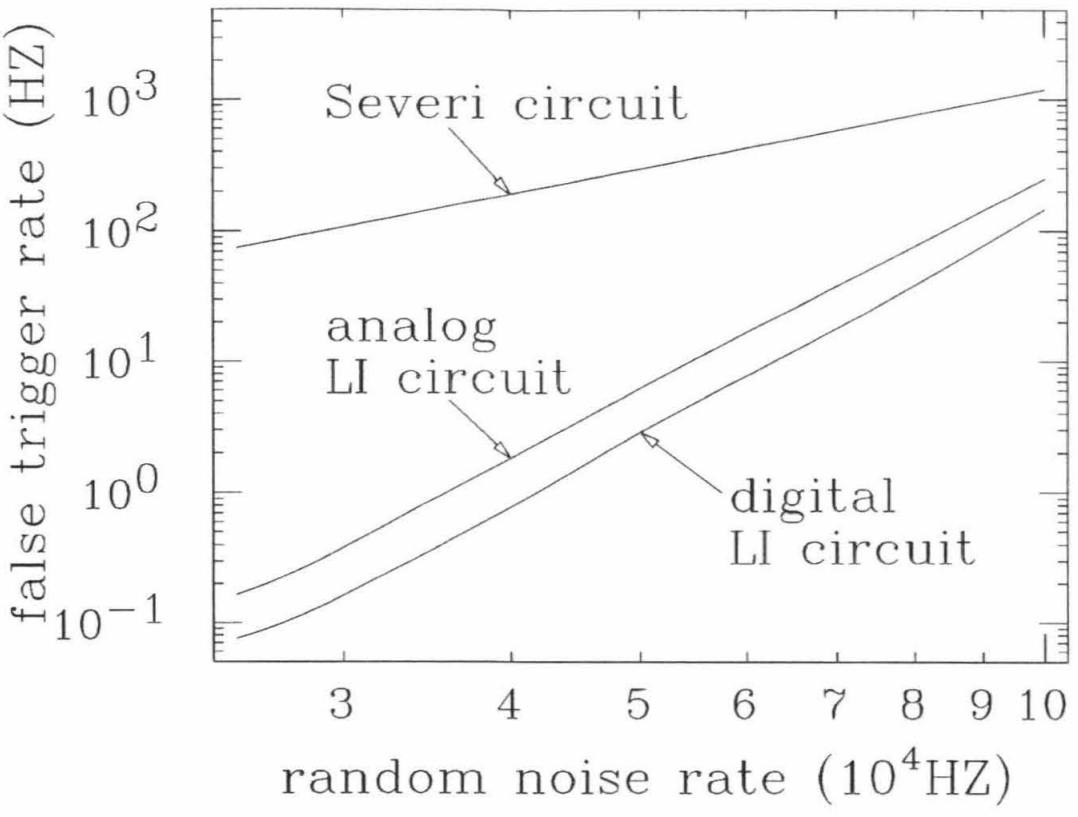

Fig. 4.2.9 — Background trigger rate of a single circuit as a function of the random noise rate. The trigger parameters are the same as in Figures 4.2.6, 4.2.7 and 4.2.8.

possible *genuine* parameters for the Severi circuit (not making it equivalent to a self-delayed coincidence logic) and have used the same LI circuit parameters as before. It can be seen from the graph, that the LI circuit trigger covers a β range of $2.3 \times 10^{-5} - 10^{-2}$ for dyons, comfortably containing Earth's escape velocity and the orbital velocity around Earth, while the coverage of the Severi circuit just misses these important velocities. For 1/5 charge particles, the LI circuit starts its coverage at $\beta = 1.1 \times 10^{-4}$, including the escape velocity of the sun, which is outside the coverage of the Severi circuit. It is also seen from the graph that, although there is a large difference in the ionization thresholds of the

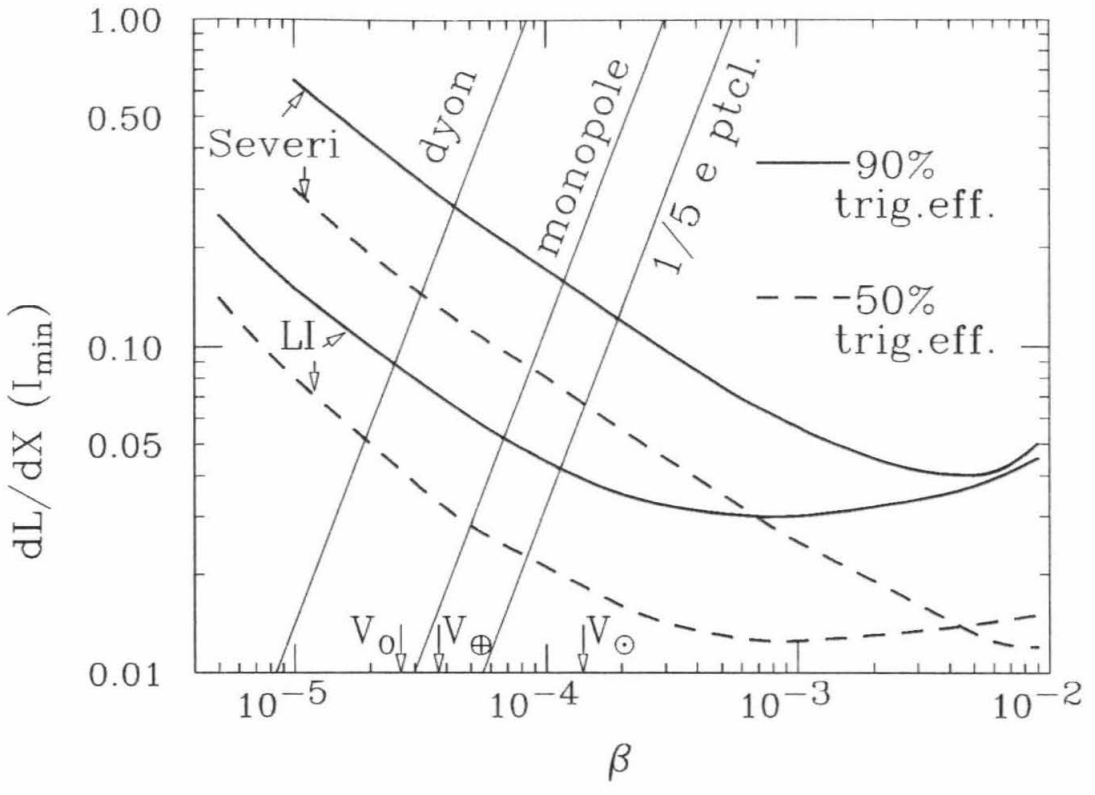

Fig. 4.2.10 — 50% and 90% efficiency contours drawn on the β versus ionization plane. The contours for the Severi circuit are generated using $T_0 =$ 100ns, $t_0 =$ 70ns, $W =$ 20ns. For the LI circuits, the same parameters as in Fig. 4.2.6 and Fig. 4.2.7 are used. Note that the digital and the analog LI circuits have the same efficiencies so that only one set of the contours is shown. The straight lines are the extrapolated tails of the dL/dX curves from Ref. 3. The escape velocities from Earth ($V_\oplus$) and from the sun ($V_\odot$) and the orbital velocity around Earth (V_o) are also indicated on the β axes.

two circuits, the difference in the β coverage is quite small (only a factor of 2) because of the steep cutoff of the particles' dL/dX curves. The dL/dX curves have been calculated by multiplying a nearly constant scintillation efficiency to the electronic stopping power and applying a steep "adiabatic correction factor" (see Ref. 3). Such an "adiabatic correction factor" has been added in an *ad hoc* fashion and it is just as plausible to fit the data and extrapolate them with a much less steep function, such as a power law[6]. The nuclear stopping power that

dominates at low β may also contribute some light yield and make the dL/dX curves even less steep. For all these reasons, I consider it very likely that the actual dL/dX tails are much less steep than those shown in Fig. 4.2.10, and that the difference in the β coverage of the two circuits is much larger.

If an acceptable background trigger rate can be obtained in the real conditions for the above LI trigger parameters, the conclusion is very impressive. When the new trigger circuit is used, MACRO may have the sensitivity for all conceivable SIMPs having a velocity as low as the escape velocity of the sun and for some species it is even sensitive to the orbital velocity around Earth. Since this is the lowest velocity possible for SIMPs, the MACRO experiment may provide an *exhaustive* search for these SIMP species over the whole conceivable β range.

References of Chapter 4

[1] *Proposal for a Large Area Detector Dedicated to Monopole Search, Astrophysics, and Cosmic Ray Physics at the Gran Sasso Laboratory*, by MACRO Collaboration (1984).
[2] Ref. 19-20 of Chapter 1.
[3] Ref. 5 of Chapter 3.
[4] G. Tarlé, S.P. Ahlen and T.M. Liss, *Monopole '83*, page 551.
[5] W. Pecorella, L. Petrillo, G. Salina, M. Severi, Nucl. Instrum. Methods **A23**, 566 (1985).
[6] C. Lane, *GUT Monopole Detection With Scintillator*, Ph.D. thesis, California Institute of Technology (1987).

Chapter 5

Conclusions

The conclusions of this work are the following:

1) The acoustic signal produced by a particle traveling through matter is reliably calculated, taking into account the heat conduction, the finite velocity of the particle and the size of the heat source it produces. These effects are explicitly evaluated and in certain cases they are *proven* to be negligible.

2) The method of acoustic detection of Slow-moving Ionizing Massive Particles (SIMPs) in an *infinite medium* is severely limited by thermal noise. Although such techniques could be made sensitive to particles like nuclearites having extremely large dE/dx, for other SIMPs, the thermal noise would dominate as previously stated by Akerlof.

3) In contrast to Akerlof's assertion, his limit does not apply to finite detectors in which energy dissipation is minimized. I conclude that, by simply reducing the size, the technology of today's gravitational wave detectors should be able to make a particle detector sensitive to $dE/dx \sim 1\mathrm{GeV/cm}$, and I point out that many running and finished gravitational wave detection experiments are already

sensitive to nuclearites and the available data may be useful for finding such particles or setting a flux limit. As an example, the result of a gravitational wave search published in 1982 is used to obtain a flux limit of $4.4 \times 10^{-11} \mathrm{cm}^{-2}\mathrm{s}^{-1}\mathrm{sr}^{-1}$ for nuclearites, which is only slightly higher than the limit of a scintillator search three years later.

4) Other acoustic and mechanical techniques for particle detection have been studied. In theory, measuring the thermal expansion of a bar may yield a much higher signal-to-noise ratio than measuring the change of the normal mode oscillations, and the method of measuring the stopping force directly may have sensitivity for extremely low β. Whether such techniques are feasible in practice is worth experimental investigation.

5) The result of a SIMP search experiment at Caltech implies that the flux of any massive particles having $I \geq \frac{1}{3} I_{min}$ and $2.7 \times 10^{-4} < \beta < 5 \times 10^{-3}$ cannot be larger than $4.7 \times 10^{-12}\ \mathrm{cm}^{-2}\mathrm{sr}^{-1}\mathrm{s}^{-1}$ (90% c.l.) at Earth's surface.

6) Although this flux limit is above the limits from underground experiments, it applies to particles about two orders of magnitude lighter than those that can be detected underground (see Fig. 3.5.1). When other published experiments on Earth's surface are corrected to address such relatively light particles, none of

them have better sensitivity than our experiment in the same β and ionization region.

7) The flux limit presented here implies a stringent limit on the fraction of the dark matter that can be attributed to massive electrically and/or magnetically charged particles, as shown in Fig. 3.5.2 and Fig. 3.5.3.

8) The test of a prototype shows that the MACRO scintillator detector has adequate light level and time resolution for achieving its physics goals.

9) When the new SIMP trigger circuit presented in this work is used in MACRO, it may be sensitive to all conceivable SIMPs having β as low as the escape velocity of the sun and for some species as low as the orbital velocity around the earth.